

INFORMATION TO USERS

This manuscript has been reproduced from the microfilm master. UMI films the text directly from the original or copy submitted. Thus, some thesis and dissertation copies are in typewriter face, while others may be from any type of computer printer.

The quality of this reproduction is dependent upon the quality of the copy submitted. Broken or indistinct print, colored or poor quality illustrations and photographs, print bleedthrough, substandard margins, and improper alignment can adversely affect reproduction.

In the unlikely event that the author did not send UMI a complete manuscript and there are missing pages, these will be noted. Also, if unauthorized copyright material had to be removed, a note will indicate the deletion.

Oversize materials (e.g., maps, drawings, charts) are reproduced by sectioning the original, beginning at the upper left-hand corner and continuing from left to right in equal sections with small overlaps.

Photographs included in the original manuscript have been reproduced xerographically in this copy. Higher quality 6" x 9" black and white photographic prints are available for any photographs or illustrations appearing in this copy for an additional charge. Contact UMI directly to order.

ProQuest Information and Learning
300 North Zeeb Road, Ann Arbor, MI 48106-1346 USA
800-521-0600

UMI[®]

University of Alberta

The Transport Processes in Soil Bioremediation

by

Soheila Karimi Lotfabad



A thesis submitted to the Faculty of Graduate Studies and Research in partial

fulfillment of the requirements for the degree of Doctor of Philosophy

in

Chemical Engineering

Department of Chemical and Materials Engineering

Edmonton, Alberta

Spring 2000



**National Library
of Canada**

**Acquisitions and
Bibliographic Services**

**395 Wellington Street
Ottawa ON K1A 0N4
Canada**

**Bibliothèque nationale
du Canada**

**Acquisitions et
services bibliographiques**

**395, rue Wellington
Ottawa ON K1A 0N4
Canada**

Your file Votre référence

Our file Notre référence

The author has granted a non-exclusive licence allowing the National Library of Canada to reproduce, loan, distribute or sell copies of this thesis in microform, paper or electronic formats.

The author retains ownership of the copyright in this thesis. Neither the thesis nor substantial extracts from it may be printed or otherwise reproduced without the author's permission.

L'auteur a accordé une licence non exclusive permettant à la Bibliothèque nationale du Canada de reproduire, prêter, distribuer ou vendre des copies de cette thèse sous la forme de microfiche/film, de reproduction sur papier ou sur format électronique.

L'auteur conserve la propriété du droit d'auteur qui protège cette thèse. Ni la thèse ni des extraits substantiels de celle-ci ne doivent être imprimés ou autrement reproduits sans son autorisation.

0-612-59983-3

Canada

University of Alberta

Library Release Form

Name of Author: *Soheila Karimi Lotfabad*


Title of Thesis: *The Transport Processes in Soil Bioremediation*

Degree: *Doctor of Philosophy*

Year this Degree Granted: *2000*

Permission is hereby granted to the University of Alberta Library to produce single copies of this thesis and to lend or sell such copies for private, scholarly or scientific research purposes only.

The author reserves all other publication and other rights in association with the copyright in the thesis, and except as hereinbefore provided, neither the thesis nor any substantial portion thereof may be printed or otherwise reproduced in any material from whatever without the author's prior written permission.

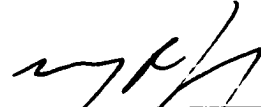

#210, 11532 – 40 Avenue
Edmonton, AB
T6J 0R6

Date: Jan 31, 2000

University of Alberta

Faculty of Graduate Studies and Research

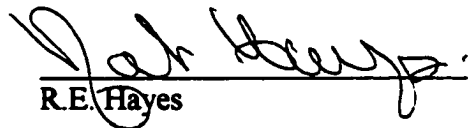
The undersigned certify that they have read, and recommend to the Faculty of Graduate Studies and Research for acceptance, a thesis entitled *The Transport Processes in Soil Bioremediation* submitted by *Soheila Karimi Lotfabad* in partial fulfillment of the requirements for the degree of *Doctor of Philosophy in Chemical Engineering*.



M.R. Gray (supervisor)



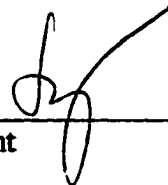
J. Ramsay (external examiner)



R.E. Hayes



M. Dudas



J. Foght

Date: January 6, 2000

This thesis is dedicated to my father Ali Karimi Lotfabad for his continuous support and encouragement

Abstract

The availability of contaminants is a major issue in soil bioremediation. Numerous studies have shown that even in the presence of active culture, bioremediation does not achieve the desired level of clean up. This study considers the physical structure of oil and clay as the key factor in bioremediation, and reviews the transport processes that limit the bioavailability of polynuclear aromatic hydrocarbons (PAHs). This research focuses on diffusion of contaminants in non-aqueous phase liquid (NAPL) and through porous structure of soil aggregates. Preliminary experiments on pristine soil, spiked with anthracene, suggested that reducing the size of the soil aggregates enhanced the rate of degradation. This hypothesis was tested on a creosote-contaminated soil. The aggregate size was reduced by sonication, and degradation of 6 target PAHs was monitored during the course of bioremediation. Sonication increased the rate of microbial degradation up to 5 fold, however there was no significant difference in the final residual concentrations between the two soil treatments. The aggregate size distribution after three weeks of treatment in a slurry bioreactor was comparable in both the sonicated and non-sonicated soils which was consistent with the equivalent residual concentrations of PAHs.

Two microscopy methods, confocal scanning laser microscopy (CSLM) and cryogenic scanning electron microscopy (cryo-SEM), were employed to investigate the microstructure of contaminated soils and to examine the distribution of non-

aqueous phase liquid (NAPL) in clay aggregates. Based on the information obtained, a physical model was proposed for the distribution of NAPL in soil microstructure. This model suggested that the distribution of NAPL change from liquid-filled pores for large aggregates, to a surface film for small aggregates.

Based on the physical model of the distribution of NAPL in soil aggregates and the data obtained in bioremediation experiments, a mathematical model was developed. This model suggested a diffusion-controlled mass transfer mechanism in soil aggregates. The effective diffusivity of PAHs in NAPL was estimated to be in the range of $0.5 \times 10^{-14} - 5 \times 10^{-14} \text{ cm}^2/\text{s}$. A model based on competitive inhibition of the substrates was developed and partially accounted for the initial lag phase in degradation of higher ring PAHs.

Acknowledgements

There are many people who helped me at various points throughout my thesis. It is not possible to acknowledge everyone here, but I do thank them.

I would like to thank my supervisor Dr. Murray Gray for his guidance in this thesis and continuous support and encouragement during my studies at the University of Alberta.

I would like to thank Dr. Sieghard Wanke and all the faculty members and staff in the Department of Chemical and Materials Engineering who provided me with the opportunity to study in such a pleasant environment.

My special thanks to Andree Koenig, Walter Boddez, Bob Borton and Jack Gibeau for timely discussions and valuable technical helps.

I give heartfelt thanks for the emotional support provided to me by my sons Peyman and Roozbeh, my father Ali and my sisters Mahin, Soraya and Sima.

Finally I would like to acknowledge the financial support from Environmental Science and Technology Alliance of Canada (ESTAC), the Natural Science and Engineering Research Council of Canada (NSERC), the Department of Chemical and Materials Engineering and my supervisor Dr. Murray Gray.

Table of Contents

Chapter		Page
1.	Introduction	1
1.1	Scope of Soil Contamination	1
1.2	Research Objectives	2
1.3	Thesis Overview	3
1.4	Literature Cited	5
2.	Literature Review	6
2.1	Significance of Non –aqueous Phase Liquid (NAPL)	6
2.1.1	Physical and Chemical Properties of DNAPLs	7
2.1.2	Distribution of DNAPL in Vadose Zone	10
2.2	Principles of bioremediation	13
2.2.1	Bioavailability Limitations	15
2.2.2	Overview of Mass Transfer in Bioremediation	16
2.3	Transport of Contaminants in Porous Structure of Soil	22
2.3.1	Diffusion Controlled Mass Transfer	22
2.3.2	Bulk Diffusivity	23
2.3.3	Knudsen Diffusivity	24
2.3.4	Dependence of Diffusivity on Viscosity of the Solvent	25
2.4	Partitioning Assumption	27
2.4.1	Nonlinear Equilibrium partitioning	28
2.4.2	Linear Equilibrium partitioning	29
2.5	Slurry Phase Reactors	30
2.5.1	Solid Liquid Mass Transfer from a single Spherical Particle	30
2.5.2	Mass Transfer to Suspensions of Small Particles	31
2.5.3	Rotating Drum Bioreactors	32
2.6	Microorganisms	35
2.6.1	Growth of Microorganisms on Hydrocarbons	35

2.6.2	Mechanism of PAH Transformation and Degradation by Microorganisms	36
2.6.3	Cometabolism and Substrate Inhibition	38
2.7	Literature Cited	42
3.	The Effect of Aggregate Size on the Kinetics of Bioremediation	48
3.1	Introduction	48
3.2	Materials and Methods	51
3.2.1	Soil Characteristics	51
3.2.2	Chemicals	52
3.2.3	Active Culture	52
3.2.4	Soil Preparation	53
3.2.5	GC Analysis	54
3.2.6	Bioreactor Operation	55
3.2.7	Aggregate Size Analysis	56
	3.2.7.1 Hydrometer Method	56
	3.2.7.2 Wet Sieving Method	57
3.3	Results	57
3.3.1	Degradation of Target PAHs in C-horizon and Creosote-contaminated soils	57
	3.3.1.1 Anthracene in C-horizon Soil	57
	3.3.1.2 Degradation of Six Target PAHs in Creosote-contaminated Soil	60
	3.3.1.3 Total Extractable Organics	64
	3.3.1.4 Biodegradation Rate Constants	65
3.3.2	Aggregate Size Distribution in Slurry-phase Bioreactors	68
	3.3.2.1 C-horizon Soil	68
	3.3.2.2 Creosote-contaminated Soil	71
3.4	Discussion	75
	3.4.1 Substrate Preference	75
	3.4.2 Kinetic Analysis	76

3.4.3	Comparison between $k_{\text{mean}}^{\text{APP}}$ and Literature Values	78
3.4.4	Dependence of $k_{\text{mean}}^{\text{APP}}$ on Aggregate Size	79
3.4.5	Extent of Biodegradation	82
3.5	Conclusion	83
3.6	Literature Cited	84
4.	Characterization on Contaminated Soils Using Confocal Scanning Laser Microscopy and Cryogenic Scanning Electron Microscopy	87
4.1	Introduction	87
4.2	Materials and Methods	89
4.2.1	Soils	89
4.2.2	Embedding	92
4.2.3	Microtomy	92
4.2.4	Confocal Scanning Laser Microscopy (CSLM)	93
4.2.5	Scanning Electron Microscopy	93
4.2.6	Freeze Fracturing	94
4.3	Results	94
4.3.1	Fluorescent CSLM	95
4.3.2	SEM	106
4.3.3	Elemental Analysis and Mapping	111
4.4	Discussion	113
4.5	Model for Distribution of NAPL in Soil Microstructure	115
4.6	Conclusion	118
4.7	Literature Cited	119
5.	A Diffusion Controlled Model for Interaaggregate Mass transfer	121
5.1	Introduction	121
5.2	Theory	124
5.2.1	Mass Transfer in Soil Aggregates	124
5.3	Results and Discussion	128
5.3.1	Feasibility of the Model	128

5.3.2	Aggregate Size Distribution and Corresponding Surface Area	130
5.3.3	Determination of Model Parameters	133
5.3.4	Estimated Diffusion Coefficients in NAPL	139
5.3.5	The Effect of Solvent Molecular Weight and Viscosity	140
5.3.6	Time Dependent Diffusivity	141
5.3.7	Formation of Semi-rigid Film on the Surface of NAPL	142
5.3.8	Comparison of Diffusion Coefficients in NAPL with Literature Values	142
5.3.9	Analogy to Diffusion in Polymers	145
5.3.10	Fraction of NAPL as a Film	146
5.4	Summary and Conclusion	147
5.5	Literature Cited	149
6.	Inhibitory Effect with Multiple Carbon Sources	153
6.1	Introduction	153
6.2	Qualitative Discussion	155
6.3	Experiments with C-horizon Soil	158
6.3.1	Results	159
6.4	Modeling	163
6.4.1	Development of a Substrate Inhibition Model	164
6.4.2	Results and Discussions	167
6.4.2.1	Evaluation of Model Parameters	167
6.4.2.2	Validity of the Competitive Inhibition Model	168
6.5	Conclusion	175
6.6	Literature Cited	177
7.	Conclusions and Recommendations	179
7.1	Conclusions	
7.1.1	Kinetics of Bioremediation	179
7.1.2	Characterization of Contaminated Soils	180

7.1.3	Modeling	181
7.2	Recommendations	183
Appendices		185
Appendix A		186
A.1.	Raw data on bioremediation of C-horizon soil and Edmonton creosote-contaminated soil	187
A.2.	Sample Calculation of the Rate Constants	199
A.2.1.	Estimation of the Apparent First Order Rate Constants	199
A.2.2.	Statistical analysis	203
A.2.3.	Apparent Rate Constants for 6 PAHs	210
Appendix B		213
Images from scanning electron microscopy and confocal scanning laser microscopy		
Appendix C		226
C.1.	Mass Balance and Governing Equations for Pore Diffusion	227
C.2.	Mass Balance and Governing Equation for Film Diffusion	231
C.3.	Calculation of average concentration in the pores	233
C.4.	Calculation of average concentration in the film	234
C.5.	Non-linear Regression for Diffusivity in NAPL	235

List of Tables

Table 2.1.	The physical properties of selected dense Non-Aqueous Phase Liquids	8
Table 2.2.	Properties of the 16 priority pollutant PAHs	9
Table 3.1.	Physical characteristics of the soils	51
Table 3.2.	Total Extractable Organics in different fractions of sonicated creosote-contaminated soil	64
Table 3.3.	Apparent first-order rate constants for degradation of anthracene in C-horizon soil	66
Table 3.4.	Apparent first order rate constants for degradation of 6 PAHs in creosote-contaminated soil	67
Table 4.1.	Characteristics of the contaminated soils and clay samples	91
Table 5.1.	Kinematic viscosity of NAPL from different sources	129
Table 5.2.	Model parameters estimated from experimental data on Edmonton Creosote-contaminated soil	134
Table 5.3.	Measured kinematic viscosity of creosote	141
Table 5.4.	Diffusion coefficients of organic compounds in different media	144
Table 5.5.	The mass fraction of slowly desorbing PAHs	147
Table 6.1.	Statistical analysis of the slope of the lag phase in bioremediation of creosote-contaminated soil	158
Table 6.2.	Data on the first phase of degradation of PAHs in C-horizon soil	163
Table 6.3.	Model parameters for degradation of PAHs based on competitive inhibition kinetics	168

List of Figures

Figure 2.1.	Schematic diagram of distribution of NAPL in porous structures	12
Figure 2.2.	Schematic diagram of steps involved in transport of contaminants from a soil aggregate to the biochemical reaction sites inside the cell	18
Figure 2.3.	Schematic diagram of PAH degradation pathway	37
Figure 3.1.	Biodegradation of anthracene in the C-horizon soil after 9 days of incubation	59
Figure 3.2.	Time course concentration of phenanthrene, fluoranthene and pyrene during bioremediation in creosote-contaminated soil	63
Figure 3.3	Hydrometer readings for the samples of C-horizon soil from the bioreactor and sonicated soil	70
Figure 3.4.	Aggregate size distribution in bioreactor and in soils sonicated at different intensities	72
Figure 3.5.	The time course of mass average diameter of the aggregates in the bioreactor compared to the samples sonicated at different intensities	74
Figure 3.6.	The effect of aggregate size on the apparent first order degradation rate constant	80
Figure 3.7.	The plot of apparent first order degradation rate constant versus $1/R^2$ for six PAHs	81
Figure 4.1.	Samples of contaminated and pristine soils under bright-field microscope (A, C and E) and fluorescent microscope (B, D and F)	96
Figure 4.2.	An aggregate of Edmonton creosote contaminated soil	98
Figure 4.3.	Aggregate of Prince Albert creosote-contaminate soil	102
Figure 4.4.	Microtome number 5 from an aggregate of Edmonton creosote-contaminated soil	105
Figure 4.5.	Electron micrographs of A) Montmorillonite, B) Kaolinite, C) C-horizon soil, D) Edmonton creosote-contaminated soil	107

Figure 4.6.	Electron micrographs of different soil samples	110
Figure 4.7.	A map of Devon hydrocarbon-contaminated soil, which shows the distribution of chemical elements obtained by elemental analysis of EDX	112
Figure 4.8.	Schematic diagram of distribution of NAPL in soil aggregate	117
Figure 5.1.	Aggregate size distribution in the process of bioremediation of Edmonton creosote-contaminated soil in slurry phase bioreactor	132
Figure 5.2.	Variation of $\alpha A(t)/A_{max}$ for non-sonicated soil during slurry phase bioremediation	135
Figure 5.3.	Time course of concentration of acenaphthene, anthracene and chrysene during bioremediation of Edmonton creosote-contaminated soil	137
Figure 5.4.	Time course of concentration of phenanthrene, fluoranthene and pyrene during bioremediation of Edmonton creosote-contaminated soil	138
Figure 6.1.	Time course concentration of 6 PAHs in the process of bioremediation of creosote-contaminated soil in slurry phase reactor	157
Figure 6.2.	Time course degradation of fluoranthene in spiked C-horizon soil	160
Figure 6.3.	Time course degradation of chrysene in spiked C-horizon soil	161
Figure 6.4.	Time course degradation of pyrene in spiked C-horizon soil	162
Figure 6.5.	The time course of concentration of fluoranthene during bioremediation of creosote-contaminated soil in slurry phase reactor	171
Figure 6.6.	The time course of concentration of chrysene during bioremediation of creosote-contaminated soil in slurry phase reactor	172
Figure 6.7.	The time course of concentration of pyrene during bioremediation of creosote-contaminated soil in slurry phase reactor	173

Nomenclature

\bar{C}_f	average concentration in the film
\bar{C}	average concentration in the film
\bar{C}_p	average concentration in the pores
$1/n$	Freundlich exponent
$A(t)$	available external surface area for mass transfer at any time t
a_c	surface area of cell per unit mass
A_{max}	maximum external surface area of soil
a_s	soil surface area per unit mass
b	Langmuir intensity coefficient
C	concentration of contaminant in soil aggregate
C_0	initial concentration in the soil
C_b^*	concentration in the bulk of aqueous phase
C_c	concentration inside the cell
C_e	aqueous phase concentration at equilibrium
C_f	concentration in the film
C_{ib}	concentration in aqueous phase, at the soil interface
C_{ic}	aqueous concentration at the cell interface
C_p	concentration in the pores
D	diffusivity of contaminants in the medium (aqueous phase or NAPL)
D_d	drum diameter
D_{eff}	effective diffusivity in soil aggregate
D_{eff-c}	effective diffusivity across the cell membrane
D_K	Knudsen diffusivity
$D_{K,eff}$	effective Knudsen diffusivity
D_{mean}	mass average diameter
D_{NAPL}	Diffusivity of component A in NAPL

D_p	particle diameter
e_0	total enzyme concentration
$Flux_I$	flux of inhibitor from NAPL
$f_{oc/om}$	mass fraction of organic carbon in soil organic matter
Fr	Froude number
g	acceleration due to gravity
h	the height of DNAPL
h_{hs}	height of slurry in the drum
i	inhibitor concentration
k	the intrinsic permeability
K	hydraulic conductivity
k_{app}	apparent first order rate constant
k^{app}_{mean}	mean apparent rate constant
k_{bio}	intrinsic rate constant for biochemical reaction
k_c	mass transfer coefficient to the cell
K_f	Freundlich capacity coefficient
K_I	dissociation constants of inhibitor
K_{oc}	organic carbon partition coefficient
K_{ow}	octanol water partition coefficient
K_p	partition coefficient
K_S	dissociation constants of substrate
K_s	half saturation concentration
k_s	mass transfer coefficient for dissolution of contaminants
l	film thickness
l_c	thickness of cell membrane
m	mass fraction
M	molecular weight
m_c	mass concentration of cells
m_s	mass concentration of soil

N	rotational speed
N_c	critical rotational speed
N_{Kn}	Knudsen number
P	pressure
P_c	capillary pressure
P_g	gravity pressure
Q	maximum uptake in the first layer
q_e	immobile phase concentration at equilibrium
R	radius of the soil aggregate
R_A	overall rate of degradation of component A
Re	Reynolds number
R_{mean}	mass average radius
r_p	the pore radius
R_r	rate of reaction
S	substrate concentration in aqueous phase
s	specific surface area
Sc	Schmidt number
Sh	Sherwood number
S_I	inhibitor concentration in aqueous phase
S_w	solubility in water
T	temperature
t	time
TEO	Total Extractable Organics
V	molar volume at the boiling point
v	velocity
V_w	velocity of the drum wall
v_{max}	maximum rate of degradation
X	cell concentration

$\bar{\tau}$	tortuosity of soil
γ	interfacial tension between DNAPL and water
ε_{aq}	water filled porosity
ρ_c	density of the fluid
μ_g	specific growth rate
μ_{max}	maximum growth rate
ρ_{NAPL}	the density of DNAPL
ε_{NAPL}	NAPL filled porosity
ρ_p	density of particles
ε_t	total porosity
φ	association parameter of the solvent
σ	constriction factor
Φ	contact angle
μ	fluid absolute viscosity
ρ	fluid density
λ	mean free path
ε	porosity of soil
τ	tortuosity factor

1. Introduction

1.1 Scope of Soil Contamination

Release of organic chemicals during transportation, storage and production has led to contamination problems in soil, water and air in the past two centuries. The contaminants cover a wide range of organics including polynuclear aromatic hydrocarbons (PAHs), petroleum hydrocarbons and compounds with a wide range of functional groups. Wood preserving sites and manufactured gas plants (MGPs) are the major industries that contributed to releases of creosote and coal tar, which contain considerable amounts of PAHs. It is estimated that more than 900 gasification plants were operational in U.S. by 1920 (Rhodes, 1979). The number of wood preserving plants was estimated between 188 and 631 in 1978 (USDA, 1980). The U.S. Environmental Protection Agency (EPA) regulates 16 PAHs as indicators of contamination in soil and groundwater. Seven of these PAHs such as benzo[a]pyrene are considered carcinogens and have been placed on the EPA's first priority list of hazardous substances (Sitting, 1991).

Transport of soil contaminants to surface water by heavy rains, or leaching into groundwater, are major concerns that motivate research into finding the most efficient, economic and applicable methods of site reclamation. Researchers have used different approaches to investigate the fate of contaminants in the natural environment. These studies have been mainly focussed on laboratory experiments (Weissenfels et al., 1992; Pennell et al., 1996), field experiments (Mackay et al.,

1986; Barker et al, 1992), investigation at contaminated sites (Blaszkiwicz et al., 1997) and mathematical modeling (Ahn et al., 1996).

Although there has been a great deal of research activity towards incorporating the transport of contaminants into bioremediation kinetics, there has been little attempt towards independent characterization of the structure of contaminants in soil aggregates and linking this geometry to the transport and remediation characteristics. This dissertation attempts to address these issues as they relate to bioremediation of creosote-contaminated soil. The objectives of the research are outlined below.

1.2 Research Objectives

The objective of this research was to increase knowledge of the transport mechanisms involved in soil bioremediation, with particular emphasis on determining the rate controlling processes. More specific objectives were as follows:

1. Experimental determination of the rate of bioremediation of polynuclear aromatic hydrocarbons (PAHs) in a creosote-contaminated soil.
2. Investigation of the role of aggregate size on the rate and extent of bioremediation.
3. Determination of the aggregate size distribution in slurry phase reactors.
4. Characterization of contaminated soil with respect to distribution of non-aqueous phase liquid (NAPL) in the soil microstructure.

5. Determination of rate controlling processes.
6. Development of an appropriate model based on the rate controlling mechanism(s).

1.3 Thesis Overview

This thesis has been divided into 7 chapters. Chapter 2 covers the theoretical background information related to the work. Chapter 3 provides an overview of the experimental methods along with choice of contaminated soil(s). In this chapter the effect of aggregate size on the rate and extent of bioremediation has been investigated. In addition, stability of the soil aggregates under experimental conditions in a slurry phase reactor and during the process of bioremediation has been discussed.

Chapter 4 describes the characterization of contaminated soils using two different microscopy techniques. Confocal scanning laser microscopy (CSLM) along with cryogenic scanning electron microscopy (cryo-SEM) was used to verify the physical structure and the distribution of NAPL in soil microstructure.

Chapter 5 is devoted to developing a diffusion model that can best explain the kinetics of bioremediation in the period when mass transfer is the limiting step in bioremediation. This mathematical model is based on the proposed model of distribution of NAPL in soil microstructure, developed in chapter 4, and is tested with data obtained in chapter 3.

Chapter 6 focuses on biological aspects of bioremediation and the period where biological activity is a rate limiting factor in bioremediation. The possibility of

catabolic repression or substrate inhibition is discussed in this chapter. Finally Chapter 7 summarizes the most important results and the conclusions of the work.

1.4 Literature Cited

Ahn, I.S.; Lion, L.W.; Shuler, M.L., "Microscale based modeling of polynuclear aromatic hydrocarbon transport and biodegradation" *Biotech. Bioeng.*, 1996, 51, 1-14.

Barker, J.F.; Hubbard, C.E.; Lemon, L.A.; Wooro, K.A., "The influence of methanol in gasoline fuels on the formation of dissolved plumes and on the fate and natural remediation of methanol and BTEX desolved in groundwater." *Proceedings, 1st Annual West Coast Conference on Hydrocarbon Contaminated Soils and Groundwater*, Newport Beach, California, USA. Feb., 1992, 2, 103-113.

Blaszkiwicz, H.; Connolly, M.; Mazur, M., "Full-scale on site bioremediation of PAH in soil" *Fourth International In-situ and On-site Bioremediation Symposium*, New Orleans, April 28-May 1, 1997.

Mackay, D.M.; Freyburg, D.L.; Roberts, p.V.; Cherry, J.A., "A natural gradient experiment on solute transport in a sand aquifer: 1. Approach and overview of plume movement." *Water Resources Research*, 1986, v.30, 2, 369-383.

Pennell, K.D.; Abriola, I.M.; Loverde, L.E., "The use of surfactants to remediate NAPL-contaminated aquifers" *Non-Aqueous Phase Liquids (NAPLs) in Subsurface Environment: Assessment and Remediation*. L.N. Reddi. ASCE, New York, 1996.

Rhodes, E.O., "The history of coal tar and light oil, in bituminous materials: asphalts, tars and pitches, Volume III: Coal Tars and Pitches" A.J. Hoiberg ed, R.E. Krieger Publishing Co., Huntington, New York, 1979.

Sitting, M., "Handbook of toxic and hazardous chemicals and carcinogens" 3rd edition, Noyes Publications, Park Ridge. 1991.

USDA, "The biologic and economic assessment of pentachlorophenol, inorganic arsenicals, creosote, Volume I: Wood preservatives" *U.S. Department of Agriculture Technical Bulletin*, 1658-I, 1980.

Weissenfels, W.D.; Klewer, H.J.; Langhoff, J., "Adsorption of polynuclear aromatic hydrocarbons (PAHs) by soil particles: influence on biodegradability and biotoxicity." *Appl. microbiol. Biotechnol.*, 1992, 36, 689-696.

2. Literature Review

2.1 Significance of Non-Aqueous Phase Liquid (NAPL)

When a solution of contaminants enters the soil, the solvent and the volatile compounds are partially removed by weathering or by biological processes. As NAPL migrates through the subsurface, a fraction of the NAPL is retained by porous soil aggregates. This fraction, which is called residue NAPL, may occupy between 5 to 40% of the pore volume of the soil (Schwille, 1984; Hunt et al., 1988). Upon entering the groundwater, the fraction that is lighter than water (LNAPL) such as petroleum hydrocarbons spread on the water table, while the NAPL which is denser than water (DNAPL) such as chlorinated solvents and creosote will continue to migrate downward in the saturated zone until it reaches a low permeability zone. The movement of the NAPL in the vadose zone (unsaturated zone) is partially controlled by the viscosity of the NAPL components as the hydraulic conductivity is inversely related to viscosity by the following equation:

$$K = k\rho g / \mu \quad (2.1)$$

K	= hydraulic conductivity
k	= the intrinsic permeability
ρ	= fluid density
g	= acceleration due to gravity
μ	= fluid absolute viscosity

The viscosity of NAPL in the vadose zone will increase gradually. Volatilization, dissolution of more volatile components and selective biodegradation will contribute to developing more viscous and thicker NAPL with time. The presence of viscous NAPL with low solubility can be a source of long term groundwater contamination.

2.1.1 Physical and Chemical Properties of DNAPLs

Dense non-aqueous phase liquids (DNAPLs) such as coal tar wastes, creosote-based wood-treating oils, chlorinated solvents, polychlorinated biphenyl compounds (PCBs) and pesticides are immiscible fluids with a density greater than water. Organic chemicals in the form of DNAPLs exhibit complex physical and chemical behavior in highly heterogeneous soil-water systems. The physical and chemical properties of pure components are well defined but the properties of DNAPLs in the subsurface environment may be considerably different from those of pure compounds due to the effects of weathering and the presence of complex chemical mixtures. The composition of tars and wastes generated at gas plants and wood preserving sites depended on the raw materials and manufacturing processes used. Table 2.1 outlines the physical properties of selected DNAPLs. Creosote and coal tar are complex mixtures containing more than 250 individual components. The composition of coal tar is similar to creosote, except that coal tar contains approximately 5% of light monocyclic aromatic compounds including benzene, toluene, ethylbenzene and xylene (BTEX). As mentioned earlier, PAHs are the major components of creosote.

In Table 2.2 the properties of 16 PAHs along with their molecular weight, water solubility and octanol water partition coefficient (K_{ow}) are listed and compared.

Table 2.1. The physical properties of selected dense non-aqueous phase liquids (DNAPLs). (Cohen and Mercer, 1993)

DNAPL, type	Specific Gravity	Viscosity, cp
Halogenated Hydrocarbon Solvents, at 20 °C	1.08 – 2.89	0.36 – 2.04
Polychlorinated biphenyl compounds (PCBs), 25 °C and 38 °C		
Aroclor 1221 – 1254	1.18 – 1.53	12 – 1900
Aroclor 1260	1.62	sticky resin
Coal Tar	1.01 – 1.18	10 - 70
Creosote (85% PAHs, 10% phenolic compounds, 5% N-, S- and O-heterocycles)	1.01 – 1.14	10 - 70

Table 2.2. Properties of the 16 priority pollutant PAHs*

PAH	Number of rings	MW g/mol	Aqueous solubility mg/L	Log(K _{ow})
Naphthalene	2	128.2	31.0	3.37
Acenaphthylen	3	150.2	3.93	4.0
Acenaphthene	3	154.2	3.47	3.92
Fluorene	3	166.2	1.90	4.18
Phenanthrene	3	178.2	1.10	4.57
Anthracene	3	178.2	0.07	4.54
Fluoranthene	4	202.3	0.26	5.22
Pyrene	4	202.3	0.13	5.18
Benzo[a]anthracene	4	228.3	0.011	5.91
Chrysene	4	228.3	0.004	5.65
Benzo[b]fluoranthene	5	252.3	0.00115	5.80
Benzo[k]fluoranthene	5	252.3	0.0008	6.0
Benzo[a]pyrene	5	252.3	0.0038	6.04
Benzo[g,h,i]pyrene	5	268.4	0.00026	6.50
Dibenz[a,h]anthracene	6	278.3	0.0006	6.75
Indeno[1,2,3-c,d]pyrene	6	276.3	0.062	7.66

* Data from Mackay et al., 1992

2.1.2 Distribution of DNAPL in the Vadose Zone

Distribution of DNAPL in the environment occurs by three distinct mechanisms:

- Immiscible subsurface flow
- Dissolution and solute transport
- Volatilization and vapor transport

Transport of DNAPL in subsurface soil is governed by several principles and transport mechanisms such as hydrostatic and hydrodynamic forces, inertial forces, interfacial forces and electrostatic forces. These forces, however, operate at different length scales with different magnitudes. The nature of the porous media, the volume and properties of DNAPL, the time duration of release and the interaction between DNAPL and soil components are parameters influencing the subsurface transport of DNAPL (Feenstra and Cherry, 1988).

The subsurface movement of DNAPL is determined by the three major forces: gravity forces, capillary forces and viscous forces. When DNAPL is released to the subsurface, it moves downward through the vadose zone by the action of gravity.

The gravity pressure is defined as:

$$P_g = \rho_{DNAPL}gh \quad (2.2)$$

- P_g = gravity pressure
- ρ_{DNAPL} = the density of DNAPL
- g = the acceleration due to gravity
- h = the height of DNAPL

Small variations in soil texture and water content at different layers can cause sufficient capillary pressure to resist the migration of DNAPL from larger to smaller pores in water saturated porous zones. The capillary pressure is a surface phenomenon and is expressed by the following equation:

$$P_c = 2\gamma \cos \Phi / r_p \quad (2.3)$$

- P_c = capillary pressure
- γ = interfacial tension between DNAPL and water
- Φ = contact angle
- r_p = the pore radius

The gravity pressure needs to overcome the capillary pressure ($P_g \geq P_c$), in order for DNAPL to move to small pores. Sufficient capillary pressure can prevent downward penetration of DNAPL and cause lateral spreading in the vadose zone. A simple model shown in Figure 2.1 illustrates the effect of different forces in the movement of DNAPL in different pore structures. In Figure 2.1a the upward capillary gradient is large enough to prevent the penetration of DNAPL into the pore. In contrast downward movement of DNAPL in Figure 2.1b continues because of a larger gravity force acting on the lower base. The NAPL has been immobilized in Figure 2.1c, as the underlying layer has a finer texture with smaller pores and higher capillary pressure. As a result the DNAPL spreads over the layer, finding its way through fractures, large pores and root holes (2.1d). Similar behavior is reported by Schuille (1988) and Wilson et al., (1990). They conducted a laboratory experiment

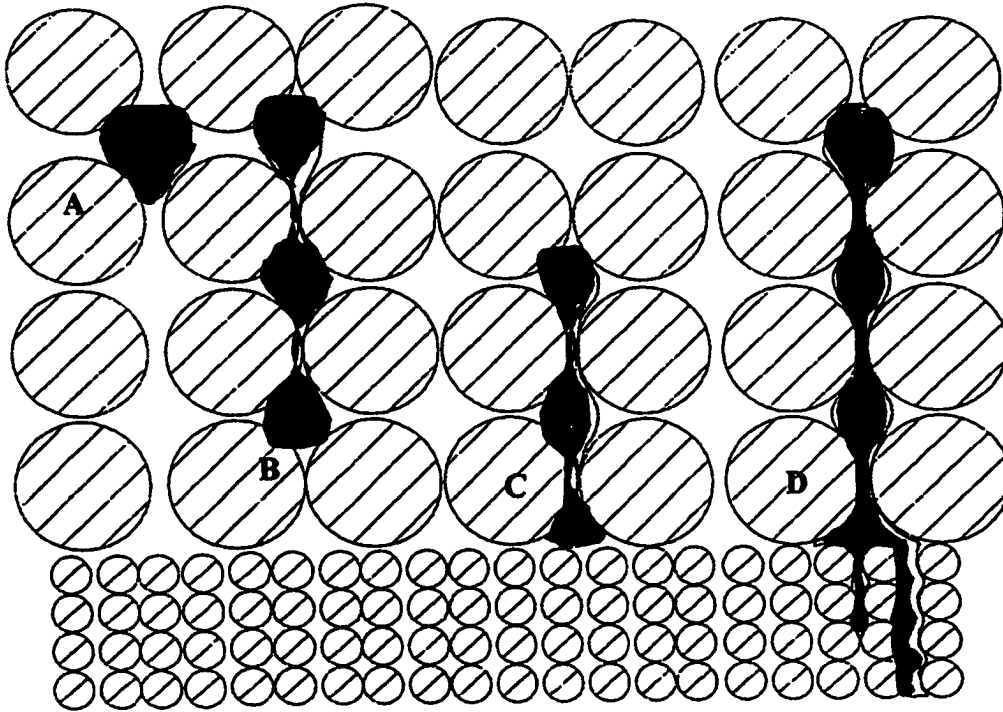


Figure 2.1. Schematic diagram of distribution of NAPL in porous structures.

and observed that in the saturated zone, hydrophobic DNAPL flowed selectively through the coarser fractions of heterogeneous media, avoiding the fine media with greater capillary resistance to the flow. As the result of this flow pattern, DNAPL appeared as structured globules along the fractures and macro-pores while the smaller pores were filled with water. As the DNAPL moves through the vadose zone a significant portion of DNAPL is trapped in the porous media and, depending on the volume of DNAPL it may or may not reach the water table.

2.2 Principles of bioremediation

Bioremediation is an extension of a natural process of biological degradation of contaminants which can be accelerated by optimizing the key variables (Loehr, 1992). Bioremediation can operate either in-situ (bioventing, bioaugmentation and biostimulation) or ex-situ (biofilters, composting, land farming and slurry bioreactors). Regardless of the method, all bioremediation techniques rely on the ability of an active microbial population to utilize the contaminants and convert them to CO₂ and water. Some microorganisms can grow directly on the surface of NAPL (Tongpim & Pickard, 1996), but in general consumption of contaminants by microorganisms occurs in aqueous phase (Wodzinski and Coyle, 1974). The contaminants need to dissolve into the aqueous phase and then be transported to the microorganisms. Oxygen and supplementary nutrients such as nitrogen and phosphorus may be added to the soil to stimulate biological activity. Trace elements are usually not limited in soil so a deficiency in them is rarely encountered (Dibble

and Bartha, 1979). The pH should be adjusted for the optimum microbial activity, which typically is in the range of 6 – 8. Temperature is critical in some bioremediation methods. Mesophilic microbes have an optimum temperature range between 25 – 45 °C. This class of microorganisms appears to be the most effective in biodegradation of organic contaminants. Hogan et al. (1989) reported that 35 °C provided better degradation of aliphatic petroleum hydrocarbons and PAH than 50 °C. The major differences between the bioremediation methods are the degree of mixing and the level of moisture content. In composting and land farming, the mixing is performed periodically and the moisture content is in the range of 40-80% of the field capacity (Peramaki et al, 1997), while in situ bioremediation provides no mixing with variable moisture content, depending on the location of the contaminants (vadose zone in contrast to saturated zone). Slurry phase bioremediation provides complete mixing and water content well above the field capacity saturation.

In terms of PAH degradation, both low and high molecular weight compounds are degradable by indigenous microorganisms in soils and sediments. As a result bioremediation is considered to be a potential remediation option at PAH contaminated sites. The major drawback of bioremediation methods is that the contaminant concentrations often decline to an asymptotic value, which is still above the required level of treatment. There are at least five factors that may lead to slow or incomplete removal of PAHs from contaminated soils during bioremediation: 1) slow rate of mass transfer from soil aggregates; 2) the lack or insufficient number of microorganisms capable of degrading a specific compound; 3) insufficient growth

substrate to sustain a population of PAH degrading microorganisms; 4) accumulation of toxic metabolites and 5) competitive inhibition of less readily degradable PAHs by the more readily degradable compounds.

2.2.1 Bioavailability Limitations

Many investigators have reported partial degradation of contaminants and slow desorption of residual contaminants. The persistence of organic compounds in the soil due to poor availability to the active organisms is a major concern in bioremediation. Limited availability of target compounds to bacteria can cause long treatment times of months or years, and apparent resistance to degradation, especially in static systems such as composting and soil columns.

Reduced bioavailability of contaminants as the result of slow rate of mass transfer is due to different interactions between contaminants and soil. Four interactions have been proposed to contribute to reducing the bioavailability of organic compounds in soil with increasing age of contamination:

- 1- Migration of contaminants into soil organic matter. Such contaminants are suggested to be non-bioavailable (Chiou et al., 1988 & 1989; Murphy et al., 1990; Weissenfels et al., 1992).
- 2- Entrapment in micropores and adsorption on mineral surfaces (Steinberg et al., 1987; Ball et al., 1991; Haderline et al., 1993).

3- Chemical reactions that alter the molecular structure, such as oligomerization of PAHs (Karimi et al., 1996) and complexation of nitroaromatic compounds (Haderline et al., 1993).

4- Presence of Non-aqueous Phase Liquid (NAPL) as a highly viscous and dense material with partition coefficients higher than soil organic matter (Luthy et al., 1994; Rutherford et al., 1997).

All of the above interactions may occur simultaneously in a given soil, leading to a complex set of interactions, which render the target compounds more resistant to bioremediation. The outcome of these interactions is manifested in the slower bioremediation of aged soil compared to freshly contaminated soils. (Steinberg et al., 1987; Weissenfels et al., 1992; Pignatello et al., 1993).

In a creosote contaminated soil, the PAHs occur in a NAPL with complex composition. Laboratory experiments have shown that the compounds are more resistant to biodegradation when they are present as NAPL, and in addition the same compound may degrade at significantly different rates in the presence of different NAPLs (Efroymsen and Alexander, 1994).

2.2.2 Overview of Mass Transfer in Bioremediation

The kinetics of biological removal of contaminants from porous soil aggregates involves several sequential and parallel transport and reaction phenomena (Tabak et al., 1996; Bosma et al., 1997). Part of the transport process is abiotic,

including internal diffusion of contaminants through soil aggregates, partitioning to the aqueous phase and external diffusion from the surface to the bulk liquid. **Biological transport phenomena** include the diffusion transport through cell membranes and biochemical reactions inside the cell. Figure 2.2 shows a schematic diagram of steps involved in transport of contaminants from NAPL in the porous structure of soil aggregates. The contaminants pass through a series of transport resistances. The relative magnitude of each resistance depends on the physical and chemical properties (viscosity, density, chemical composition) of the medium that the contaminants are transported through, temperature, hydrodynamics and interfacial phenomena (Fogler, 1992).

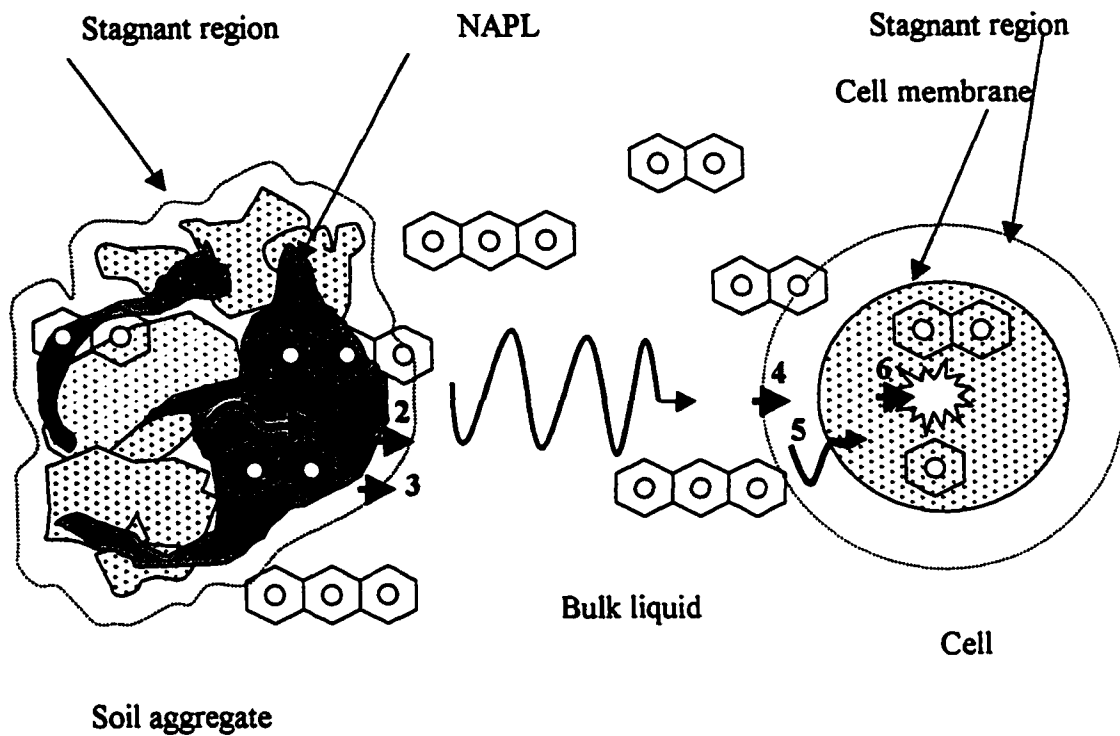


Figure 2.2. Schematic diagram of steps involved in transport of contaminants from a soil aggregate to the biochemical reaction sites inside the cell.

To illustrate the resistance to mass transfer in each step a simple steady state model is discussed below. The infinite series solution for non-steady state model with appropriate boundary conditions will be discussed in Chapter 5.

The transport mechanism and the rate of mass transfer in each step can be listed as follows:

1. Diffusion of contaminants from inside the soil aggregate to the surface of the aggregate can be illustrated with the following differential equation:

$$\frac{\partial C}{\partial t} = D_{eff} \nabla^2 C \quad (2.4)$$

D_{eff} = effective diffusivity in soil aggregate
 R = radius of the soil aggregate
 C = concentration of contaminant in soil aggregate
 t = time

The flux of contaminants is controlled by the effective diffusivity of the contaminants in the soil aggregates.

2. Partitioning to the aqueous phase

$$K_p = \frac{C_s}{C_{ib}} \quad K_p = \frac{C}{C_b^*} \quad (2.5)$$

K_p = partition coefficient
 C_{ib}^* = concentration in aqueous phase, at the soil interface
 C_b^* = concentration in the bulk of aqueous phase

3. Diffusion through stagnant region around the soil aggregate into the bulk aqueous phase

$$R_A = k_s a_s m_s (C_{ib} - C_b) \quad (2.6)$$

- k_s = mass transfer coefficient for dissolution of contaminants
 a_s = soil surface area per unit mass
 m_s = mass concentration of soil
 R_A = overall rate of degradation of component A

Transport through the bulk liquid phase, usually by means of convection

4. Diffusion through stagnant region around the cell

$$R_A = k_c a_c m_c (C_b - C_{ic}) \quad (2.7)$$

- k_c = mass transfer coefficient to the cell
 a_c = surface area of cell per unit mass
 m_c = mass concentration of cells
 C_{ic} = aqueous concentration at the cell interface

5. Diffusion through cell membrane

$$R_A = \frac{D_{eff-c} a_c m_c}{l_c} (C_{ic} - C_c) \quad (2.8)$$

- D_{eff-c} = effective diffusivity across the cell membrane
 l_c = thickness of cell membrane
 C_c = concentration inside the cell

6. Biochemical reaction inside the cell

$$R_A = k_{bio} C_c \quad (2.9)$$

k_{bio} = intrinsic rate constant for biochemical reaction

The overall rate of reaction can be expressed as:

$$R_A = k_{app}C \quad (2.10)$$

k_{app} = apparent first order rate constant

Combining equations (2.5) through (2.9) and comparing the result with equation (2.10) we can derive an expression for the external resistance to mass transfer as follows:

$$\frac{1}{k_{app}} = \left[\frac{1}{k_s a_s m_s} \right] + \left[\frac{1}{k_c a_c m_c} + \frac{l}{D_{eff-c} a_c m_c} \right] + \left[\frac{1}{k_{bio}} \right] \quad (2.11)$$

The terms in the first bracket correspond to external resistance to mass transfer associated with aggregates. The second bracket demonstrates the resistance to transport of contaminants to the cells. Similarly, it includes a resistance to external mass transfer and the resistance to diffusion across the cell membrane. The third bracket demonstrates the intrinsic resistance of cells to biochemical reaction.

The challenge in any bioremediation process is to reduce and ultimately to eliminate the overall resistance to mass transfer by reducing the resistance in each stage. The focus of this work will be on reducing the internal resistance to mass transfer inside the soil aggregates.

2.3 Transport of Contaminants in Porous Structure of Soil

The fundamental transport equation most commonly used in transport of contaminants in porous media is the convection/dispersion equation, which may include source and sink terms to account for chemical reactions, adsorption/desorption and bioremediation. The one dimensional form of such an equation can be written as follows (Bird *et al.*, 1960; Geankoplis, 1993):

$$\frac{\partial C}{\partial t} = D_{eff} \nabla^2 C - v \nabla C + R_r \quad (2.12)$$

D_{eff} = effective diffusivity
 v = velocity
 R_r = rate of reaction

2.3.1 Diffusion Controlled Mass Transfer

In bioremediation processes the convection transport through soil aggregates ($d < 1000 \mu\text{m}$) is negligible and we can assume that diffusion is the only transport mechanism within the soil aggregates. Further, we assume that the contaminants can be utilized only at the outer surface of the aggregates and in the aqueous phase. With these assumptions equation (2.12) reduces to:

$$\frac{\partial C}{\partial t} = D_{eff} \nabla^2 C \quad (2.13)$$

2.3.2 Bulk Diffusivity

Bulk diffusivity and Knudsen diffusivity are the two mechanisms involved in diffusion in porous structures. Bulk diffusion applies in the conditions where the mean free path of the diffusive molecule is much smaller than the pore diameter. The molecular size of contaminants in the soil is in the range of nanometers, while the minimum accessible pore size for diffusion of NAPL is 0.05 μm (Hoque et al., 1983). For diffusion of dense materials such as liquids in large pores, bulk diffusion is a valid assumption (Satterfield, 1991). The effective diffusivity is defined by the following equation (Satterfield, 1991, Fogler, 1992):

$$D_{\text{eff}} = \frac{D\varepsilon}{\tau} \quad (2.14)$$

$$\tau = \frac{\sigma}{\bar{\tau}} \quad (2.15)$$

- D = diffusivity of contaminants in the medium (aqueous phase or NAPL)
- ε = porosity of soil
- τ = tortuosity factor
- $\bar{\tau}$ = tortuosity of soil
- σ = constriction factor

Tortuosity is a property of a porous medium, which depends on the pore structure. Tortuosity factor is an adjustable parameter ($\tau > 1.0$) which accounts for the fact that pathways for diffusion in porous media are longer and more tortuous than in aqueous solution. It also allows for the variation in the cross sectional area that is normal to diffusion. Values of 2-7 are suggested for tortuosity factor of different catalysts (Satterfield, 1991). Freeze and Cherry (1979) reported apparent tortuosity

factors of 0.01-0.5 ($D_{\text{eff}} = \tau_{\text{app}} D$, $\tau_{\text{app}} = \varepsilon/\tau$) for a wide range of geological deposits. Values of 0.15-0.2 (Barone et al., 1992), 0.1-0.3 ($\varepsilon=0.13-0.26$) (Overcash et al, 1991) and 0.26-0.38 ($\varepsilon=0.4-0.48$) (Mott et al., 1991) are reported for apparent tortuosity factor of mudstone, a loamy sand and bentonite cutoff barriers. Oscarson and Hume (1994) suggested that a large amount of soil compaction is required to reduce the tortuosity factor in geological deposits, thus we can assume that the tortuosity of a given soil remains constant in the processes such as bioremediation.

2.3.3 Knudsen Diffusivity

Knudsen diffusivity applies when the pores are very small or the density of diffusive molecule is very low (gases). In this situation the mean free path of the molecule is comparable to the pore size and the effect of collision with the pore wall is significant. The molecules hitting the wall are momentarily adsorbed and desorbed in random direction. This phenomenon hinders the diffusivity of the molecule and can lead to very low effective diffusivity. When the Knudsen number N_{Kn} , defined as

$$N_{Kn} = \frac{\lambda}{2r_p} \quad (2.16)$$

is larger than 10 the diffusion is primarily Knudsen. In equation (2.17), r is the average pore diameter and λ is the mean free path for a gas molecule which is defined by the following equation (Geankoplis, 1993):

$$\lambda = \frac{3.2\mu}{p} \sqrt{\frac{RT}{2\pi M}} \quad (2.17)$$

where μ is viscosity, P is pressure, T is temperature and M is molecular weight. Knudsen diffusivity in porous media using the kinetic theory of gases is defined by the following equation (Satterfield, 1991):

$$D_{K,eff} = \frac{D_K \varepsilon}{\tau} = 19400 \frac{\varepsilon^2}{\tau \rho} \sqrt{\frac{T}{M}} \quad (2.18)$$

- $D_{K,eff}$ = effective Knudsen diffusivity
- D_K = Knudsen diffusivity
- s = specific surface area
- ρ = density
- T = temperature
- M = molecular weight of diffusive molecule

As mentioned earlier Knudsen diffusivity applies to diffusion of gases in porous structures and does not apply to diffusion transport in soil bioremediation.

2.3.4 Dependence of Diffusivity on Viscosity of the Solvent

The equations for predicting diffusivities of solute in liquids are semiempirical, since the theory for diffusion in liquids is not well established. Hydrodynamic theory is one approach that gives expressions for diffusion coefficient for spherical molecules in dilute solutions. Stokes-Einstein equation has been developed based on this theory for predicting the diffusivity of large spherical

molecules in a solvent of small molecules. This relation shows that diffusion coefficient is inversely proportional to viscosity (Bird, 1960).

$$D = \frac{kT}{6\pi\mu r} \quad (2.19)$$

where, T is temperature, μ is viscosity, r is the radius of diffusive molecule and k is the Boltzmann constant.

Because of the approximate nature of the foregoing theories, a number of empirical relations have been proposed to predict diffusivity coefficients. The Wilke-Chang correlation has been developed based on Stokes-Einstein equation and can be used for most general purposes where the solute (A) is dilute in the solvent (B) (Geankoplis, 1993).

$$D_{AB} = 1.173 \times 10^{-13} (\varphi M_B)^{\frac{1}{2}} \frac{T}{\mu_B V_A^{0.6}} \quad (2.20)$$

where, M_B is the molecular weight of solvent, μ_B is the viscosity of B, V_A is the solute molar volume at the boiling point and φ is an association parameter of the solvent.

Tyn and Calus have proposed a similar correlation to estimate the diffusion coefficient in the form (Reid et al., 1987):

$$D_{AB} = 8.93 \times 10^{-8} \frac{V_B^{0.267}}{V_A^{0.433}} \frac{T}{\mu_B} \left(\frac{\gamma_B}{\gamma_A} \right)^{0.15} \quad (2.21)$$

Similarly V_A and V_B are the molar volume of solute A and solvent B, T is the temperature, μ_B is the viscosity of the solvent and γ_A and γ_B are the surface tension of the solute and the solvent.

Stokes-Einstein equation along with Wilke-Chang and Tyn-Calus Equations all predict that diffusivity is inversely correlated to viscosity. Some researchers have proposed that the relation ($D \propto \mu^{-1}$) may not hold for diffusion of solutes in viscous solvents. Davies found that diffusion coefficient of CO₂ in various solvents ranging in viscosity 1-27 cP is in the form of $D \propto \mu^{-0.45}$. Hiss and Cussler (1973) studying diffusion of naphthalene through hydrocarbon oils, ranging in viscosity between 0.5 – 5000 cP, suggested that diffusion coefficient is related to $\mu^{-0.69}$. These studies show that over a wide solvent viscosity range simple empirical correlations such as Wilke-Chang, Tyn-Calus and even Stokes-Einstein may not give an accurate estimate of diffusion coefficient and that diffusion coefficient is proportional to $\mu^{-0.45}$ to μ^{-1} .

2.4 Partitioning Assumption

In modeling a desorption/bioremediation process, some assumptions are made and justified in order to simplify the equations by ignoring the less important processes. One of these assumptions, which is well documented (Bahr and Rubin, 1987), is the equilibrium partitioning of the contaminants between the immobile phase (NAPL, soil) and mobile phase (water). With this assumption the immobilized solute concentration can be expressed in terms of aqueous phase concentration. Different

models have been developed to describe the functional relationship between the two phases, expressed as equilibrium isotherms.

2.4.1 Nonlinear Equilibrium Partitioning

Many researchers have suggested that nonlinear partitioning is more appropriate to express the relation between mobile phase and immobile phase. The two most commonly used nonlinear isotherms are Freundlich isotherm and Langmuir isotherm. The Freundlich isotherm is expressed as:

$$q_e = K_f C_e^{\frac{1}{n}} \quad (2.22)$$

- q_e = immobile phase concentration at equilibrium
- C_e = aqueous phase concentration at equilibrium
- K_f = Freundlich capacity coefficient
- $1/n$ = Freundlich exponent, $n > 1$

Another commonly applied isotherm is the Langmuir isotherm. In the Langmuir isotherm, the concentration in immobile phase asymptotically approaches a maximum limit. The isotherm has a basis in theory for monolayer gas adsorption, but when applied to soil water system, it should be considered empirical. At low concentrations, this isotherm simulates linear partitioning which tends to higher non-linearity at high concentrations. The Langmuir isotherm can be expressed as:

$$q_e = \frac{QbC_e}{1+bC_e} \quad (2.23)$$

- Q = maximum uptake in the first layer
- b = Langmuir intensity coefficient (related to enthalpy of adsorption)

2.4.2 Linear Equilibrium Partitioning

In many cases the equilibrium concentration in the immobile phase is linearly related to aqueous phase concentration. In particular, linear isotherms are applicable for non-polar organic compounds and compounds with low solubility in the aqueous phase (Chiou et al., 1988, 1989; Murphy et al., 1990). The equilibrium relation can be expressed as:

$$q_e = K_p C_e \quad (2.24)$$

K_p = partition coefficient

The partition coefficient can be expressed as partition coefficient based on the carbon content of the soil:

$$K_{oc} = \frac{K_p}{f_{oc/om}} \quad (2.25)$$

$f_{oc/om}$ = Mass fraction of organic carbon in soil organic matter
 K_{oc} = organic carbon partition coefficient

Many investigators have successfully measured the partition coefficient for various compounds and have found a good correlation between partition coefficient and octanol water partition coefficient (K_{ow}). For nonionic organic compounds, which have low solubility in water, the octanol water partition coefficient is related to solubility in water (S_w):

$$\text{Log}(K_{oc}) = A\text{Log}(K_{ow}) + B \quad (2.26)$$

$$\text{Log}(K_{ow}) = -C\text{Log}(S_w) + D \quad (2.27)$$

A, B, C and D are regression coefficients. Variations in the nature of the soil organic matter due to the age, source, and developing conditions, have a strong effect on the partition coefficient. Rutherford et al. (1992) and Xing et al. (1994) have proposed that the polarity of soil organic matter is inversely proportional to the partition coefficient for non-polar compounds.

2.5 Slurry Phase Reactors

In an attempt to overcome the external mass transfer limitations and to improve the mixing conditions in bioremediation, slurry phase bioreactors have been developed and their performance has been investigated (Muller, 1991; Gray et al. 1994; Banerjee et al., 1995). This method has been effectively used for a variety of wastes such as herbicides, pentachlorophenol and wood preserving wastes (Ross, 1991) and PAHs (Liu et al, 1994). The rate of degradation of contaminants in slurry phase reactors is reported to be 10 times faster than other bioremediation methods (Ross, 1991).

2.5.1 Solid Liquid Mass Transfer from a Single Spherical particle

Ranz and Marshal (1952) studied mass transfer coefficient for flow past a single sphere. They suggested that in the conditions where the particles are sheared by the fluid motion, the following equation could be used to predict the mass transfer coefficient (Ranz and Marshal, 1952; Fogler, 1992):

$$Sh = 2 + 0.6Re^{\frac{1}{2}} Sc^{\frac{1}{3}} \quad (2.28)$$

The dimensionless numbers (Sherwood number, Sh , Reynolds number, Re and Schmidt number, Sc) are defined as:

$$Sh = \frac{k_s D_p}{D} \quad (2.29)$$

$$Re = \frac{D_p v_t \rho}{\mu} \quad (2.30)$$

$$Sc = \frac{\mu}{\rho D} \quad (2.31)$$

- k_s = the mass transfer coefficient,
- D_p = the particle diameter,
- D = diffusion coefficient,
- v = the relative velocity of the sphere,
- μ = viscosity of the fluid
- ρ = density of the fluid.

In the conditions where there is no shear between the particles and the fluid, equation (2.29) reduces to $Sh = 2$.

Garner et al. (1958) suggested similar equations for different ranges of Reynolds number.

$$Sh = 2 + 0.95 Re^{0.5} Sc^{\frac{1}{3}} \quad 2 < Re < 2000 \quad (2.32)$$

$$Sh = 0.347 Re^{0.62} Sc^{\frac{1}{3}} \quad 2000 < Re < 17000 \quad (2.33)$$

2.5.2 Mass Transfer to Suspensions of Small Particles

Many investigators have studied the mass transfer from suspended particles in agitated solutions. The general conclusion is that increased agitation above that

necessary to freely suspend the small particles has very little effect on mass transfer coefficient to the particle (Blakebrough, 1967; Calderbank et al, 1991). They have suggested that the small particles in the range of a few μm , which is the size of many microorganisms and some catalyst particles, are smaller than turbulent eddies which are in the range of 100 μm . Hence increased agitation will have very little effect on the mass transfer coefficient. They have proposed the following equation for the particles smaller than 600 μm :

$$Sh = 2 + 0.31Sc^{\frac{1}{3}} \left(\frac{D_p^3 \rho_c \Delta \rho g}{\mu_c^2} \right)^{\frac{1}{3}} \quad (2.34)$$

where, D_p is the diameter of the particle, ρ_c is the density of the liquid, μ_c is the viscosity of fluid and $\Delta \rho = \rho_p - \rho_c$, ρ_p is the density of the particle. A similar correlation has been developed for particles in different size ranges.

2.5.3 Rotating Drum Bioreactors

Rotating drums are widely used for processing of granular materials such as drying, mixing, incineration, humidification and heating. Rotary drums have been used in large scale for hot water extraction of bitumen from Athabasca tar sands (Carrigy, 1963). The rotating drums can be used in batch and continuous operation and are designed with or without lifters. In slurry phase reactors, the lifters provide a good mixing condition and a good contact between solid and liquid by showering the slurry into the main volume of the slurry. This method of mixing consumes less energy compared to mixing with impellers in baffled tanks. A literature review of

rotating drums indicates that drum rotational speed, slurry holdup and liquid solid ratio are important parameters affecting the solid liquid mass transfer. Extensive studies have been done on mixing patterns in rotating drums. In drums with lifters, the lifts carry the solid to the top and shower it to the main stream of the slurry. Sherritt et al. (1996) observed three levels of loading in the lifters which depended on the angle of rotation at which the lifter began to discharge the solids. The lifters may be underloaded, overloaded with no buried lifters or overloaded with at least one buried lifter. Extensive studies have been done on the mixing conditions in drums without lifters (Oyama, 1980; Henein et al., 1983; Woodle and Munro, 1993). They observed different patterns of bed motion such as slipping, slumping, rolling, cascading and centrifuging. The centrifuging pattern happens when the drum rotational speed is above the critical rotational speed, defined as (Henein et al., 1983b):

$$N_c = \frac{30}{\pi} \sqrt{\frac{2g}{D_d}} \quad (2.35)$$

where, D_d is drum diameter.

Studies have been conducted to correlate the mass transfer coefficient in the rotating drum to the physical parameters such as rotational speed, slurry holdup and mass fraction of the solids. Different definitions of Froude number (Fr) were developed by different researchers. Miwa et al (1991) suggested that the mass transfer coefficient was linearly related to Froude number up to the point where the

rotational speed reached the critical value. They defined Froude number by the following equation where D_d is drum diameter and N is rotational speed.

$$Fr = \frac{N^2 D_d}{g} \quad (2.36)$$

This definition, however, does not include the liquid holdup in the drum. A more detailed definition was derived by Gray et al (1993) to include the drum rotational speed and liquid holdup.

$$Fr = \frac{V_w}{\sqrt{gh_s}} \quad (2.37)$$

where V_w is the velocity of the drum wall and h_s is the height of slurry in the drum. Further Masliyah et al. (1992) included another term ($S = \rho_p / \rho_c$) to account for the difference between the density of particles (ρ_p) and the density of the fluid (ρ_c).

$$Fr = \frac{V_w}{\sqrt{gD_d(S-1)}} \quad (2.38)$$

Parsons (1995) studied the mass transfer coefficient of β -naphthol in a sand water slurry. He observed an 8 fold increase in mass transfer coefficient by increasing the drum rotational speed from 0.33 rpm to 15 rpm. He also reported a 2.5 fold increase in mass transfer coefficient by increasing the liquid holdup from 8.7% to 17%. The increase in mass transfer coefficient was not significant when the solids volume fraction was increased up to 62%.

2.6 Microorganisms

2.6.1 Growth of Microorganisms on Hydrocarbons

In a typical batch process, the complete cycle of a bacterial growth consists of four distinct phases. 1) Initial lag phase with no increase in cell population. This is the period that cells try to adapt to new environment. 2) Exponential growth phase during which the cell population increases exponentially and the substrate depletes very fast. In this period the growth is restricted by either substrate deficiency or accumulation of toxic byproducts. 3) The stationary phase with maximum cell population. In this period the growth and death rate of the cells are balanced. 4) Death phase with exponential decrease in the cell population. The exponential growth phase can be expressed as:

$$\frac{dX}{dt} = \mu_g X \quad (2.39)$$

X = the cell concentration
 t = time
 μ_g = specific growth rate

Monod (1942) proposed a functional relationship between the specific growth rate and substrate concentration(s) of the form:

$$\mu = \frac{\mu_{\max} S}{K_s + S} \quad (2.40)$$

where μ_{\max} is the maximum growth rate achieved when $S \gg K_s$, and K_s is the concentration of substrate when the specific growth rate is half the maximum value. Some researchers have observed linear growth when different hydrocarbons were

used as substrate. Growth of *Pseudomonas sp.* and a mixed culture on naphthalene, phenanthrene and anthracene (Volkering et al., 1992), growth of *Pseudomonas* isolates on pyrene (Thibault et al., 1996) and the growth of *Mycobacterium sp.* on anthracene (Chen, 1999) are examples of this observation. This phenomenon has been attributed to the very low solubility of the substrate and the fact that the growth rate is limited by the dissolution rate of hydrocarbons.

2.6.2 Mechanism of PAH Transformation and Degradation by Microorganisms

The solubility of PAHs in water is very low, so they must be solubilized by addition of molecular oxygen. Oxygenation is accomplished by two classes of enzymes, monooxygenases and dioxygenases. These enzymes are present in several aerobic species and some possess a broad substrate specificity, which allows them to catalyze reactions with many compounds. The dioxygenases are produced exclusively by bacteria. The reaction proceeds by incorporation of two oxygen atoms in the end ring of PAHs to form *cis*-dihydrodiol (Gibson et al., 1975). The *cis* isomer is then transformed to dihydroxylated intermediate. The ring fission of aromatic compounds can occur via *ortho* fission or *meta* fission. The *ortho* fission cleaves the carbon-carbon bond between the hydroxyl groups of the catechol intermediate while the *meta* fission cleaves the bond beside the hydroxyl group (Cerniglia, 1984). After the fission of the first ring in the compound, pyruvate and CO₂ are released and the cycle repeats itself for another ring to form catechol, pyruvate and CO₂. Figure 2.3 represents a schematic pathway for degradation of anthracene.

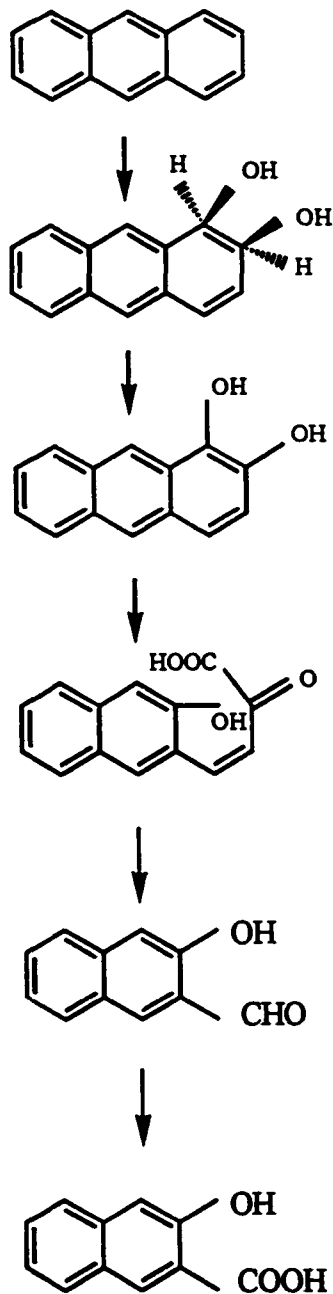


Figure 2.3. Schematic diagram of a typical PAH degradation pathway (Cerniglia and Heitkamp, 1989)

2.6.3 Cometabolism and Substrate Inhibition

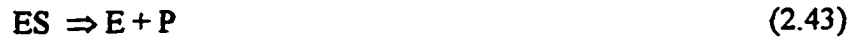
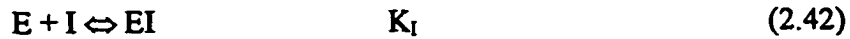
Most enzymes are highly specific in the reactions they catalyze and in the substrate they accept. However the monooxygenase and dioxygenase enzyme systems, present in many bacteria, possess a broad substrate specificity which allows them to catalyze reactions with compounds other than their growth substrate. Atlas and Bartha (1993) defined cometabolism as a process, which occurs when an organism growing on a particular substrate metabolizes a second substrate it is unable to utilize as sole nutrient or energy source. The metabolite can then serve as a possible carbon source for another organism present in mixed culture. Bioremediation with mixed cultures takes advantage of the capability of such enzyme systems to degrade recalcitrant pollutants.

Many microorganisms can degrade the lower molecular weight PAH (2 & 3 rings) and use them as the sole carbon source (Cerniglia et al., 1989; Southerland et al., 1995). A few bacteria have been recently isolated that can degrade four ring compounds such as fluoranthene, pyrene and chrysene (Mueller et al., 1990; Dean-Ross and Cerniglia, 1996). Until recently, no pure culture had been found to degrade five or more rings and use them as the only energy source, instead, degradation of these compounds by pure cultures usually is observed after growth on another PAH substrate. The advantage in soil bioremediation is the multisubstrate environment and the presence of mixed cultures. Cometabolic transformation in a multi-substrate environment happens when a microorganism produces specific enzymes to metabolize certain compound. If the enzyme has a broad substrate specificity it can

oxidize cosubstrates as well. However, the second enzyme involved in metabolism of the substrate may be more specific and not capable of further metabolizing the cometabolite. In a pure culture, this will be the end of the transformation of the cometabolite, however, in a mixed culture the cometabolites can be used as substrates by other species of microorganisms. Complex molecules can be degraded in a mixed culture as the result of cometabolism. Microorganisms can use the compounds with similar structures (analogues) as sole carbon source and cometabolized substrate (Keck et al., 1989). In the degradation of analogue PAHs, the competition for the same initial enzyme in the pathway (oxygenase) can result in competitive inhibition of the substrate. This phenomenon leads to fast degradation of specific compounds and hinders the degradation of other analogues (Stringfellow et al., 1995). The decrease in the reaction rate will depend on the relative affinity of the substrates for the enzyme. In addition to competitive inhibition, unproductive binding of non-growth substrate can cause non-competitive inhibition of growth substrate oxidation (Dixon and Webb, 1979).

Modeling of competitive inhibition in cometabolism can be accomplished using the Michaelis-Menten approach for enzyme kinetics. The binding of growth substrate and non-growth substrates to the initial enzyme in a competitive inhibition model follows the following steps:





E = enzyme

S = substrate

I = inhibitor

P = product

K_S and K_I are dissociation constants. In this model the inhibitor binds with the enzyme, thus, all the enzyme is not available for catalyzing substrate conversion. The reaction rate for such conditions is as follows:

$$R_r = \frac{ke_0s}{s + K_s(1 + i/K_i)} \quad (1.44)$$

R_r = reaction rate
 e_0 = total enzyme concentration
 s = substrate concentration
 i = inhibitor concentration
 K_s & K_i = dissociation rate constants

Competitive inhibition is only one of many different phenomena that can happen in a multi-substrate environment. Some researchers have observed different behaviors such as catabolic repression (diauxie) in multi-substrate environments. This phenomenon has been observed in multi-sugar substrates (Kompala et al., 1984) and can happen when each substrate needs a different enzyme to initiate the metabolic reactions. Thus the microorganisms initially grow on one substrate and

after the substrate is depleted they move on to a different substrate, showing a lag phase to produce the required enzymes.

2.7 Literature cited

Atlas, R.M.; Bartha, R., "*Microbial Ecology: Fundamental and applications*" 3rd. Ed. The Benjamin/Cummings Publishing Company, Rewood City, CA. 1993.

Bahr, J.M.; Rubin, J., "Direct comparison of kinetic and local equilibrium formulation for solute transport affected by surface reactions" *Water Resour. Res.* 1987, 23(3), 438-452.

Bailey, J.E.; Ollis, D.F., "*Biochemical Engineering Fundamentals*" McGraw-Hill, U.S.A., 1986.

Ball, W.P.; Roberts, P.V., "Long term sorption of halogenated organic chemicals by aquifer material. 1. Equilibrium." *Environ. Sci. Technol.* 1991, 25, 1223-1236.

Banerjee, D.K.; Fedorak, P.M.; Hashimoto, A.; Masliyah, J.H.; Pickard, M.A.; Gray, M.R., "Monitoring the biological treatment of anthracene contaminated soil in a rotating drum bioreactor." *Appl. Microbiol. Biotechnol.* 1995, 43, 521-528.

Barone, F.S.; Rowe, R.K.; Quigley, R.M., "Estimation of chloride diffusion coefficient and tortuosity factor for mudstone" *J. Geotech. Eng.* 1992, 118, 1031-1046.

Bird, R.B.; Stewart, W.E.; Lightfoot, E.N., "*Transport Phenomena*" John Wiley & Sons, Inc., New York. 1960.

Bosma, T.N.P.; Middeldorp, P.J.M.; Zehnder, A.J.B., "Mass transfer limitation of biotransformation: quantifying bioavailability." *Environ. Sci. Technol.* 1997, 31, 248-252.

Carrigy, M.A.; The K.A. Clark Volume, A collection of papers in Athabasca oil sands presented to K.A. Clark on the 75th anniversary of his birthday, *Research Council of Alberta, Edmonton, AB*, 1963.

Cerniglia, C.E.; Heitkamp, M.A., "Microbial degradation of polycyclic aromatic hydrocarbons in the aquatic environment" in *Metabolism of Polycyclic Aromatic Hydrocarbons in the Aquatic Environment*. Ed. U.Varasani. CRC Press, Inc., Boca Raton, FL. 1989, 41-68.

Cerniglia, C.E., "Biodegradation of polycyclic aromatic hydrocarbons" *Adv. Appl. Microbiol.* 1992, 30, 371-377.

Chen, P., "*Effects of surfactants on microbial growth on anthracene*" M.Sc. thesis, *University of Alberta*. 1999.

Chiou, C.T., "Theoretical considerations of the partition uptake of nonionic organic compounds by soil organic matter" *Reactions and movement of organic chemicals in soils*. B.L. Sawney and K. Brown eds. *SSSA Special Publication*. Number 22. 1989.

Chiou, C.T.; Kile, D.E.; Malcolm, R.L., "Sorption of vapors of some organic liquids in soil humic acid and its relation to partitioning of organic compounds in soil organic matter." *Environ. Sci. Technol.* 1988, 22, 298-303.

Cohen, R.M.; Mercer, J.W., "*DNAPL Site evaluation*" CRC Press, Inc., Boca Raton, Florida. 1993.

Dibble, J.T.; Bartha, R., "Effects of environmental parameters on the biodegradation of oil sludge." *Appl. Environ. Microbiol.* 1979, 37(4), 729-739.

Dixon, M.; Webb, E.C., "*Enzymes*" Academic Press, New York. 1979.

Efroyson, R.A.; Alexander, M., "Role of partitioning in biodegradation of phenanthrene dissolved in non-aqueous phase liquids" *Environ. Sci. Technol.* 1994, 28, 1172-1179.

Feenstra, S.; Cherry, J.A., "Subsurface contamination by dense non-aqueous phase liquid (DNAPL) chemicals." *International Groundwater Symposium, International Symposium of Hydrogeologist*, Halifax, Nova Scotia, May 1-4. 1988.

Fogler, H.S., "*Elements of chemical reaction engineering*" Prentice Hall Englewood, New Jersey. 1992.

Freeze, R.A.; Cherry, J.A., "*Groundwater*" Prentice Hall Inc., Englewood Cliffs, N.J. 1979.

Geankoplis, C.J., "*Transport Process and Unit Operations*" Prentice Hall Englewood, New Jersey. 1993.

Gibson, D.T.; Mahadevan, V.; Jerina, D.M.; Yagi, H.; Yeh, H.J.C., "Oxidation of carcinogens benzo(a)pyrene and benzo(a)anthracene to dihydrodiols by a bacterium" *Science*. 1975, 189, 295-297.

Gray, M.R.; Banerjee, D.K.; Fedorak, P.M.; Hashimoto, A.; Masliyah, J.H.; Pickard, M.A., "Biological remediation of anthracene-contaminated soil in rotating bioreactors." *Appl. Microbiol. Biotechnol.* 1994, 40, 933-940.

Gray, M.R.; Mehta, B.; Masliyah, J.H., "Liquid side mass transfer coefficients for liquids and slurries in rotating drums." *Chem. Eng. Sci.*, 1993, 48(19), 3442-3446.

Harerlein, S.B.; Schwarsenbach, R.P., "Adsorption of substituted nitrobenzenes and nitrophenols to mineral surfaces." *Environ. Sci. Technol.* 1993, 27, 316-326.

Henein, H.; Brimacombe, J.K. and Watkinson, A.P., "Experimental study of transverse bed motion in rotary kilns" *Metallurgical Transactions B*, 1983a, 14B, 191-205.

Henein, H.; Brimacombe, J.K. and Watkinson, A.P., "The modeling of transverse solids motion in rotary kilns" *Metallurgical Transactions B*, 1983b, 14B, 191-205.

Hiss, T.G.; Cussler, E.L., "Diffusion in high viscosity liquids" *AIChE J.* 1973, 19, 698-703.

Hogan, J.A.; Toffoli, G.R.; Miller, F.C.; Hunter, J.V.; Finstein, M.S., "Composting physical model demonstration: Mass balance of hydrocarbons and PCBs." *International Conference on Physiochemical and Biological Detoxification of Hazardous Waste*, Atlanta City, New Jersey, May 3-5. 1988.

Hoque, A.M.; Cabrera, J.G., "Absorption in manufactured soil aggregates" *J. Trans. Eng.* 1983, 109, 6, 800-814.

Karimi, S.; Pickard, M.A.; Gray, M.R., "Reactions of polynuclear aromatic hydrocarbons on Soil." *Environ. Sci. Technol.* 1996, 30, 1145-1151.

Keck, J.; Sims, R.C.; Coover, M.; Park, K.; Symons, B., "Evidence for co-oxidation of PAH in soil" *Water Res.* 1989, 23, 1467-1476.

Kompala, D.S.; Ramkrishna, D.; Tsao, G.T., "Cybernetic modeling of microbial growth on multiple substrates." *Biotech. Bioeng.* 1984, 26, 1272.

Loehr, R.C., "Bioremediation of PAH compounds in contaminated soil", In: *Hydrocarbon Contaminated Soils and Groundwater 2*, E.J. Calabrese and P.T. Kosteki, Eds, Lewis Publishers, Boca Raton, 1992, 213-222.

Luthy, R.G.; Dzombak, D.A.; Peters, C.A.; Roy, S.B.; Ramaswami, A.; Nakles, D.V.; Nott, B.R., *Environ. Sci. Technol.* 1994, 28, 266A-276A.

Mackay, D.; Shia, Y.W.; Ma, K.C., "*Illustrated Handbook of Physical and Environmental Fate for Organic Chemicals*" Lewis Publishers, Chelsea. MI. 1992.

Masliyah, J.H.; Afacan, A.; Wong, A.K.M.; Nasr-El-Din, H.A., "Flow of slightly settling slurries in a horizontal rotary drum" *Can. J. Chem. Eng.*, 1992, 70, 1083-1089.

Miwa, Y.; Matsubara, S.; Takagi, K., "Application of a rotary drum reactor to a diffusion controlled liquid-solid reaction" *Powder Technol.*, 1991, 64, 207-212.

Mueller, J.G.; Lantz, S.E.; Blattmann, B.O.; Chapman, P.J., "Bench-scale evaluation of alternative biological treatment processes for the remediation of pentachlorophenol and creosote-contaminated materials: Slurry-phase bioremediation." *Environ. Sci. Technol.* 1991, 25, 1055-1061.

Murphy, E.M.; Zachara, J.M.; Smith, S.C., "Influence of mineral bound humic substances on the sorption of hydrophobic organic compounds" *Environ. Sci. Technol.* 1990, 24, 1507-1516.

Oscarson, D.W.; Hume, H.B., "Diffusion of ^{14}C in dense saturated bentonite under steady state conditions" *Transport in Porous Media*. 1994, 14, 73-84.

Overcash, M.R.; McPeters, A.L.; Dougherty, E.J.; Carbonell, R.G., "Diffusion of 2,3,7,8-tetrachlorodibenzo-p dioxin in soil containing organic solvents" *Environ. Sci. Technol.* 1991, 25, 1479-1485.

Oyama, Y., "Particle motion in horizontal rotating cylinder" *International Chem. Eng.* 1980, 20 (1), 36-55.

Parson, T.G., "*Solid Liquid Mass Transfer in Rotary Drums*" University of Alberta, M.Sc. Thesis, 1995.

Peramaki, M.P.; Blomker, K.R., "Practical design considerations for composting contaminated soils." *Fourth International In Situ and On-Site Bioremediation Symposium*, New Orleans, April 28 - May 1. 1997.

Pignatello, J.J.; Ferrandino, F.J.; Huang, L.Q., "Elution of aged and freshly added herbicides from a soil." *Environ. Sci. Technol.* 1993, 27, 1563-1571.

Ranz, W.E.; Marshal, W.R., "Evaporation from drops" *Chem. Eng. Sci.*, 1952a, 48(3), 141-146.

Ranz, W.E.; Marshal, W.R., "Evaporation from drops" *Chem. Eng. Sci.*, 1952b, 48(4), 173-179.

Ross, D., "Slurry phase bioremediation: Case studies and cost Comparisons." *Bioremediation* 1, 61-74, 1990-1991.

Rutherford, D.W.; Chiou, C.T.; Kile, D.E., "Influence of soil organic matter composition on the partition of organic compounds." *Environ. Sci. Technol.* 1992, 26, 336-340.

Rutherford, P.M.; Gray, M.R.; Dudas, M.J., "Desorption of ¹⁴C naphthalene from bioremediated and nonbioremediated soils contaminated with creosote compounds" *Environ. Sci. Technol.* 1997, 31, 2515-2519.

Satterfield, C.N., "*Heterogeneous catalysis in industrial practice*" McGraw-Hill, Inc. New York, 1991.

Schwille, F., "*Pollutants in Porous Media; Ecology Studies*" Springer-Verlag, New York, 1991, 47, 27-48.

Schwille, F., "*Dense Chlorinated Solvents in Porous and Fractured Media.*" Lewis Publisher, Chelsea, MI, 1988.

Sherritt, R.G.; Behie, L.A.; Mehrotra, A.K., "The movement of solids in flighted rotating drums, Mixed flow hydrodynamics" *Advances in Engineering Fluid Mechanics Series* Cheremisinoff, N.P., ed., Gulf Publishing Company, Houston. 1996.

Steinberg, S.M.; Pignatello, J.J.; Sawhney, B.L., "Persistence of 1,2-dibromoethane in soils: entrapment in intraparticle micropores." *Environ. Sci. Technol.* 1987, 21, 1201-1208.

Tabak, H.; Fu, C.; Pfanstiel, S.; Gao, C.; Yan, X.; Govind, R., "Studies on contaminants biodegradation in slurry, wafer, and compacted soil tube reactors." *Environ. Sci. Technol.* 1996, 30, 743-750.

Thibault, S.L.; Anderson, M.; Frankerberger, W.T., "Influence of surfactants on pyrene desorption and degradation in soils" *Appl. Environ. Microbiol.*, 1996, 62, 283-287.

Tongpim, S.; Pickard, M.A., "Growth of *Rhodococcus SI* on anthracene" *Can. J. Microbiol.*, 1996, 42, 289-294.

Volkering, F.; Breure, A.M.; Sterkenburg, A.; Van Andel, J.G., "Microbial degradation of polycyclic aromatic hydrocarbons: effect of substrate availability on bacterial growth kinetics" *Appl. microbiol. Biotechnol.* 1992, 36, 548-552.

Weissenfels, W.D.; Klewer, H.J.; Langhoff, J., "Adsorption of polynuclear aromatic hydrocarbons (PAHs) by soil particles: influence on biodegradability and biotoxicity." *Appl. microbiol. Biotechnol.* 1992, 36, 689.

Wilson, J.L.; Conrad, S.H.; Mason, W.R.; Peplinski, W.; Hagen, E., "Laboratory investigation of residual liquid organics, USEPA600/6-90/004, Kerr, R.S.; Environmental Research Laboratory" Ada, Oklahoma. 1990.

Wodzinski, R.S.; Coyle, J.E., "Physical state of phenanthrene for utilization by bacteria" *Appl. Microbial. Biotechnol.* 1974, 27, 1081-1084.

Woodle, G.R.; Munro, J.M., "Particle motion and mixing in rotary kiln" *Powder Technol.*, 1993, 76, 241-245.

Xing, B.; McGill, W.B.; Dudas, M.J., " Cross-correlation of polarity curves to predict partition coefficients of nonionic organic contaminants." *Environ. Sci. Technol.* 1994, 28, 1929-1933.

3. THE EFFECT OF AGGREGATE SIZE ON THE KINETICS OF BIOREMEDIATION

3.1 Introduction

In the past century, wood preserving operations and manufactured gas plants commonly gave severe contamination of soil with creosote and coal tars. Creosote is a complex mixture derived from coal, and contains considerable amounts of polynuclear aromatic hydrocarbons (PAHs) which can cause significant health hazards because of their toxicity and carcinogenicity. Coal tars from manufactured gas plants are also rich in PAHs. Bioremediation has been extensively used to clean up creosote-contaminated sites. This method relies on the ability of microorganisms to utilize the contaminants and convert them to CO₂ and water or to partially oxidized metabolites. Degradation requires the availability of contaminants to microorganisms by dissolution and diffusion through the soil particles. Many microorganisms are known to have enzymatic capacity to degrade PAHs that range in size from naphthalene to benzopyrene (Foght and Westlake, 1988; Cerniglia, 1992).

Bioremediation of creosote-contaminated soils effectively decreases the concentration of contaminants, but even in the presence of active culture it often fails to achieve the target concentrations set by environmental regulations. Many investigators have reported partial degradation of contaminants (Weissenfels et al., 1992; Gray et al., 1994). Bioremediation of soils and sediments often displays biphasic behavior. An initial fast decline in the concentration is followed by

degradation at a much slower rate, which eventually levels off at a constant residual concentration. Unfortunately, the residual concentration is often above the regulatory targets. The biological activity is believed to control the first phase of degradation in many studies. The rate of metabolism of the target substrates can be a limiting factor during the rapid phase of degradation. The slow degradation phase is commonly attributed to the persistence of the residual contaminants in soils and sediments due to aging (Karickhoff and Morris, 1985; Hatzinger and Alexander, 1995).

The kinetics of biological removal of contaminants from porous soil aggregates involves several sequential and parallel transport and reaction phenomena (Tabak et al., 1996; Ahn et al., 1996; Bosma et al., 1997). Part of the transport process is abiotic, including internal diffusion of contaminants through soil aggregates, partitioning to the aqueous phase and external diffusion from the surface to the bulk liquid. Biological transport phenomena include the diffusion transport through cell membranes and biochemical reactions inside the cell.

In an attempt to overcome the mass transfer limitations and to improve the operating conditions in bioreactors, mixed-slurry-phase reactors have been developed. Mixing provides a uniform distribution of nutrients, oxygen and contaminants, as well as increasing the contact between microorganisms and contaminants. Slurry-phase bioreactors eliminate the external resistance to mass transfer. Bioremediation studies employing such reactors have shown a higher rate of degradation relative to static systems (Gray et al., 1994; Mueller et al., 1991; Banerjee et al., 1995).

The unresolved problem, even with slurry-phase reactors, is the persistence of

the residual contaminants in soil, although at relatively low concentrations. What has been overlooked is the role of diffusion within soil aggregates of diameter 40 – 1000 μm and their stability when shear force is applied. Some researchers have addressed the effect of aggregate size on adsorption/desorption of organic compounds by soils and sediments. Ball and Roberts (1991) observed an increase in uptake of halogenated organic compounds in pulverized sediments. Steinberg et al. (1987) have reported that desorption of ethylene dibromide (EDB) from two different soils was increased by pulverization. A few studies have addressed the effect of aggregate size in bioremediation. Some researchers have observed a lower rate of degradation in the presence of aggregates (Scow and Alexander, 1992; Geerdink et al., 1996), however this idea is not supported by Mihelcic and Luthy (1991). These contradictory results are partly related to the difficulty in discriminating between the rate of desorption and the rate of biodegradation.

The objectives of this study were to determine the effect of aggregate size on the rate of bioremediation and to evaluate how the extent of bioremediation is affected by aggregate size in the range 40 – 1000 μm .

Experiments were carried out in slurry-phase reactors using a creosote-contaminated soil and a pristine soil that was spiked with anthracene. The aggregate sizes were reduced by sonication. Bioremediation was then carried out on batches of sonicated and non-sonicated soils. Six PAHs were selected as target compounds and the concentrations of these compounds were determined in samples taken during three weeks of bioremediation in slurry-phase reactors.

3.2 Materials and Methods

3.2.1 Soil Characteristics

C-horizon soil was obtained from a site south of Edmonton, Canada, sampled at a depth of 75+ cm. It had a dark grayish brown color with a sandy clay loam texture and was moderately calcareous with a low content of organic matter (0.62%). The surface area was 348 m²/g by ethylene glycol adsorption.

Creosote-contaminated soil was collected from a wood preserving site in Edmonton, Canada, which was in operation from 1924 – 1988. This site was contaminated with creosote components. The soil was classified as silty clay. Properties of the two soils are listed in Table 3.1.

Table 3.1. Physical Characteristics of the Soils

Type	C-horizon	Creosote-contaminated
Sand, %wt	51	16
Silt, %wt	25	43
Clay, %wt	24	41
pH	7.8	7.5
Organic matter %wt	0.62	3.29
Surface area, m ² /g	348	ND
CEC. mequiv/100 g	12.1	0.40

The pH for C-horizon soil was measured in distilled water, while for creosote-contaminated soil was determined in 0.01 M CaCl₂.

3.2.2 Chemicals

The anthracene used in this experiment was purchased from Sigma Chemical Co. (St. Louis, MO) with 98% purity. Methylene chloride was purchased from Fisher Scientific (New Jersey) in HPLC grade.

The mineral salts medium used for the biodegradation experiment with C-horizon soil consisted of 1.33 g/L KH_2PO_4 , 2.67 g/L K_2HPO_4 , 1 g/L NH_4Cl , 2 g/L Na_2SO_4 , 2 g/L KNO_3 , 0.05 g/L $\text{FeSO}_4 \cdot 7\text{H}_2\text{O}$, and 1 ml of trace metal solution. After autoclaving the mineral salts medium at 120 °C for 20 minutes $\text{MgSO}_4 \cdot 7\text{H}_2\text{O}$ was added to a concentration of 0.2 g/L (Fedorak et al., 1991). The mineral salts medium used for creosote-contaminated soil consisted of 28.6 g/L NH_4NO_3 , 1.46 g/L KH_2PO_4 , 1.87 g/L K_2HPO_4 , 0.54 g/L K_2SO_4 and the pH was adjusted to 7.2 with 1 N KOH.

3.2.3 Active Culture

The anthracene degrading culture was a mixed culture enriched from a creosote-contaminated soil. This culture was grown on anthracene as the sole carbon source. Initially 7 g of soil and 0.1 g of anthracene were added to 200 ml buffer solution and was shaken at 27 °C. The culture was maintained by monthly transfers of 10% by volume and growth was monitored by plating on agar plates. After the culture was stabilized, the cells were harvested and suspended in 20% glycerol to a concentration of 10^8 CFU/ml and stored at -80 °C in 1 ml vials.

The inoculum used for Creosote-contaminated soil was the transfer of slurry

from previous batch experiments with the same soil. Addition of 10% slurry at the beginning of each batch experiment provided a sufficient amount of active culture to initiate degradation of PAHs.

3.2.4 Soil Preparation

The soils were air dried, ground and sieved with a 1.7 mm sieve. To prepare the C-horizon soil containing 400 mg anthracene per kg of soil and to provide uniform distribution of anthracene in soil, a solution of 4 g/L anthracene in methylene chloride was prepared and mixed with the soil at a ratio of 200 ml solution per kg of soil. The flasks containing loaded soil were sealed and covered with aluminum foil to prevent photooxidation of anthracene. These flasks were kept at room temperature (23°C) for a period of 17 days and then methylene chloride was evaporated using a rotary evaporator with a water bath at 60°C. The soil was then used for the bioremediation experiment.

Two different sonifiers with different operating conditions were used in this experiment thus, the effectiveness of sonication was determined by measuring the aggregate size distribution. The C-horizon soil and the mildly sonicated creosote-contaminated soil were prepared using a sonifier operating at 400 W (2.5 cm probe, Braun). For vigorous sonication of creosote-contaminated soil a high intensity ultrasonic processor (600 watt model, 13 mm probe, Cole-Parmer, Vernon Hills, U.S.A.) was used. No treatment was applied before sonication. This method permitted separation of soil particles without the use of oxidants, acids or dispersing

agents. The sonicated C-horizon soil samples were prepared by adding 100 ml water to 200 g soil and sonicating for 21 minutes. To sonicate creosote-contaminated soil, 200 g soil was divided into four portions of 50 g. Each portion was sonicated in 200 ml water for periods of 21 and 30 minutes (mild and vigorous sonication). The probe was inserted about 3 cm below the surface of the soil suspension and the suspension was stirred periodically to insure uniform and effective distribution of energy. An ice bath was used to remove the heat generated during the process to maintain temperature below 30°C and prevent temperature rise. After the sonication was complete the slurry was centrifuged to remove the excess water.

3.2.5 GC Analysis

PAHs were recovered from the soil by Soxhlet extraction for 4.5 h, using methylene chloride as the solvent (EPA Method 3540). The solvent was evaporated using a rotary evaporator and the residue was dissolved in a known volume of methylene chloride. The extracts were analyzed by gas chromatography (EPA Method 8000) for six PAH components: acenaphthene, phenanthrene, anthracene, fluoranthene, pyrene and chrysene. For GC analysis of anthracene in the C-horizon soil, phenanthrene was used as the internal standard. In the case of Creosote-contaminated soil, 1-methylnaphthalene served as the internal standard. The gas chromatograph was a Hewlett Packard 5890, equipped with a DB-1 capillary column 30 m long, 0.25 mm diameter with a 0.025 mm film thickness, flame ionization detector, an HP 6890 autosampler, and HP Chemstation. The operating conditions

were: initial oven temperature 40 °C, held for 1 minute, detector 310 °C, injector 300 °C. The oven was programmed to increase the temperature with three different ramps over a period of 46 minutes to a final temperature of 300 °C. The temperature was increased from 40 °C to 180 °C with the rate of 20 °C/min and kept at 180 °C for 10 minutes. In the second stage the temperature was increased from 180 °C to 250 °C with the rate of 15 °C /min and kept at 250 °C for 5 minutes. Finally the temperature was increased from 250 °C to 300 °C with the rate of 15 °C /min and kept at 300 °C for 15 minutes. This programming provided a good separation of the peaks. The identity of the peaks of the six PAHs was verified by retention time of pure standards and by mass spectrometry.

3.2.6 Bioreactor Operation

The bioreactor was a glass bottle of 2 L volume, 11.5 cm in diameter and 21 cm long sealed with a steel screw top. The holes of the lid were covered with filter paper to provide good circulation of air. The slurry consisted of 200 g air-dried soil, a desired amount of medium to ensure a sufficient amount of N and P, and enough water to keep the ratio of liquid to slurry at about 41- 45 weight%. The bottles were inoculated either by 1 ml of cells with concentration of 10^8 CFU/ml which had been stored in glycerol at -80 °C (C-horizon), or by 10% slurry of the previous run (creosote-contaminated soil). The bottles were rotated at 3 rpm at a room temperature of about 23°C.

Daily samples of about 4 g were removed from the bottles for a period of two to three weeks. The samples were air-dried, Soxhlet extracted and analyzed by GC.

3.2.7 Aggregate Size Analysis

Size analysis of the distribution of aggregates in different size fractions was determined by sedimentation and by sieve analysis.

3.2.7.1 Hydrometer Method

This method is a sedimentation technique based on Stokes' Law, which is extensively used in particle size distribution analysis in soil classification (Sheldrick, and Wang, 1993). Based on Stokes' Law, larger particles settle faster, leaving behind the smaller particles in suspension. As the particles settle, the density of the suspension decreases. A standard hydrometer (ASTM No. 1. 152 H with Bouyoucos scale in g/L) was used to measure the difference between the density of soil suspension and water at different settling times. Initially 40 g of soil was suspended in distilled water in a 1 L cylinder and completely mixed by moving a plunger up and down. After mixing, the suspension was allowed to settle. At each time interval the hydrometer was submerged in the suspension and the reading was recorded. Samples were taken directly from the bioreactor and no treatment was done before the sedimentation experiment.

3.2.7.2 Wet Sieving Method

This method is used to determine the aggregate size distribution in wet samples. The slurry or wet soil is exposed to disruptive forces by wet sieving, and the proportion of aggregates remaining on each sieve represents the mass of stable aggregates in each size fraction. 40 g of soil, or a proportional amount of slurry, was spread on top of the nest of sieves with openings ranging from 991 to 38 μm . The sieves were immersed in water and were stroked up and down for 20 minutes. The sieves were then removed and the aggregates accumulated on each sieve were washed with water, air dried and weighed.

3.3 Results

3.3.1 Degradation of Target PAHs in C-horizon and Creosote-contaminated Soils

3.3.1.1 Anthracene in C-horizon Soil

Degradation of anthracene in C-horizon soil was measured for sonicated and non-sonicated samples. The experiment was carried out in duplicate for sonicated and non-sonicated soils and the results were averaged. The data of Fig 3.1 illustrate the results of this experiment. Although the soils were initially loaded with 400 ppm of anthracene, the measured initial concentration was 300 ppm. The 100 ppm loss was attributed to polymerization (Karimi et al., 1996). The concentration of anthracene in the sonicated sample dropped from the initial concentration of 300 ppm down to 10 ppm in 5 days, while the parallel runs for non-sonicated samples gave a concentration of 40 ppm after 9 days, however, the concentration of anthracene continued to

decrease with time. In the absence of the inoculum, the concentration remained constant at the initial level for at least 5 days, consequently the removal of anthracene was due to biological activity. This experiment was repeated with different batches of C-horizon soil in duplicate for each of the sonicated and non-sonicated soils. The results of the second series of experiments (data not shown) confirmed the results obtained from the first series of experiments.

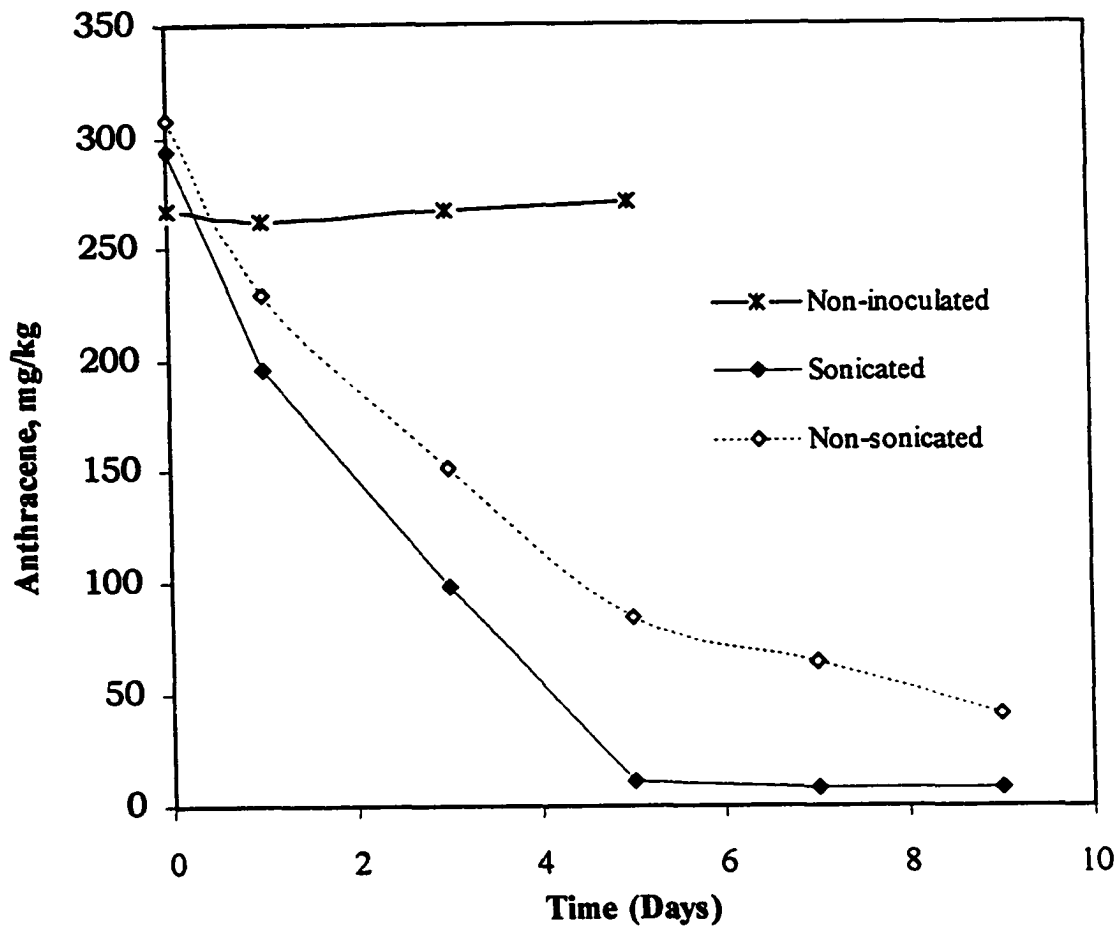


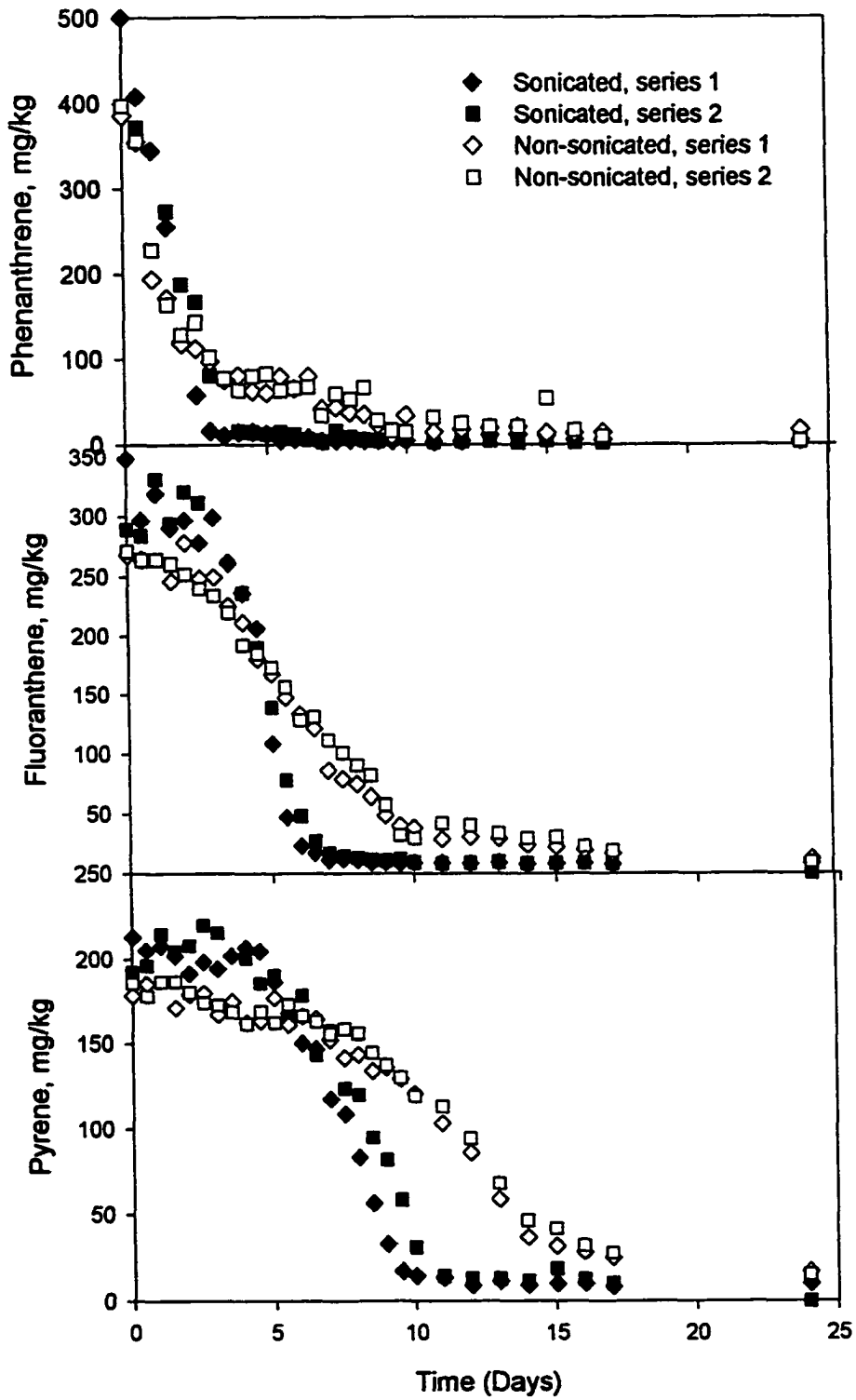
Figure 3.1. Biodegradation of anthracene in the inoculated C-horizon soil after 9 days of incubation

3.3.1.2 Degradation of Six Target PAHs in Creosote Contaminated Soil

A similar experiment was carried out on the creosote-contaminated soil. The inoculum for this experiment was 10% slurry from a stock culture. Daily samples were taken from the bioreactor. The samples were air dried, extracted and analyzed by GC. The concentration of six target compounds: acenaphthene, phenanthrene, anthracene, fluoranthene, pyrene and chrysene were monitored as a measure of biodegradation. As in the previous experiment, the results of sonicated and non-sonicated runs were compared. The data of Figure 3.2 present the results of four parallel experiments: two sonicated and two non-sonicated. The data illustrate the time course concentration of phenanthrene, fluoranthene and pyrene during bioremediation (the data for acenaphthene, anthracene and chrysene are not shown). The concentration of phenanthrene, as the most degradable carbon source, dropped rapidly from 400 ppm to 15 ppm in 4 days, and then it gradually decreased to 5 ppm in a week for sonicated samples. There was no significant change in the concentration of phenanthrene after the first week. The concentration of phenanthrene in the non-sonicated slurry exhibited a rapid drop to about 90 ppm in the first 3 days, then slowly dropped to 40 ppm in a week, and 15 ppm in 16 days.

The concentration of fluoranthene remained almost constant for about 3 days. In sonicated samples the concentration dropped to 10 ppm by day 7, while the non-sonicated runs required 9 days to drop to 50 ppm. Slow degradation for fluoranthene continued down to a level of 8 ppm after 24 days of treatment. Similar results were obtained for pyrene, except that the time lag before degradation began was

approximately 5 days. Pyrene showed an initial rapid drop in concentration to 15 ppm in sonicated runs, with subsequent slow degradation, which decreased the concentration of pyrene to 9 ppm in two weeks. The non-sonicated samples showed a significantly lower rate of degradation of pyrene. The concentration of pyrene dropped to 40 ppm in two weeks and continued with a slower rate, to decrease to 14 ppm in 24 days.



3.3.1.3 Total Extractable Organics (TEO)

A sonicated sample of creosote-contaminated soil was sieved (using the wet sieving technique) and different fractions were isolated. Samples from each fraction were extracted with methylene chloride and the total extractable organics were measured by gravimetric method. The results tabulated in Table 3.2 clearly showed that the highest concentrations of total extractable organics were heavily accumulated in the smallest aggregates ($D_p < 38 \mu\text{m}$) and the largest aggregates ($D_p > 991 \mu\text{m}$) with a concentration of circa 1%. The aggregates between the two size limits had lower concentrations of TEO in the range of 0.3% ~ 0.6%.

Table 3.2. Total Extractable Organics (TEO%) in different fractions of sonicated creosote-contaminated soil:

Aggregate Size μm	%Mass Fraction	%TEO	%Fraction of Total TEO
$D_p > 991$	4.41	1.06	5.05
$495 < D_p < 991$	3.39	0.605	2.19
$246 < D_p < 495$	3.74	0.388	1.46
$124 < D_p < 246$	4.46	0.363	1.72
$53 < D_p < 124$	3.74	0.500	2.01
$38 < D_p < 53$	5.68	0.434	2.66
$D_p < 38$	74.5	1.074	84.8

3.3.1.4 Biodegradation Rate Constants

The apparent first-order rate constants were calculated for each PAH in the period where maximum rate of degradation occurred. The rate constants for degradation of anthracene in C-horizon soil are presented in Table 3.3. The rate constants are the average of four sets of data in each of the sonicated and non-sonicated experiments. The rate constants for degradation of six PAHs in creosote-contaminated soil with three different treatments are presented in Table 3.4 (the raw data on degradation of anthracene in C-horizon soil and degradation of 6 PAHs in creosote-contaminated soil with different treatments, are presented in Appendix A). The results represent experiments for non-sonicated, mildly sonicated and vigorously sonicated soil slurries. The mean apparent rate constant ($k_{\text{mean}}^{\text{app}}$) for PAHs in non-sonicated Creosote-contaminated soil is the average of six experiments, which is presented along with the time average of the mass-average diameter of the aggregates during the time period when first-order degradation was observed. The data for sonicated samples are presented as average values from two experiments. The table also shows the confidence level for calculated $k_{\text{mean}}^{\text{app}}$ and the standard deviations.

The observed increase in the apparent rate constant for anthracene in C-horizon soil due to sonication was significant (student t-test, 95% confidence). The $k_{\text{mean}}^{\text{app}}$ was significantly increased by vigorous sonication of the creosote-contaminated soil for all PAHs except phenanthrene and fluoranthene. The mild sonication also showed significant increase in $k_{\text{mean}}^{\text{app}}$ for anthracene, fluoranthene, pyrene and chrysene (student t-test, 95% confidence). The increase of $k_{\text{mean}}^{\text{app}}$ for

phenanthrene and fluoranthene (in the case of vigorous sonication) and acenaphthene and phenanthrene (in the case of mild sonication) was significant at the 90% confidence level.

Table 3.3. Apparent first-order rate constants* for degradation of anthracene in C-horizon soil.

	k^{app}_{mean} (95%CI) (d) ⁻¹	SD
Sonicated	0.583±0.090	0.092
Non-sonicated	0.238±0.118	0.120

* The rate constant in each case is the mean of four different experiments.

Table 3.4. Apparent first order rate constants¹ for degradation of 6 PAHs in Creosote-contaminated soil.

	$k_{\text{mean}}^{\text{app}}$ (95%CI) (d) ⁻¹	SD	Time Average ² Aggregate Size (μm)
Acenaphthene			
Non-sonicated	0.246±0.065	0.081	301
Sonicated (mild) ³	0.405	0.122	134
Sonicated (vigorous) ⁴	1.112	0.142	78
Phenanthrene			
Non-sonicated	0.447±0.053	0.067	474
Sonicated (mild)	0.662	0.129	134
Sonicated (vigorous)	1.418	0.364	78
Anthracene			
Non-sonicated	0.277±0.072	0.090	432
Sonicated (mild)	0.309	0.110	134
Sonicated (vigorous)	0.537	0.0003	78
Fluoranthene			
Non-sonicated	0.221±0.026	0.033	271
Sonicated (mild)	0.417	0.030	134
Sonicated (vigorous)	1.245	0.338	78
Pyrene			
Non-sonicated	0.229±0.044	0.056	213
Sonicated (mild)	0.339	0.018	134
Sonicated (vigorous)	0.984	0.115	78
Chrysene			
Non-sonicated	0.107±0.041	0.051	245
Sonicated (mild)	0.207	0.016	134
Sonicated (vigorous)	0.513	0.083	78

1. The data for non-sonicated soil is the mean of six experiments.
The data for sonicated soil is the mean of duplicate experiments.
2. The aggregate size is the time average of mass average diameter in the period that the kinetic data is extracted.
3. 50 g of soil was sonicated in 200 ml water for 21 minutes.
4. 50 g of soil was sonicated in 200 ml water for 30 minutes.

3.3.2 Aggregate Size Distribution in Slurry-phase Bioreactors

As the results of the experiments on C-horizon and creosote-contaminated soils suggest, the extents of degradation of PAHs were not significantly affected by sonication. Considering that sonication breaks down the aggregates to smaller size and decreases the diffusion path length, it was expected that the extent of bioremediation should increase as well as the rate. The contradictory results suggested an analysis of the aggregate size distribution in slurry-phase reactors to determine the range of particle sizes in each case.

3.3.2.1 C-horizon Soil

The hydrometer method was selected to examine the changes in aggregate size distribution during bioremediation for C-horizon soil. The readings on the hydrometer were directly proportional to the difference between the density of the suspension and a reference liquid (water in this case). A higher reading indicated that higher concentrations of aggregates remained in suspension. The measurements started 30 seconds after the suspension was left to settle down, and continued for about 7 hours. In Fig 3.3 the results of 6 experiments are summarized. The curve depicting the data for untreated soil that had been soaked for 2.5 h, constituted the lower limit. In this case very few soil aggregates remained in suspension. The concentration of aggregates dropped dramatically in the first 25 minutes, suggesting that the soil initially contained a considerable amount of large aggregates. The sonicated sample on the other hand served as the upper limit curve, which shows the contribution of

more small aggregates. The four curves falling between these two limits show the data for samples taken from the bioreactor at different time intervals. The data show that the curves for 5 and 16 days shifted upwards compared to the data on day one, indicating that the samples, which had spent a longer time in the bioreactor, were enriched in smaller aggregates. The most dramatic shift in the profile was during the first 5 days, when the large unstable aggregates were disrupted. The data also imply that there was not a significant change in the aggregate size distribution after 16 days and that the aggregate size distribution approached the properties of the sonicated sample asymptotically.

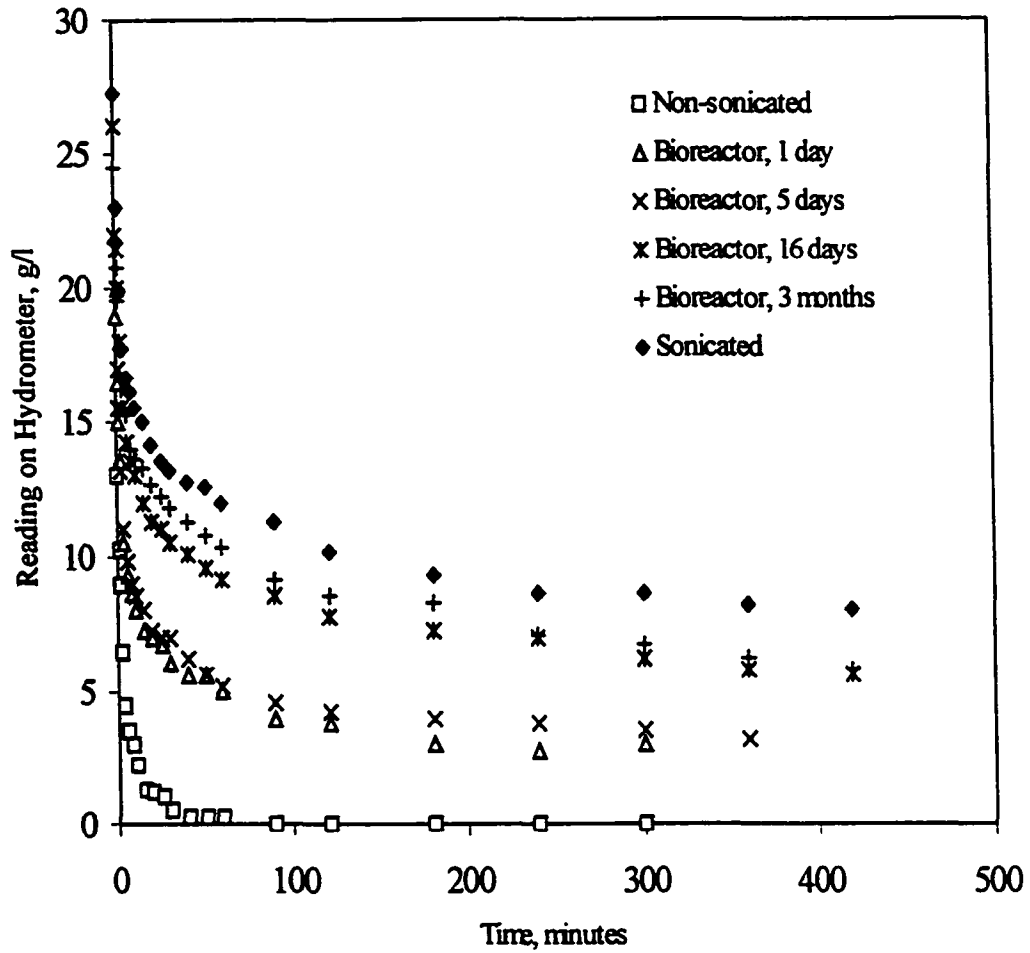


Figure 3.3. Hydrometer readings for the samples of C-horizon soil from the bioreactor and sonicated soil

3.3.2.2 Creosote-contaminated Soil

It was not possible to quantify the changes in aggregate size distribution by the hydrometer method for creosote-contaminated soil, because the soil flocculated very rapidly and separated into two phases, with an interface that settled with time. As an alternative, the wet sieving method was used to quantify the aggregate size distribution in creosote-contaminated soil. The data of Fig 3.4 illustrate the aggregate size distribution for slurry samples taken from the bioreactor at different time intervals and compares them with the aggregate size distribution in two sonicated soils. In the first sampling after 30 minutes, aggregates larger than 246 μm constituted 60% of the mass of the soil, while aggregates of smaller than 38 μm were only 22% of the total. After 9 days the former size range dropped to 30% of the mass while the latter increased up to 57%. The results show good agreement with the analysis of C-horizon soil by the hydrometer method and indicate that the slurry in the bioreactor was disaggregated, approaching the aggregate size distribution of the sonicated sample after 16 days.

A comparison parameter was needed to compare the aggregate size distribution in the bioreactor at different time intervals with sonicated samples. The mass average diameter was selected as a measure of average aggregate size for the purpose of comparison. The correlation in equation 3.1 gives the variation of mass average diameter (D_{mean} , μm) with respect to time (t , days) in the bioreactor. The parameters were determined by least squares.

$$D_{mean} = 182.61 + 414.66EXP(-0.22t) \quad (3.1)$$

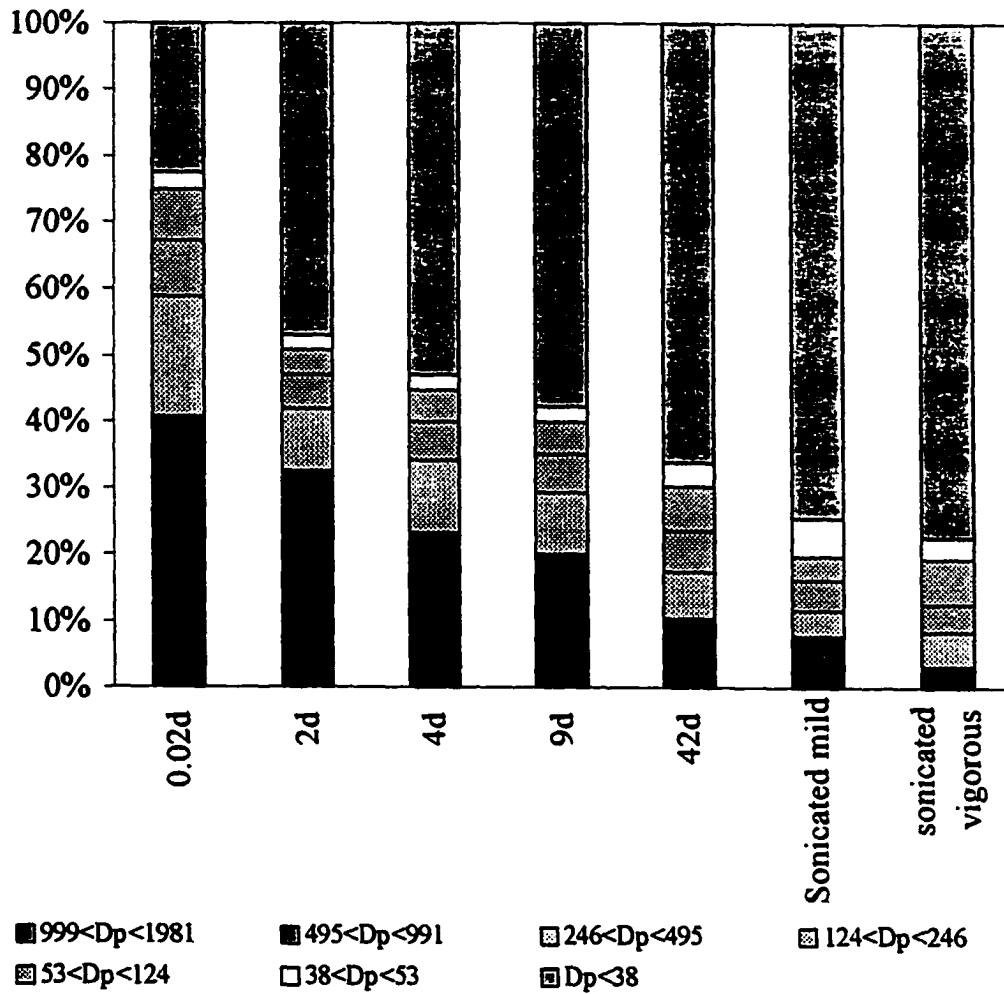


Figure 3.4. Aggregate size distribution in bioreactor and in soils sonicated at different intensities

The mass-average diameter was calculated for each sample during the process of bioremediation and was compared with the two samples sonicated with different intensities. The results depicted in Fig 3.5 show that the mass-average diameter of the aggregates dropped exponentially for the first two weeks and then approached the final value of 184 μm . This terminal value was slightly higher than the mean diameters of sonicated samples, with values of 134 μm and 78 μm from mild and intense sonication. At this point, it is important to mention that in the two sonicated samples, 75% and 77% of the aggregates were < 38 μm , however, the methods used in these experiments were not able to give any information on the distribution of aggregates smaller than 38 μm . This limitation might have caused some inaccuracy in determining the mass-average diameters.

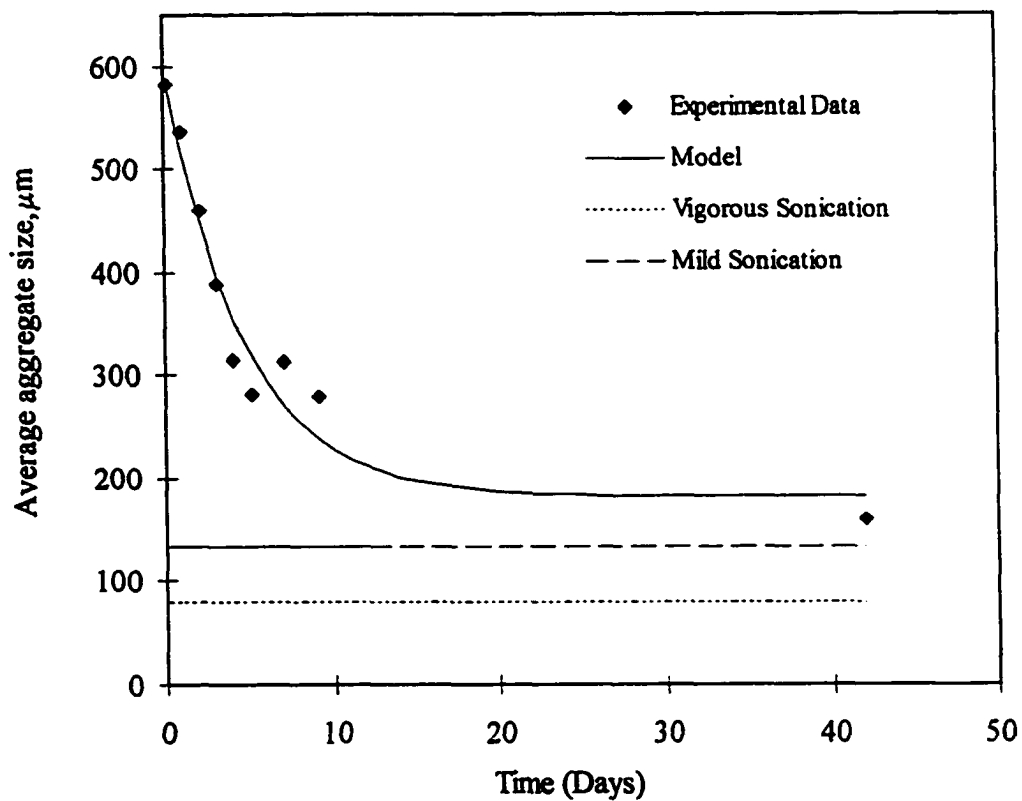


Figure 3.5. The time course of mass average diameter of the aggregates in the bioreactor compared to the samples sonicated at different intensities

3.4 Discussion

A qualitative analysis of the biodegradation curves revealed that degradation of PAHs followed three distinct phases.

- 1- An initial lag phase during which no degradation occurred. The duration of this phase depended on the chemistry of the PAH molecule.
- 2- The rapid phase of degradation: In this period considerable amounts of PAHs were degraded.
- 3- The slow phase of degradation, which was attributed to a resistant or strongly-retained fraction of contaminants in the soil.

The time course and the extent of degradation in each phase were variable and depended on the component of PAHs and the treatment applied to the soil.

3.4.1 Substrate Preferences

The data depicted in Figure 3.2 imply that there is a definite sequence in utilization of the PAHs by microorganisms. The preferential sequence appears to be related to the structure and complexity of the molecules (Banerjee et al., 1995). Degradation of phenanthrene began immediately, followed by degradation of fluoranthene, pyrene and chrysene after a considerable time delay, providing clear evidence that the active culture had more affinity for simpler compounds as long as they were present in sufficient concentration. In the absence of easily degradable compounds, the microorganisms showed the ability to utilize more complex aromatics such as fluoranthene, pyrene and chrysene. Degradation of fluoranthene, pyrene and

chrysene started after lag phases of 3, 4.5 and 4 days respectively. During this period the concentration of phenanthrene and anthracene had dropped significantly. This behavior may be attributed to diauxic growth on the multiple carbon sources. This phenomenon has been observed and well documented for growth of microorganisms on mixtures of sugars (Bailey and Ollis, 1986), however, there is very little evidence of such catabolic repression in the systems that hazardous organic wastes are treated. The lack of evidence is mostly due to the fact that in any waste treatment system, the carbon source is complex and consists of hundreds of different compounds. One example was reported by Anciaux et al. (1989), who reported a two phase growth curve due to diauxic growth on a mixture of straight and branched-chain fatty acids.

3.4.2 Kinetic Analysis

Following the initial lag phase, the rapid phase of degradation started. During this period the concentration of PAHs dropped significantly for both sonicated and non-sonicated samples. The data depicted in Fig. 3.1 suggest that the rate of degradation of anthracene in pristine soil was improved by sonication. The same conclusion can be drawn from the data of Fig. 3.2 for degradation of phenanthrene, fluoranthene and pyrene in the Creosote-contaminated soil. Two sets of results are presented for sonicated experiments. The mild sonication resulted in a mass average diameter (D_{mean}) of 134 μm , while a more vigorous sonication broke down the aggregates to 78 μm . The strong effect of aggregate size on the degradation rate constants is demonstrated in Table 3.2 for six PAHs. The data of Figs 3.1 and 3.2

along with information illustrated in Table 3.2 suggest that the effect of sonication was most significant during the rapid phase of degradation. The data provided strong evidence that the rapid phase of degradation was controlled by mass transfer rather than microbial activity. The highest apparent rate constants (k^{app}_{mean}) for degradation, in the range 0.513~1.418 d⁻¹, were for the aggregates of size 78 μm, followed by a lower k^{app}_{mean} of 0.207~0.662 d⁻¹ for the aggregates of size 134 μm. The non-sonicated experiment showed the lowest k^{app}_{mean} for all six PAHs, in the range 0.122~0.447 d⁻¹. Similar results were reported by Scow and Alexander (1992) for degradation of phenol. They suggested that the rate of degradation of phenol in the presence of porous clay aggregates of size 0.55 and 0.75 cm was significantly lower than the rates measured in the absence of aggregates. In contrast, Mihelcic and Luthy (1991) developed a diffusion model for the sorption/desorption of naphthalene from soil aggregates, which suggested that diffusion-desorption rate was very fast compared to the microbial degradation rate and hence diffusion in small aggregates would not limit the rate of degradation. The aggregates used in their experiment were in the range of 0.25 – 50 μm with a geometric mean diameter of 1.5 μm and the volume mean diameter of 35 μm.

Another implication of the results in Table 3.2 is that the chemical properties of the diffusing molecule have also a strong effect on bioremediation. The effect of sonication was more significant for the higher molecular weight compounds while phenanthrene and anthracene, the 3 ring compounds, were less affected by sonication.

Degradation of fluoranthene, pyrene and chrysene was significantly improved by sonication, with increases in the apparent first-order rate constants of 5,4 and 4 fold respectively. Phenanthrene and anthracene showed only a 2-3 fold increase in the apparent rate constants due to sonication.

3.4.3 Comparison between $k_{\text{mean}}^{\text{APP}}$ and Literature Values

A number of studies have tried to measure and compare the relative rates of desorption and mineralization. These studies were carried out with different chemicals, porous materials, soils and sediments, different microorganisms and different aging times. Some of the reported values for mineralization rate constants are: (I)* 0.02 d⁻¹ up to 0.90 d⁻¹ for mineralization of phenanthrene from various porous media and glass beads (Nam and Alexander, 1998); (II)* 0.122 d⁻¹ and 0.027 d⁻¹ for phenanthrene in freshly spiked soil and aged soil (Hatzinger and Alexander, 1995); (III)* 1.99 d⁻¹ and 0.14 d⁻¹ for 4-nitrophenol in freshly spiked soil and aged soil (Hatzinger and Alexander, 1995); (IV) 26.1-34.1 d⁻¹ for naphthalene from coal tar coated on silica beads and 4.7 d⁻¹ for naphthalene in 2,2,4,4,6,8,8-heptamethylnonane (Ghoshal et al., 1996). It can be inferred from these data that the rate of mineralization is strongly influenced by the physical properties of the material that has been used as a support for coating.

* The rate constants are calculated based on the data in the corresponding papers

The apparent rate of mineralization was clearly influenced by transport processes such as diffusion, desorption and dissolution. The values of $k_{\text{mean}}^{\text{APP}}$ from our study fall in the mid-range of the reported data for phenanthrene.

3.4.4 Dependence of $k_{\text{mean}}^{\text{APP}}$ on Aggregate Size

The $k_{\text{mean}}^{\text{APP}}$ values are plotted in Fig. 3.6 as a function of time average diameter (D_{mean}) during the rapid degradation phase. The important conclusion drawn from this plot is that the most dramatic change for $k_{\text{mean}}^{\text{APP}}$ occurs where the mean diameter D_{mean} is below 134 μm . In this range, the size of aggregates has stabilized and the large aggregates have been broken to aggregates of size 78 – 134 μm . Increasing the aggregate size over 134 μm had very little effect on the mean apparent rate constants. This observation is consistent with the data on total extractable organics presented in Table 3.2, which confirmed that the smaller aggregates were more heavily loaded with organic matter. This observation is also in agreement with the findings of Bremner and Genrich (1990), who characterized different fractions of the soil and reported that the clay fraction had a higher concentration of organic carbon compared to sand and silt fractions. A more linearized form of dependence of $k_{\text{mean}}^{\text{APP}}$ to aggregate size is illustrated in Figure 3.7, where, the $k_{\text{mean}}^{\text{APP}}$ is plotted against $1/(R_{\text{mean}})^2$. The linear correlation between $k_{\text{mean}}^{\text{APP}}$ and $1/(R_{\text{mean}})^2$ is observed for all PAHs and is consistent with diffusion controlled mass transfer mechanism from the aggregates to the aqueous phase.

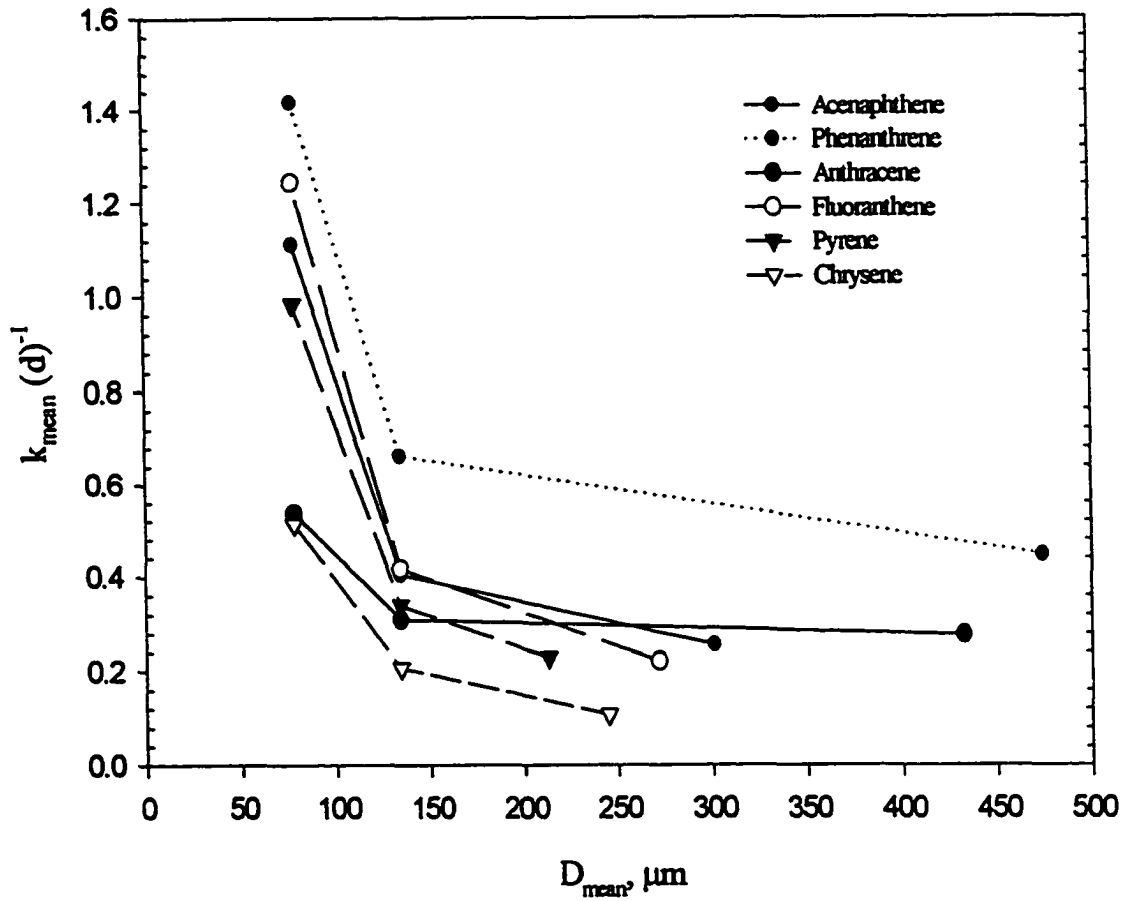


Figure 3.6. The effect of aggregate size on the apparent first order degradation rate constant

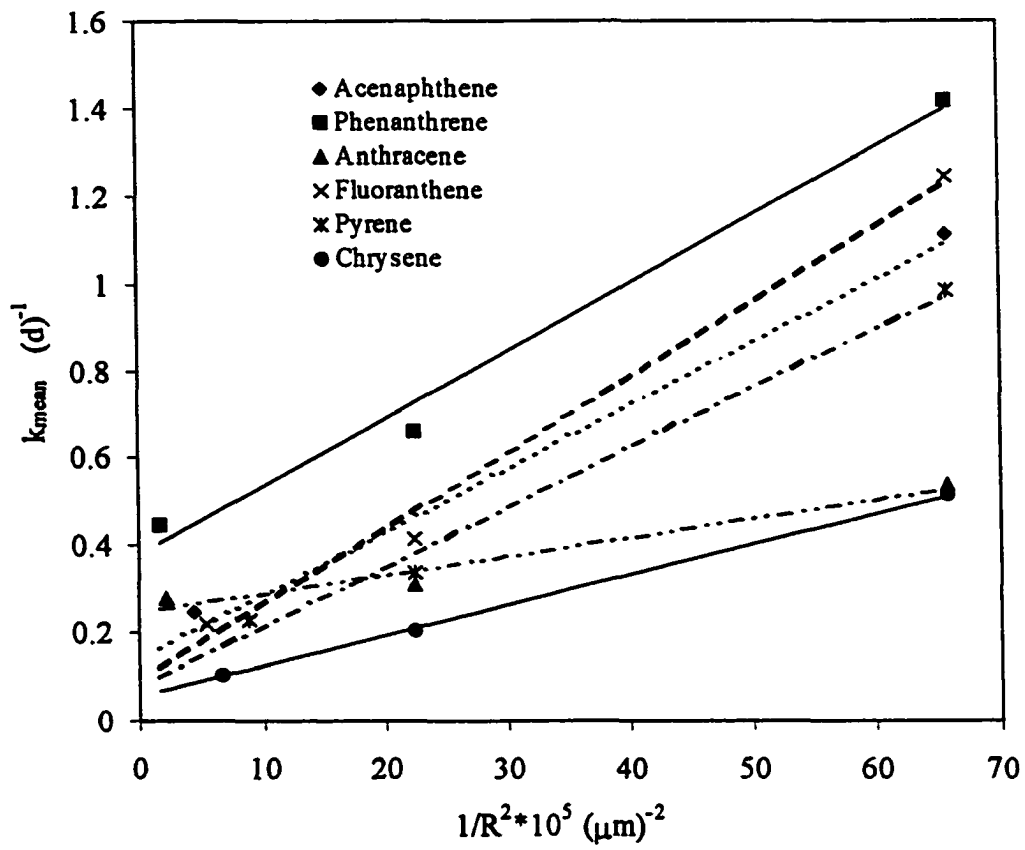


Figure 3.7. The plot of apparent first order degradation rate constant versus $1/R^2$ for six PAHs

3.4.5 Extent of Biodegradation

Regardless of the preparation method, within 3 weeks of treatment both sonicated and non-sonicated samples showed similar amounts of residual contaminants, suggesting that in all cases the final extent of degradation was not significantly affected by sonication. The fact that degradation of sonicated and non-sonicated samples of Creosote-contaminated soil reached the same ultimate value likely result from two distinct phenomena:

- 1- The hydration and shear forces in the bioreactor were sufficient to change the aggregate size distribution and reduce it to values comparable to sonication.
- 2- There was a limited power for sonication. At some point sonication was no longer effective and the microstructures responsible for retaining the contaminants were no longer affected by sonication.

The results of this study are in agreement with the data published by Hatzinger and Alexander (1995), who reported that both in aged and unaged soils sonication increased the rate of degradation of phenanthrene, but the extent of degradation remained unaffected. Although they did not give any quantitative explanation for the behavior of their system, the fact that their experiments were carried out in a rotary shaker implies that the shear effects might have been a contributing factor on breaking down the aggregates in the non-sonicated soil samples.

Stability of the aggregates is due to the grouping of the aggregates by cementing agents or pore fluid characteristics. Breaking down the aggregates not only releases the contaminants that are trapped in macropores and interaggregate spaces,

but provides higher surface area for mass transfer. More study is needed to reveal the microstructure of aggregates in contaminated soils and the distribution of non-aqueous phase liquid in the soil matrix.

3.5 Conclusion

This research showed that aggregate size in the range 40 – 1000 μm influenced the rate but not the extent of bioremediation in slurry-phase reactors. The apparent rate constant for degradation of anthracene in the sonicated soil spiked with anthracene was twice the rate in the non-sonicated soil. The rates of degradation of 6 PAHs, monitored in the course of bioremediation of creosote-contaminated soil, were increased up to 5 fold by reducing the aggregate size to 78 μm . Approximately three weeks of bioreactor operation was enough to reduce the aggregate size distribution in soil to a final stable value, comparable to a sonicated sample.

3.6 Literature cited

Ahn, I.S.; Lion, L.W.; Shuler, m.L., "Microscale-based modelling of polynuclear aromatic hydrocarbon transport and biodegradation in soil." *Biotech. and Bioeng.* 1996, 51, 1-14.

Anciaux, C.M.; Meyer, M.De.; Levert, J.M., Vanthournhout, M., "Influence of several parameters on the growth of *Candida Ingens* in controlled batch culture using volatile fatty acids as substrate." *Biological wastes.* 1989, 30, 21-34.

Bailey, J.E.; Ollis, D.F., 'Biochemical Engineering Fundamentals" *McGraw-Hill. USA*, 1986.

Ball, W.P.; Roberts, P.V., "Long term sorption of halogenated organic chemicals by aquifer materials." *Environ. Sci. Techol.* 1991, 25, 1223-1249.

Banerjee, D.K.; Fedorak, P.M.; Hashimoto, A.; Masliyah, J.H.; Pickard, M.A.; Gray, M.R., "Monitoring the biological treatment of anthracene contaminated soil in a rotating drum bioreactor." *Appl. Microbiol. Biotechnol.* 1995, 43, 521-528.

Bosma, T.N.P.; Middeldorp, P.J.M.; Zehnder, A.J.B., "Mass transfer limitation of biotransformation: quantifying bioavailability." *Environ. Sci. Technol.* 1997, 31, 248-252.

Bremner, J.M.; Genrich, D.A., " Characterization of the sand, silt, and clay fractions of some mollisols." *Soil Colloids and Their Association in Aggregates.*" Chapter 15, Plenum Press, New York, 1990.

Cerniglia,C.E., "Biodegradation of polycyclic aromatic hydrocarbons." *Biodegradation* 1992, 3, 351-368.

Fedorak, P.M.; Grbic Galic, D., "Aerobic microbial cometabolism of benzothiophene." *Appl. Environ. Microbiol.* 1991, 57, 932-942.

Foght, J.M.; Westlake, D.W.S., "Degradation of polycyclic aromatic hydrocarbons and aromatic heterocycles by a *Pseudomonas* species." *Can. J. Microbiol.* 1988, 34, 1135-1141.

Geerdink, M.I.; Van Loosdrecht, M.C.M.; Luyben, K.CH.A.M., "Model for microbial degradation of nonpolar organic contaminants in a soil slurry reactor." *Environ. Sci. Technol.* 1996, 30, 779-786.

Ghoshal, S.; Ramaswami, A.; Luthy, R.G., "Biodegradation of naphthalene from coal tar and heptamethylnonane in mixed batch systems" *Environ. Sci. Technol.* 1996, 30, 1282.

Gray, M.R.; Banerjee, D.K.; Fedorak, P.M.; Hashimoto, A.; Masliyah, J.H.; Pickard, M.A., "Biological remediation of anthracene-contaminated soil in rotating bioreactors" *Appl. Microbiol. Biotechnol.* 1994, 40, 933-940.

Hatzinger, P.B.; Alexander, M., "Effect of aging of chemicals in soil on their biodegradability and extractability." *Environ. Sci. Technol.* 1995, 29, 537-545.

Karickhoff, S.W.; Morris, K.W., "Sorption dynamics of hydrophobic pollutants in sediment suspensions" *Environ. Toxicol. Chem.* 1985, 4, 469-479.

Karimi, S.; Pichard, M.A.; Gray, M.R., "Reactions of polynuclear aromatic hydrocarbons on soil." *Environ. Sci. Technol.* 1996, 30, 1145-1151.

Mihelcic, J.R.; Luthy, R.G., "Sorption and microbial degradation of naphthalene in soil-water suspensions under denitrification conditions." *Environ. Sci. Technol.* 1991, 25, 169-177.

Mueller, J.G.; Lantz, S.E.; Blattmann, B.O.; Chapman, P.J., "Bench-scale evaluation of alternative biological treatment processes for the remediation of pentachlorophenol and creosote-contaminated materials: Slurry-phase bioremediation." *Environ. Sci. Technol.* 1991, 25, 1055-1061.

Nam, K.; Alexander, M., "Role of nanoporosity and hydrophobicity in sequestration and bioavailability: tests with model solids." *Environ. Sci. Technol.* 32:71-74.

Scow, K.M.; Alexander, M., "Effect of diffusion on the kinetics of bioremediation: experimental results with synthetic aggregates." *Soil Sci. Soc. Am. J.* 1998, 56, 128-134.

Sheldrick, B.H.; Wang, C., "Particle size distribution." *Soil sampling and methods of analysis*. M.R. Carter Ed., Canadian Society of Soil Science. Chapter 47, 1993.

Steinberg, S.M.; Pignatello, J.J.; Sawhney, B.L., "Persistence of 1,2-dibromoethane in soils: entrapment in intraparticle micropores." *Environ. Sci. Technol.* 1987, 21, 1201-1208.

Tabak, H.; Fu, C.; Pfanstiel, S.; Gao, C.; Yan, X.; Govind, R., "Studies on contaminants biodegradation in slurry, wafer, and compacted soil tube reactors." *Environ. Sci. Technol.* 1996, 30, 743-750.

Weissenfels, W.D.; Klewer, H.J.; Langhoff, J., "Adsorption of polynuclear aromatic hydrocarbons (PAHs) by soil particles: influence on biodegradability and biotoxicity." *Appl. Microbiol. Biotechnol.* 1992, 36, 689-696.

4. Characterization of Contaminated Soils Using Confocal Scanning Laser

Microscopy and Cryogenic-Scanning Electron Microscopy

4.1 Introduction

Although many researchers have observed a slow rate of desorption of contaminants from soil, our knowledge of the causes of these slow kinetics is very limited. There is very little information on the distribution of non-aqueous phase liquid (NAPL) in contaminated soils at the micro-scales. The association of NAPL with soil aggregates is important in determining the transport processes that control the desorption of contaminants. In this study, we used microscopy techniques to get an insight into the distribution of NAPL in the soil matrix at a length scale of 1 μm to 100 μm .

The association of NAPL with soil may be analogous to crude oil in porous media in petroleum reservoirs. Various microscopy techniques have been used in petroleum engineering to analyze reservoir rock porosity and to characterize the pore structure. Computed microtomography (CMT) has been used in the characterization of porous media for geological applications (Coles et al., 1994; Spanne et al., 1994). Application of this technique provided two and three dimensional descriptions of pore structure and mineral distribution of core materials with resolution of 30 μm . Using this technique Coles et al. (1998) have been able to observe oil and brine phases within the rock matrix. Scanning electron microscopy (SEM) was used to

characterize the pore structure of oil reservoirs (Sneider and Erickson, 1997) and study wettability in pores (Robin et al., 1995).

There are very few published studies on the application of confocal scanning laser microscopy (CSLM) to opaque objects. Munoz et al. (1997) used CSLM to characterize oil-water emulsions, and suggested that the 3D image analysis obtained by this method provided similar information to cryogenic scanning electron microscopy analysis. Li et al. (1995) used CSLM to characterize the asphaltene particles precipitating in bitumen processing. The method has successfully been used by Postma and Altemuller (1989) to visualize the rhizobial cells added to a soil by staining them with the fluorescent brightener Calcofluor White M2R. Farahani et al. (1996) managed to display crack growth and crack depth on the surface of aluminum alloys using CSLM.

CSLM with fluorescent probes has been used extensively in biochemistry, molecular biology and medical sciences to detect particular components within complex cellular assemblies. All the fluorescent probes contain polynuclear aromatic hydrocarbons (PAHs) bonded to aliphatic chains, and the fluorescence is a common characteristic of aromatic, polar aromatic and asphaltenes (Haugland, 1996). Most mineral particles do not exhibit fluorescent characteristics with the same intensity and colour that organics do, therefore, it is possible to distinguish between the oil phase and mineral phase using fluorescent CSLM.

This study characterized contaminated soils by CSLM, using the fluorescence properties of NAPL that is rich in PAHs. The distribution of NAPL in soil and the

association of this phase with mineral matter were also investigated. Soils were imaged down to a length scale of 1 μm or less, therefore, the interaction of contaminants with soil organic matter or mineral surfaces at the molecular level was not investigated. Cryo-SEM and CSLM were used on the same sample to compare directly the information on NAPL distribution derived from the two different techniques using very different bases of observation (fluorescent emitted light for CSLM and secondary electron imaging for SEM).

4.2 Materials and Methods

4.2.1 Soils

Edmonton soil was collected from a wood-preserving site, which was in operation from 1924 – 1988. This site was contaminated with creosote components. The soil was classified as silty clay. Devon soil was collected from Devon, Alberta, at a site contaminated with petroleum hydrocarbons in 1948. This soil was classified as intermediate loam texture. The two soils had organic contents of 3.28 and 3.2 wt% respectively. Prince Albert soil was contaminated with creosote and had an organic content of 1.41%. This soil was collected from Prince Albert, Saskatchewan at a former wood-preserving site. The three soils were selected to give a wide range of textures from high clay content of Edmonton soil to sandy soil of Prince Albert. Two pristine soils were also used as background reference. The C-horizon sub-soil was collected at a depth of 75+ cm from south of Edmonton, AB. The shale was sampled from a site on the North Saskatchewan River near Devon, AB. Montmorillonite No.

23 from Arizona and KGa-1 Kaolinite from Georgia were used as reference clays.

Properties of the soils and clays used in this experiment are listed in Table 4.1.

Table 4.1. Characteristics of the contaminated soils and clay samples

soil source/type	contaminant type	total organic content (wt%)	total extractable organics (wt%) TEO	clay (wt%)	sand (wt%)
Edmonton, AB	creosote	3.29	1.45	40.8	15.8
Devon, AB	petroleum hydrocarbons	3.20	2.23	18.4	44.8
Prince Albert	creosote	1.41	1.09	3.80	90.2
C-horizon	nil	0.62		23.9	50.6
Shale	nil	2.80		43.0	9.00
Montmorillonite	nil			100	
Kaolinite	nil			100	

4.2.2 Embedding

LKB 2218 – 500 Histo-resin kit from LKB-Produkter (Bromma, Sweden) was used to embed the soil aggregates and prepare them for sectioning. This resin is water soluble and consists of three different components:

- A) Powder Component (activator): Benzoyl peroxide with 50% plasticizer (0.5 g)
- B) Liquid Component (basic resin): Glycol methacrylate monomer, Polyethylene glycol 400 and Hydroquinone (500 ml)
- C) Hardener: Derivative of fumaric acid, Dimethyl sulfoxide (1 ml)

The activator was dissolved in basic resin and stirred with a magnetic stirrer, then the hardener was added and completely mixed. After filling the mold with the embedding medium, the soil aggregate was immersed and oriented in the medium. The mold was left under vacuum overnight until the medium was hardened and ready for sectioning.

4.2.3 Microtomy

A Sorvall JB – 4A microtome was used to prepare thin sections for CSLM. The thin sections were prepared to a thickness of 10 μm , using glass blades. A fine bristle was used to pick up the thin sections from the glass blade and to place them on a drop of water. The slides were then warmed in an oven at 45 °C to spread the sections flat and stick them to the slides for examination under the microscope.

4.2.4 Confocal Scanning Laser Microscopy (CSLM)

The microscope used in this experiment was a Molecular Dynamics 2001 (Sunnyvale, California, USA) confocal microscope. The microscope was equipped with a mercury lamp and argon/krypton medium as laser source. This combination created a broad spectral coverage of 400-800 nm. There were no laser lines below 400 nm in this microscope. The laser lines and the attenuation levels were selected by two sets of filters. The attenuation filters allowed 1,3,10, 30 and 100 percent of light to pass through. The bandpass excitation filters provided light of selected band to pass. Therefore it was possible to use excitation light at 488nm, 488/568 nm (dual band pass), 488/647 nm and 568 nm. The CSLM was equipped with two detectors. A 568 beam splitter along with 530 DF30 filter for FITC detection and a 600 DF40 filter for rhodamine detection was used to detect the emitted light. The aperture was set for 100 μ m pinhole and the photomultiplier gain was 1X. The fluorescent intensity in each pixel was measured for FITC and rhodamine signals and digitized by the image processor for quantitative analysis. The Image Space 3.2 software of the MD 2001 confocal microscope was used as the image processing tool. The threshold of fluorescence intensity measurement was set at 0 to 255 levels of grey scale.

4.2.5 Scanning Electron Microscopy

An EMI TECH K1250 was used for cryogenic preparation and transfer. The scanning electron microscope was JEOL ISM – 6301 FXV equipped with SCO software. A PRISM energy dispersive X-ray detector (EDX) was used for

microanalysis. The system was equipped with PGT IMIX software as the X-ray imaging microanalysis tool. The imaging procedure used secondary electron mode to study the region of interest. The contrast basically gave information on surface topography. The great depth of field made these images particularly well suited for examining fractured surfaces.

Energy dispersive X-ray was used for elemental analysis and to identify local changes in the composition of the surfaces. Sulfur and vanadium were used as the tracer elements for oil because light elements such as carbon were not detectable.

4.2.6 Freeze Fracturing

The soil aggregates were mounted on the sample holder then frozen with liquid nitrogen at $-180\text{ }^{\circ}\text{C}$, and transferred to the preparation chamber. Fracturing was carried out at $-180\text{ }^{\circ}\text{C}$ under vacuum to prevent condensation. The fresh surfaces were coated with gold with a thickness of 100 angstroms to increase the conductivity of the surface and to enable observations under electron beam without charging effects.

4.3 Results

Soil aggregates were randomly chosen for CSLM and SEM examination. Numerous regions of the samples were analyzed and those images representative of the samples are presented here (more images are presented in Appendix B). Figures

4.1 to 4.6 are representative photomicrographs of different contaminated soils obtained by fluorescent CSLM and SEM.

4.3.1 Fluorescent CSLM

The experiments with CSLM used the fluorescence of contaminant molecules to obtain images. Figure 4.1 illustrates a creosote-contaminated soil and two pristine soils under white light and UV light. Bright-field microscopy inspection of contaminated soil (4.1A) showed that the soil aggregates consisted of particles with different shapes and sizes, however, no information on the distribution of organic compounds could be obtained. There was no significant difference in appearance between the pristine and contaminated soil under the conventional light microscope (4.1A, 4.1C and 4.1E), except that the contaminated soils appeared to be more agglomerated while the pristine soil looked more like segregated particles. However, the examination of the same samples by UV light revealed a strong fluorescence in creosote-contaminated soil (Figure 4.1B). Montmorillonite and kaolinite were examined for background fluorescence. No detectable fluorescence was observed in the two clay samples (data not shown). The C-horizon soil and Shale were two pristine soils that were examined under fluorescent light. The C-horizon soil showed some sharp fluorescent points at some regions, due to the presence of some fluorescent minerals (4.1D). No fluorescence was observed in shale (4.1F).

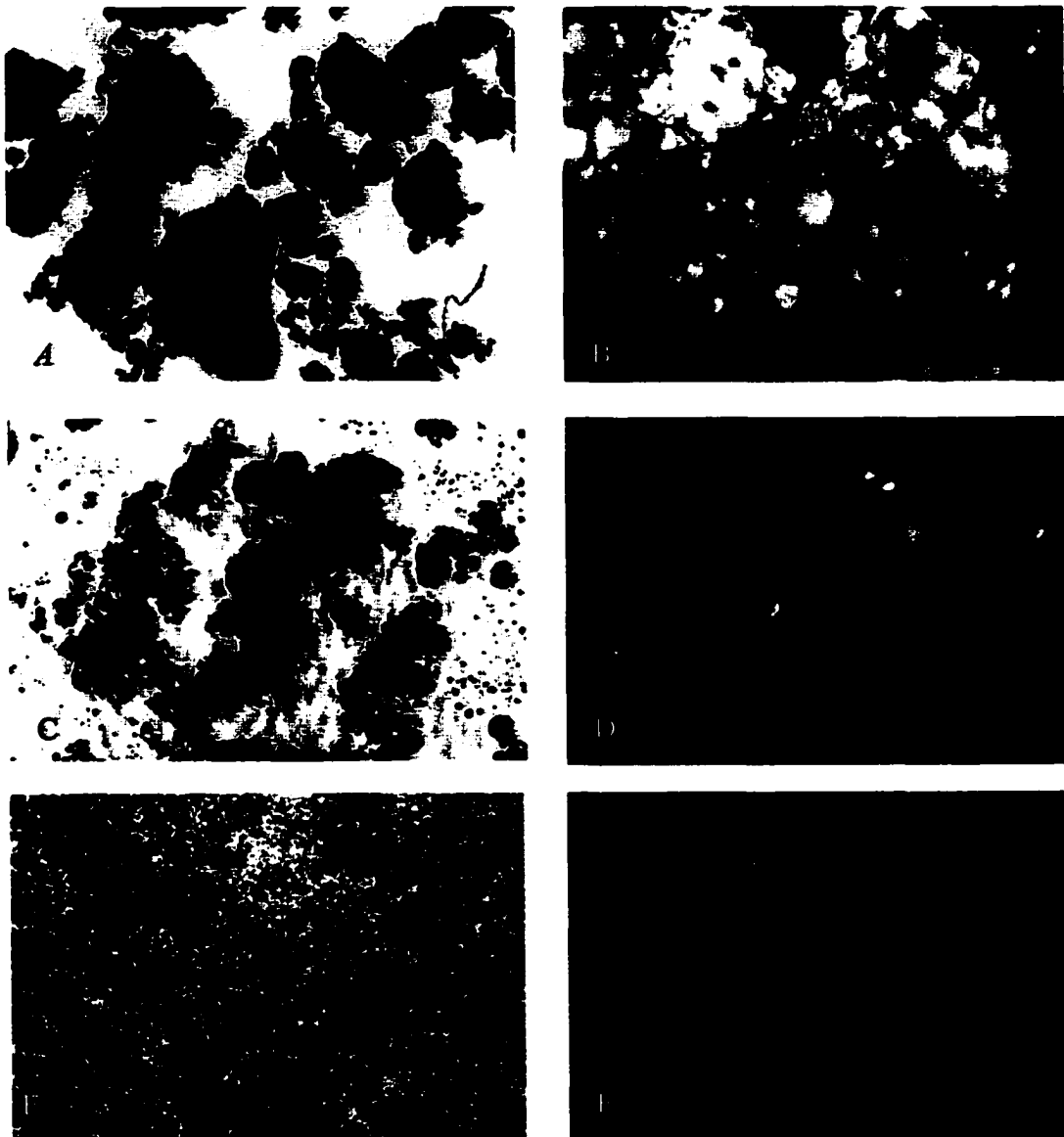


Figure 4.1. Samples of contaminated and pristine soils under bright-field microscope (A, C and E) and fluorescent microscope (B, D and F). A and B: Edmonton creosote-contaminated soil, C and D: C-horizon pristine soil, E and F: pristine shale.

To verify the fact that the fluorescence observed was from organic molecules in the soil, and to distinguish it from the natural fluorescence of soil minerals, a simple experiment was conducted. The fluorescent intensity of an aggregate of Edmonton creosote-contaminated soil was measured at different stages under exactly the same conditions (voltage = 716, photo gain = 1X, attenuation = 30%, excitation light 488/568). The aggregate was strongly fluorescent before any treatment (figure 4.2A). The sample was then extracted with methylene chloride for 6 hours and then tested for fluorescent intensity. As shown in Figure 4.2B, the sample still fluoresced, implying that a significant portion of the organic material was not extracted. This result was consistent with the data shown in Table 4.1 suggesting that of the 3.29% total organic content of the soil, less than half (1.45% by weight of soil) was extractable. The same aggregate was then incinerated at 815°C for one hour to remove all the organic material. The examination of the aggregate with CSLM (Figure 4.2C) then showed no fluorescence, although the operation conditions of the microscope were set to maximize the response of the detector (attenuation 100% and the results of 4 series of scans were summed).



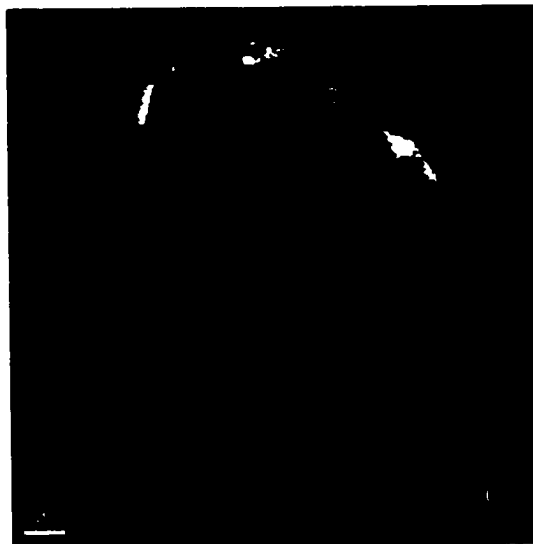
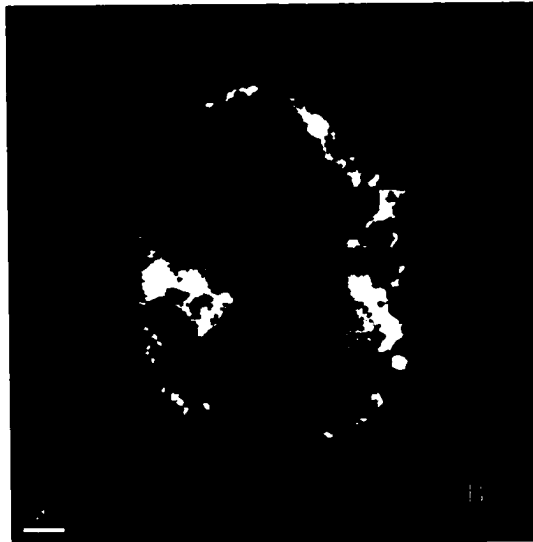
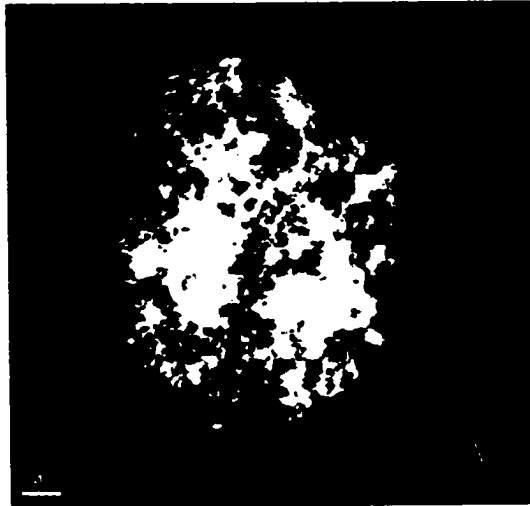
Figure 4.2. An aggregate of Edmonton creosote contaminated soil A) before any treatment, B) after extraction with methylene chloride for 6 hours, and C) after incineration at 815 °C for 1 hour.

One of the advantages of using CSLM is its ability to reconstruct and study the 3D structures without sectioning the sample. Confocal scanning laser microscope scans the sample with a laser beam. The emitted light after detection by two photomultipliers is digitized to give an image from specified depths. The series of images collected at different depths can be combined to reconstruct the three dimensional structure of the aggregate with the aid of Image Space software. Another feature of CSLM is digital frame storage. An intensity number is assigned for each pixel in the image, which is called the pixel value or gray level. Each pixel has a brightness described by its gray level usually between 0 and 255. This feature gives the ability to stretch the displayable pixel intensity range by colour coding steps that might otherwise be below the detectable difference for monochrome visual inspection. Digital frame storage allowed for several means of image display, such as exhibition of an iso-intensity map and the application of pseudo colors to display different level of fluorescent intensities.

Figure 4.3 shows 3 images of an aggregate of Prince Albert creosote contaminated soil. Figures 4.3A shows a 3D composite image obtained by FITC signal and displayed in pseudo-colours. This image was constructed from a series of 70 optical sections at 1.2 μm focus intervals. Figures 4.3B and 4.3C are images from 25th and 45th planes of focus respectively. The images taken from deeper sections were dark and did not show the detailed structure from inside of the aggregate. The last clear image was obtained from the depth of 30 μm relative to the first focused image. The main reason is that the depth of field in laser microscope is 3 μm , thus the

opaque samples thicker than the depth of field could not efficiently be radiated in deeper sections and the emitted light could not reach directly to the detector with preserved intensity. Montoto et al. (1995) reported that the signals from the depths of 300 μm for quartz and 100-130 μm for feldspars could be detected.

Figure 4.3. Aggregate of Prince Albert creosote-contaminate soil. A) 3D construction of 530 DF30 filter FITC signal in pseudo-color, the 3D image was constructed by collecting 70 series of images at 1.2 μm focus intervals. B and C) the images from 25th and 45th planes of focus respectively



To overcome this problem and to get a better insight into the internal structure and composition of the aggregates, thin sections of the samples were prepared. The aggregates were embedded in a resin and sections with thickness of 10 μm were prepared. The thin sections were then examined with CSLM. Figure 4.4 shows one of the middle sections taken from an aggregate size of 250 μm from Edmonton creosote-contaminated soil. The thin section was studied sequentially using the different microscopy techniques. The bright field illumination of a thin section is shown in Figure 4.4A. A series of large inter-connected pores are evident in the centre of the aggregate. These pores are in the range of 10–40 μm in size and are filled with air. Figure 4.4B shows the same microtom using CSLM. The two images have been taken using the same objectives. Figures 4.4C and 4.4D show the magnified image of the box in Figure 4.4B in pseudo-colours. The advantage of this method of presentation was that the background fluorescence could be easily eliminated and with the aid of image analysis software it was possible to indicate the spots of high concentration in the sample. The regions with white color have the highest intensity of fluorescence while the blue color is assigned for the lower intensities. Another advantage of this technique is its ability to increase the optical magnification by means of electronic zoom. As mentioned earlier the intensity is assigned a number between 0 and 255 on gray scale. From the previous experiments on clay and pristine soil it was observed that the fluorescent intensity for clay and soil in the same operating condition was in the range of 0 to 15. There were very few point spots with intensities of 15 to 30 in C-horizon soil. To eliminate any

background and to assure there was no interference from the minerals, the areas with intensity between 0 and 50 were eliminated and only the areas with intensity between 50 and 255 were illustrated in figure 4.4C. With the same logic, figure 4.4D illustrates the regions with intensities 150-255. With this method of analysis, it was concluded that distribution of NAPL was not uniform throughout the soil aggregates. There were spots with very high concentration of NAPL as well as clean areas. The soils with higher content of clay created suitable space in pores of size range 0.5 – 5 μm to accommodate the NAPL, however in the sandy soil the NAPL was located on the surface of the sand grains.

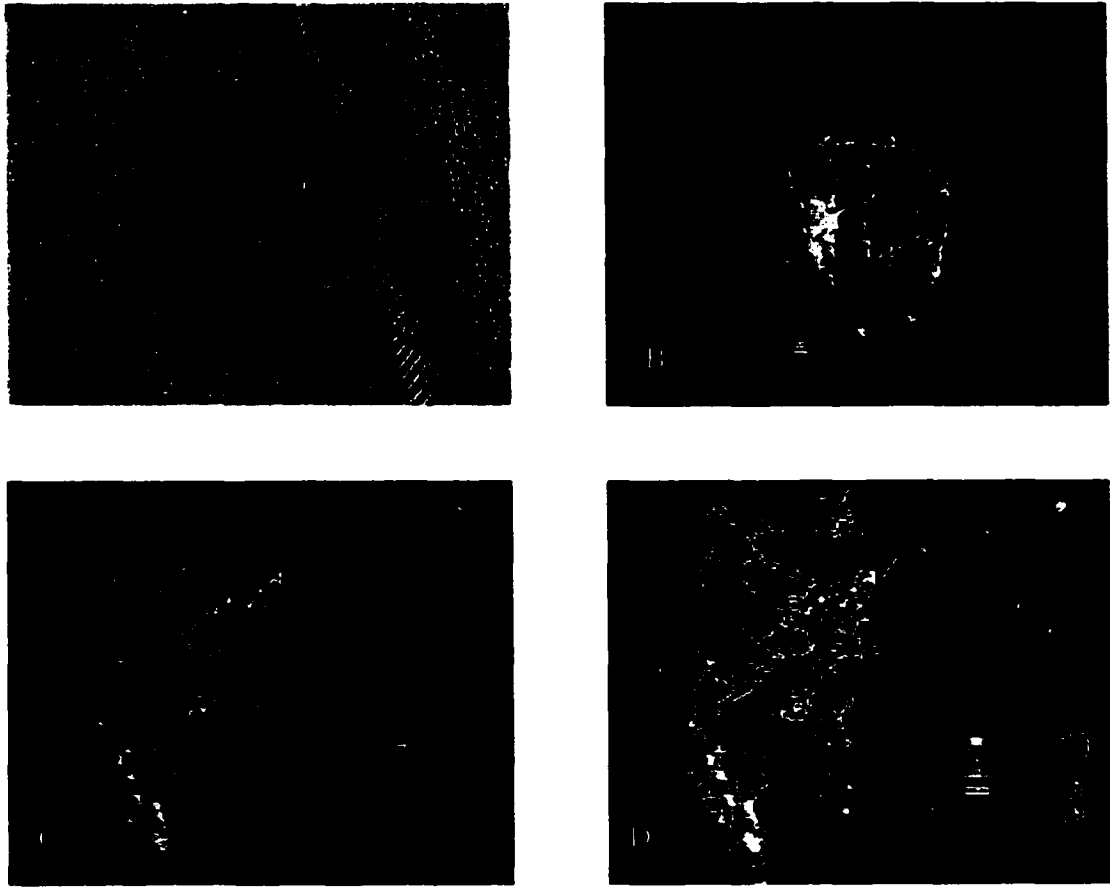
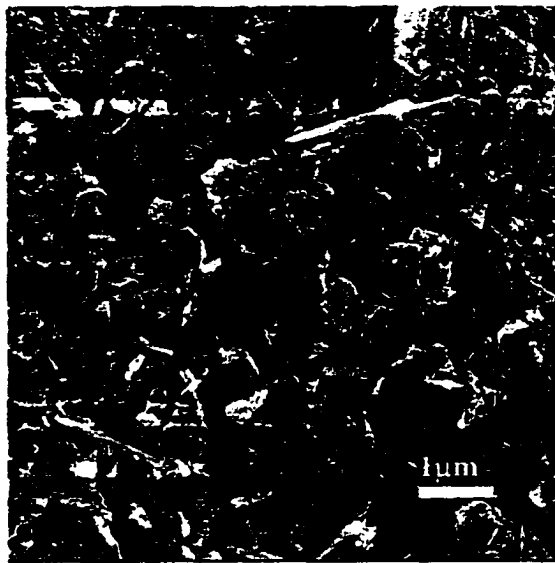


Figure 4.4. Microtome number 5 from an aggregate of Edmonton creosote-contaminated soil. Each microtome had a thickness of 10 μm . A) bright field microscope, B) CSLM, C) the magnified micrograph of the box in B showing the areas of intensity 50-255, D) the same area as C with intensity of 150-255.

4.3.2 SEM

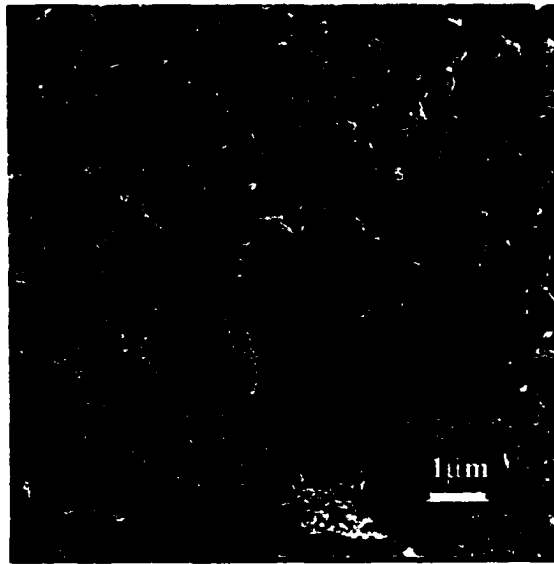
SEM observations gave topographic images with a great depth of field of up to 400 μm for a magnification of X100. Electron micrographs of two different clays along with pristine C-horizon soil and Edmonton creosote-contaminated soil are presented in Figure 4.5. Montmorillonite (4.5A) is composed of aggregates that are made up by association of a number of primary clay platelets. The orientation of hexagonal plates in kaolinite sample (4.5B) clearly shows the plate morphology of kaolinite. Kaolinite consists of a basal surface with multilayer cascade grown on the basal surface. The edges appear flat and angular. Although the C-horizon soil consisted of 50% sand and only 24% clay (4.5C), the clay stacks can easily be distinguished on top of the sand grains. The clay samples and the pristine soil were all characterized with sharp edges and discrete clay aggregates. The boundary between the aggregates was clear and well established. In contrast, the surface of the Edmonton creosote-contaminated soil (4.5D) shows curved morphology. There is no distinguishing border between the particles, although the soil consisted of 50% clay. The images of clay stacks and sharp edges are completely obscured in this micrograph.



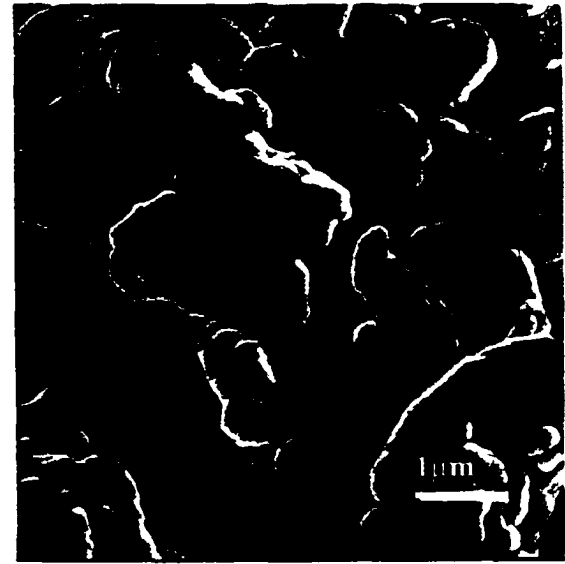
A



B



C



D

Figure 4.5. Electron micrographs of A) Montmorillonite, B) Kaolinite, C) C-horizon soil, D) Edmonton creosote-contaminated soil. For panels A and B the magnification is 11000X, and for panels C and D the magnification is 10000X and 14000X respectively. A, B and C show well defined platelets which are completely obscured in D.

Because of the volatility of the NAPL, the scanning electron microscopy was carried out under cryogenic conditions. The samples were quickly frozen with liquid nitrogen at -180°C and freeze fractured to reveal the interior surfaces of the aggregates. Rapid freezing and fracturing was important to maintain the morphology of the aggregates and provide the detailed association of different components inside the aggregates.

Figure 4.6 illustrates the sample micrographs of different contaminated soils. Under the scanning electron microscope, the surfaces of the particles were covered with a layer of NAPL and had distinct individual morphology. These aggregates were rather round with smooth surfaces and gummy texture. There was no evidence of sharp edges protruding from the aggregates, as was observed in examining pure clays and pristine soil. It was evident that the NAPL was highly associated with clay minerals.

The presence of viscous films of NAPL at the points of contact of clay aggregates was indicated by the presence of curved interfaces. Several examples are indicated by the arrows in Figures 4.6A and 4.6B. The NAPL filled the interaggregate pore spaces. When the aggregates were broken to smaller sub-aggregates, the presence of NAPL on the surface could clearly be identified. The roughness of the mineral surface was filled with organic compounds.

Some samples were frozen in liquid nitrogen at -180°C , but were fractured at room temperature. As a result the frozen NAPL had started to melt at the time of

fracturing. The micrographs of these samples clearly showed the highly viscous texture and stretched gummy materials filling the large pores (Figures 4.6B & 4.6C).

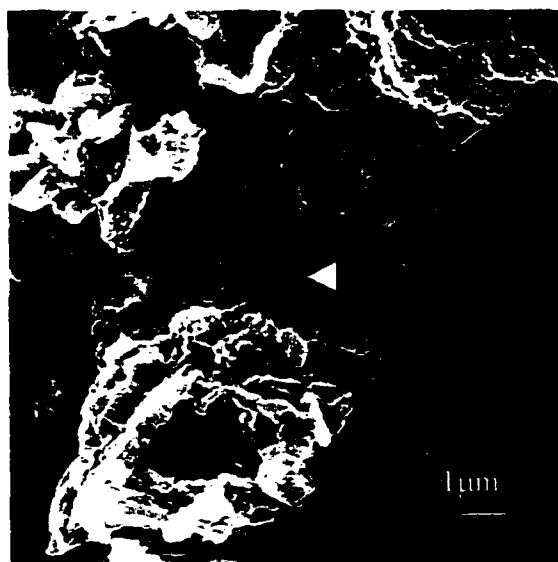
This study was not designed to investigate the microbial inhabitants of the soil, but in fracturing one of the samples a community of soil indigenous microorganisms was uncovered (Figure 4.6D). The microbial population was extensive and the microorganisms were highly associated with soil, which hindered observation of the cells. At some points the cells agglomerated and appeared as colonies rather than individual cells. The cells had a width of 0.6 to 0.8 μm and a length of 3 to 5 μm .



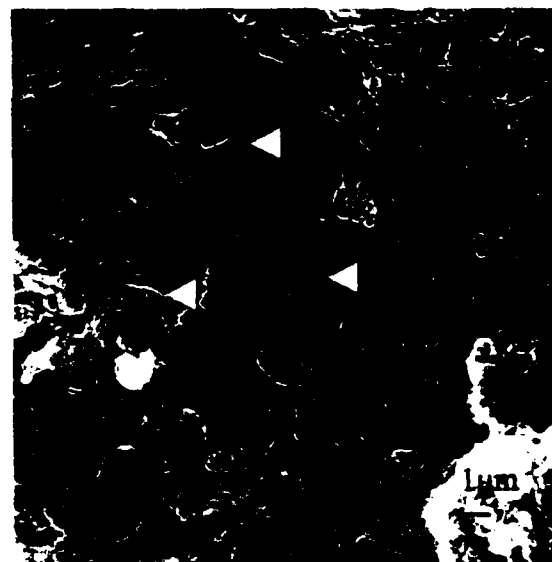
A



B



C



D

Figure 4.6. Electron micrographs of different soil samples, A) Edmonton creosote-contaminated soil (X14000). The undefined edges of the clay and the meniscus appearing at the point of contact of two aggregates are evidences for the presence of oil. B&C) Devon hydrocarbon-contaminated soil (X7000 & X2200). The viscous hydrocarbons filling the macropore spaces, D) Devon hydrocarbon-contaminated soil, (X3300), The image illustrates the macrostructure of cells highly associated with clay (the cells are indicated by arrows).

4.3.3 Elemental analysis and Mapping

The chemical composition on the surface of the fractured aggregates was determined by energy dispersive X-ray (EDX) analysis. The qualitative elemental analysis was carried out on Devon hydrocarbon-contaminated soil to detect the elements incorporated with oil such as carbon and vanadium. The major elements detected by EDX analysis were Si, Al, Fe, Ca, K, which are the common elements associated with clay. This method did not allow detection of target elements either because of low concentration (vanadium) or low atomic number (carbon).

Mapping was performed to visualize the distribution of elements in the soil aggregates. Figure 4.7 displays the maps of important elements in Devon contaminated soil. The most abundant element was Si, the major constituent of clay. The distribution of other elements such as Cl, P and Fe followed the same pattern as Si. It was hypothesized that the sulfur and vanadium content of the oil might be used to detect the organic material in soil. The concentration of sulfur was not high enough to exceed the sulfur content of the soil and for most samples analyzed, the pattern for sulfur distribution was not different from Cl and Si. Some samples showed slightly higher concentration of sulfur in the areas where the viscous organic material covered the clay minerals. The distribution pattern for vanadium could not be distinguished from the background noise as the concentration of this element was very low.

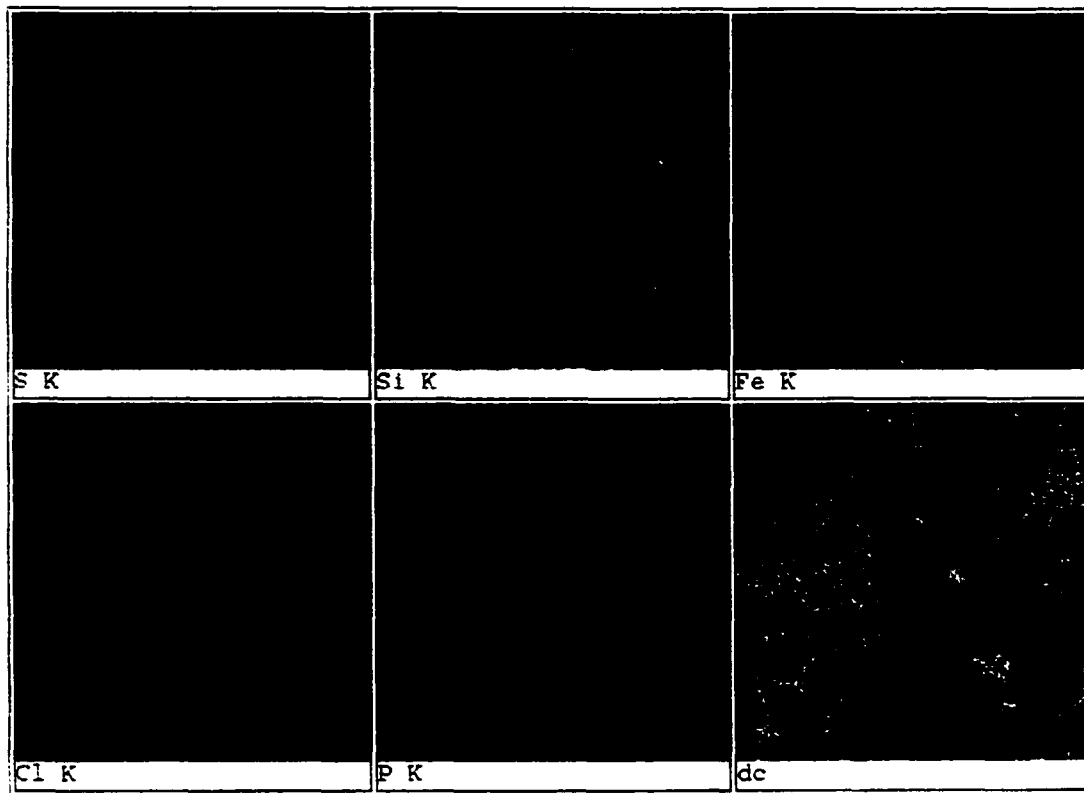


Figure 4.7. A map of Devon hydrocarbon-contaminated soil, which shows the distribution of chemical elements obtained by elemental analysis of EDX. The distribution of Cl, Fe and P followed the same pattern as Si, the major component of clay. S was used as precursor for the presence of organic materials in soil. The map of S shows its relative abundance and similar distribution as Si, Cl and Fe.

4.4 Discussion

A variety of contaminated soils with different textures were examined in this study. Heterogeneous distribution of NAPL was observed in detailed studies of thin sections with CSLM and micrographs of cro-SEM. The sandy soil (Prince Albert) generally had a layer of contaminants on the surface of mineral particles, filling the surface roughness and giving a smooth texture. The 10% clay in this soil acted as a gluing material for the sand grains, along with a considerable amount of contaminants. In Edmonton creosote-contaminated soil with 50% clay, the NAPL materials were not observed as often on the surfaces of large aggregates in the size range of 200 – 900 μm . In contrast, the NAPL was distributed in the aggregates through interaggregate macro-pores. The clay aggregates acted as sponges to accommodate the organic contaminants.

There is a limit for the distribution of NAPL in different pore sizes due to capillary pressure. Hoque et al. (1983) investigated the absorption of water and bitumen on different soil aggregates at 25 °C and 155 °C respectively. Their analysis suggested that absorption of bitumen by soil aggregates showed a good correlation with the porosity due to pores larger than 0.05 μm . Pores smaller than 0.05 μm did not contribute to absorption of bitumen, however, absorption of water took place in all ranges of capillary pores. This observation is consistent with data reported by Lettier et al. (1949). They proposed that absorption of bitumen was very well correlated to the pores of 0.05-0.7 μm . The observations from microscopy were

consistent with penetration of NAPL into pores in the range 0.05-0.7 μm , and formation of a surface film.

Clay aggregates display massive cascade structures, forming aggregates in the range of tens of nanometers to several μm . The pores in these clusters are in the order of angstroms (10^{-4} μm) in diameter and contain immobile interlayer water with different properties than bulk water (Murray and Quirk, 1990). By the action of sedimentation and compaction, the clay clusters or stacks of primary aggregates develop face to face contact with the pores in the range of 0.08 μm as observed by Fernandez and Quigley (1988). Other researchers have reported development of pores 0.02 - 0.1 μm in diameter due to the process of swelling and shrinking induced by sequential wetting and drying. This information is consistent with the observations of Robin et al. (1995), who reported that kaolinite aggregates of 10 μm were oil-wet while the aggregates of 1 μm remained water wet. Our studies of micrographs suggested that the aggregates smaller than 2 μm were glued together by NAPL, forming dense agglomerates of larger size. Small domains of clay with high concentrations of oil were observed. The contaminants appeared as viscous material filling the large pore space between clay stacks and covering the surfaces. This physical structure could easily retain the contaminants.

The distribution of oil and water within the pore structure is not only affected by pore size but is also strongly influenced by mineralogy. Robin et al. (1998) suggested that kaolinite exposed to oil was initially water wet, but after aging for two weeks gave oil-wet network of pores. Other minerals, such as quartz and illite,

remained water wet. They also suggested that carbonate minerals have mixed networks, wherein micro-pores remain water wet while macro-pores become part of an oil-wet network. They hypothesized that upon exposure to oil, the minerals which are initially water saturated become oil saturated in larger pores, while the smaller pores remain oil-free because of insufficient capillary pressure. During aging the polar components of oil are adsorbed to the mineral surfaces and create oil-wet minerals. This network can expand through interaggregate macro and meso-pores. Stallard et al. (1997) reported that the microstructure of the clay particles and the pore size distribution was altered by the presence of polar organic compounds. The migration of polar compounds into the micro-pores collapse the clay pore structure, resulting in flocculation and increase in pore size. This phenomenon leads to lower capillary pressure and higher permeability in clays. The association of polar components of oil with clay minerals at the molecular level is well documented (Flank and Williams, 1995; Murgich and Rodriguez, 1998). The adsorption of asphaltenes on clay minerals was linked to the presence of Al-OH groups at the surface of kaolinite and no interlayer adsorption was observed.

4.5 Model for Distribution of NAPL in Soil Microstructure

Based on the information obtained from CSLM and cryo-SEM, the model in Figure 4.8 is proposed for the distribution of NAPL in the soil microstructure. For this model, the pores smaller than 0.05 μm are classified as micro-pores, pores between 0.05-0.5 μm are classified as meso-pores, pores between 0.5-5 μm are

macro-pores and the pores larger than 5 μm are called mega-pores. Initially the soil is grouped as large aggregates with micropores filled with water, meso- and macro-pores filled with NAPL, and mega-pores filled with air. The viscous NAPL material acts as a gluing agent to hold the aggregate together. After the aggregate is disrupted, the NAPL appears as a film surrounding the micro-aggregates and a filling in the interior meso- and macro-pores. This model suggests that the distribution of NAPL changes from liquid-filled pores for large aggregates, to a surface film for small aggregates. Consequently, the size of the aggregates determines the nature of the diffusion process to liberate the contaminants from NAPL. This model is consistent with the extremely low cation exchange capacity of the creosote-contaminated soil (0.40 mequiv/100 g) compared to the pristine soil (12.1 mequiv/100 g), in spite of higher clay content (41% for creosote-contaminated soil compared to 24% for pristine soil).

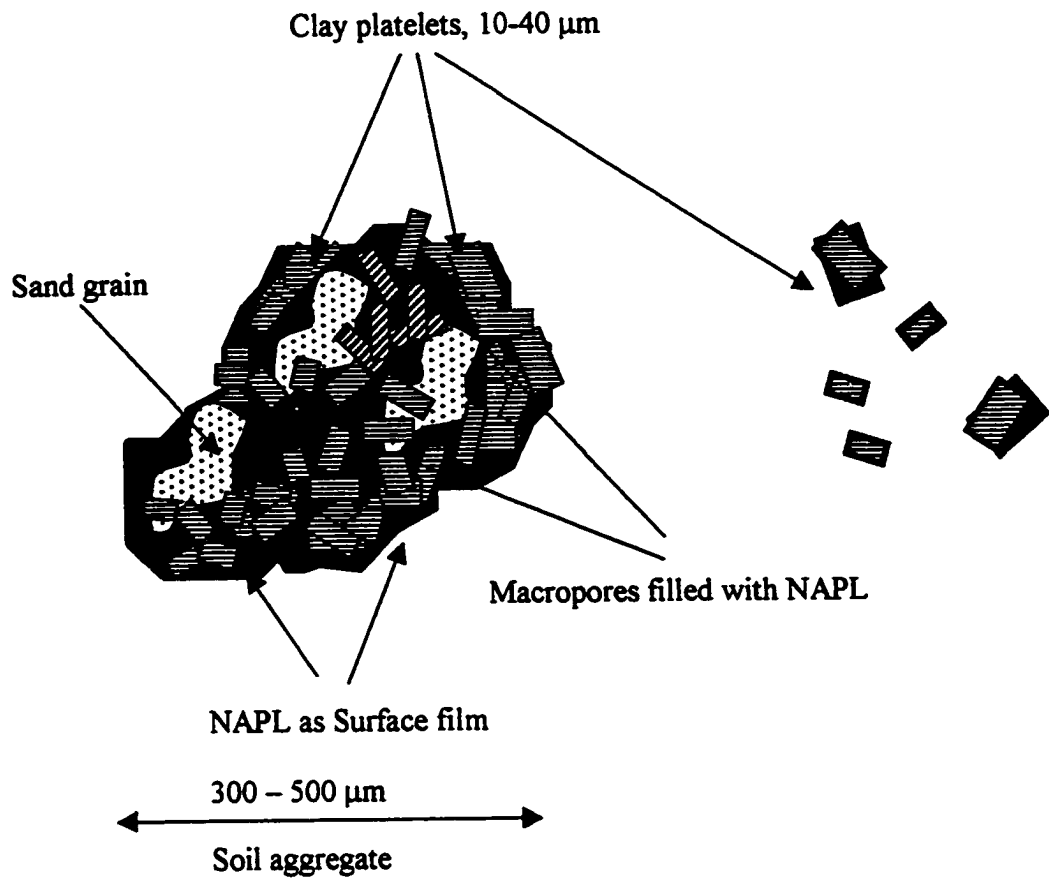


Figure 4.8. Schematic diagram of distribution of NAPL in soil aggregate.

4.6 Conclusion

Two imaging techniques, CSLM and cryo-SEM, were used to examine the microstructure of NAPL associated with soil aggregates. The images from the two techniques gave different but complementary and consistent information on distribution of NAPL in relation to the mineral surfaces. Based on the information obtained, a model was proposed for distribution of NAPL in soil micro-aggregates. The model suggests that NAPL penetrate the macro-pores in the soil, likely in the size range down to at least 0.05 μm . When the aggregates are dispersed the pore NAPL appears as a thin film on the surfaces of the microaggregates.

4.7 Literature cited:

Coles, M.E.; Hazlett, R.D.; Spanne, P.; Soll, W.E.; Muegge, E.L.; Jones, K.W., "Pore level imaging of fluid transport using synchrotron X-ray microtomography" *J. Pet. Sci. and Eng.* 1998, 19, 55-63.

Coles, M.E.; Spanne, p.; Muegge, E.L.; Jones, K.W., "Computed microtomography of reservoir core samples." *Society of Core Analysts Annual Technical Conference*, SCA9401, 1994, 9-16.

Farahani, V.A.; Topper, T.H.; Plumtree, A., 1996. "Confocal laser scanning microscopy measurements of the growth and morphology of microstructurally short fatigue cracks in A1 2024-T351 alloy." *Fatigue and Fracture of Engineering Materials and Structures*. Vol 19, No 9:1153-1159.

Fernande, F.; Quigley, R.M., 1988. "Viscosity and dielectric constant controls on the hydraulic conductivity of clayey soils permeated with water-soluble organics." *Canadian Geotechnical journal*. Vol. 25:582-589.

Bantignies, J.L.; Moulin, C.C.D.; Dexpert, H.; Flank, A.M.; Williams, G., "Asphaltene adsorption on kaolinite: characterization by infrared microspectroscopy and X-ray absorption spectroscopy" *C.R. Acad. Sci., Serie II*. 1995, 320, 699-706.

Haugland, R.P., *Handbook of Fluorescent Probes and Research Chemicals*. Sixth Edition. Molecular Probes, Inc., 1996.

Hoque, A.M.; Cabrera, J.G., "Absorption in manufactured soil aggregates." *J. Trans. Eng.* 1983, Vol. 109, No. 6, 800-814.

Lettier, J.A.; Fink, D.F.; Wilson, N.B.; Farley, F.F., "Mechanism of absorption of bituminous materials by aggregates." *Proceedings, Association of Asphalt Paving Technologists*. 1949, Vol. 18, 278-300.

Li, H.; Wan, W.K., "Investigation of the asphaltene precipitation process from Cold Lake bitumen by confocal laser scanning microscopy." *International Heavy Oil Symposium*. Calgary. AB. CA., 1995, 19-21 June.

Montono, M.; Martinez-Nistal, A.; Rodriguez-Rey, A.; Fernandez-Merayo, N.; Soriano, P., "Microfractography of granitic rocks under confocal scanning laser microscopy." *J. Microscopy*. 1995, Vol. 177, 138-149.

Munoz, V.A.; Mikula, R.J., "Characterization of petroleum industry emulsions and suspensions using microscopy." *J. Can. Pet. Tech.* 1997, 36, No.10, 36-40.

Murgich, J.M.; Rodriguez, J.M., "Interatomic interactions in the adsorption of asphaltenes and resins on kaolinite calculated by molecular dynamics" *Energy & Fuels*. 1998, 12, 339.

Murray, R.S.; Quirk, J.P., "Intrinsic failure and cracking of clay." *Soil Sci. Soc. Am. J.* 1990, 54, 1179-1184.

Postma, J.; Altemuller, H.J., "Bacteria in thin soil sections stained with the fluorescent brightener Calcofluor White MR2." *Soil Biol. & Bioch.* 1989, Vol. 22, No 1, 89-96.

Robin, M.; Rosenberg, E.; Fassi-Fihri, O., "Wettability studies at the pore level: A new approach by use of cryo-SEM." *SPE Formation Evaluation*, Mar 1995, 10 (1), 11-19.

Robin, M; Combes, R; Cuiec, L., "Two SEM techniques to investigate reservoir rock wettability." *J. Pet. Tech.* 1998, Vol. 50, No. 11, 77-79.

Sneider, R.M.; Erickson, J.W., "Rock types, depositional history, and diagenetic effects, Ivishak Reservoir, Prudhoe Bay Field." *SPE Reservoir Engineering*. 1997, Feb., 23-30.

Spanne, P.; Thovert, C.J.; Jaquin, C.J.; Lindquist, W.B.; Jones, K.W., "Synchrotron computed microtomography of porous media: topography and transport." *Phys. Rev. Lett.* 1994, 73 (14), 2001-2004.

Stallard, W.M.; Herbert, B.; Choi, H-C., Corapcioglu, M.Y., "Enhanced migration of gasohol fuels in clay soils and sediments" *Environ. & Eng. Geoscience.*, 1997, 3(1), 45-33.

5. A Diffusion Controlled Model for Intraggregate Mass Transfer

5.1 Introduction

A bioremediation process can be effectively managed and optimized, if the rate limiting step is recognized. A mathematical model is helpful to describe the limiting factors in bioremediation and to predict the outcome of the process. The kinetics of desorption and bioremediation of contaminants from the porous structure of soils and sediments involve a series of biotic and abiotic transport mechanisms. The challenge in developing any mathematical model is to recognize the relative role of all mechanisms and processes involved and justify the simplifying assumptions.

The complexity of the biodegradation of contaminants in soil has led to two types of modeling: experimental models in which the number of variables is reduced and controlled, and mathematical models. The use of experimental models to represent actual contaminated soil can lead to misleading results. For example the common practices of spiking soils with organic contaminants (Geerdink et al., 1996) or adding them to the aqueous phase (Mihelcic and Luthy, 1991) excludes the contribution of NAPL, which is a major concern in contaminated sites. Efroymsen and Alexander (1994), using model NAPLs, reported that the rate of partitioning of phenanthrene from NAPL was slower than the rate of bioremediation. This factor may be even more important in aged contaminated soils, where the NAPL is viscous and transport from one phase to another may be inhibited by surface films. The

physical and chemical properties of dense NAPL (DNAPL) is considerably different from that of model NAPL due to the presence of complex chemical mixtures, the effects of in-situ weathering and the fact that much of the DNAPLs are production process residues and spent materials (Cohen and Mercer, 1993). Consequently, a mathematical model for soil bioremediation must be validated with data from contaminated soil, not just from experimental models.

In most mathematical models, diffusion of contaminants through soil has been considered as the most important transport mechanism (Cooney, 1983; Farrell et al., 1996). In some studies, Michaelis-Menten kinetics are coupled with diffusion equations to express the microbially induced substrate depletion from the aqueous phase (Mihelcic and Luthy, 1991; Fu et al., 1996). Some investigators have observed the biphasic behavior during desorption/bioremediation and reported that the transport of contaminants does not follow a pattern that can be explained as a simple diffusion model. Wu and Gschwend (1986) reported that a pore diffusion model was adequate to describe the adsorption/desorption kinetics for nonpolar organic compounds in soils and sediments. In contrast, Farrell et al. (1994) using model solids with uniform pore and particle size, suggested that a pore diffusion model was not adequate to describe both the fast and slow desorbing fractions of organic contaminants. So far, all the mathematical models developed based on pore diffusion assume that the contaminants diffuse through the aqueous phase in the pores of the soil matrix.

Karickhoff (1980) and Cornelissen et al. (1998) suggested two compartment models to describe desorption of contaminants from soils and sediments. These models include two rate constants or diffusion coefficients to accommodate the fast and slow desorbing regimes. This type of analysis, however, is largely empirical and does not necessarily have a mechanistic meaning. The amount of slowly desorbing material cannot be determined from any independent experiments, only from the kinetics.

In our study, as reported in Chapter 3, soil was sonicated to reduce the aggregate size and experiments were carried out with sonicated samples to study the influence of aggregate structure on the biodegradation rate. This study revealed that bioavailability is primarily controlled by diffusion. Reducing the aggregate size increased the rate of degradation, however, the extent of degradation was not improved significantly. The data implied that at some point sonication was no longer effective because the microstructures that were responsible for diffusion limitations were no longer affected by sonication.

The objective of this study was to develop a mathematical model based on physical principles that could explain the mechanism of fast and slow modes of biodegradation in slurry phase reactors. This model was based on:

- 1- The experimental data on biodegradation of creosote-contaminated soil in the slurry phase reactor

2- The results of microstructure analysis on the distribution of NAPL in soil aggregates

As mentioned in Chapter 3, three distinct phases of kinetics were observed in the degradation of PAHs in slurry phase reactor. An initial lag phase was followed by a high rate of degradation and finally a low rate of degradation. The intrinsic microbial activity limited degradation of contaminants in the first phase of bioremediation. The numerous growth substrates in the NAPL could result in either competitive inhibition of the high molecular weight PAHs or catabolic repression, leading to the kinetic behavior which was observed in the first phase. This model for the diffusion controlled mechanism was applied to biodegradation kinetics through the subsequent fast and slow phases of degradation, where the sonication experiments had demonstrated the dependence of degradation rate on the size of soil aggregates.

5.2 Theory

5.2.1 Mass Transfer in Soil Aggregates

A mathematical model was developed based on previous studies on the microstructure of contaminated soils, and the distribution of NAPL presented in chapter 4. We assumed that the fast phase of degradation was due to desorption of contaminants from a film of NAPL surrounding the aggregates. The slow phase was due to the portion of NAPL trapped in mesopores ($0.05 \mu\text{m} < D_p < 0.5 \mu\text{m}$) and macropores ($0.5 \mu\text{m} < D_p < 5 \mu\text{m}$) that were not disrupted by the forces of sonication or

agitation. In both cases, diffusion of contaminants through the NAPL phase controls transport. Desorption of contaminants from such a physical system would generate bimodal behavior in bioremediation kinetics. The aggregates were approximated as spheres with a thin film of NAPL surrounding the sphere.

It was assumed that no biodegradation takes place inside the aggregates and the active biodegradation only occurs in the biofilm surrounding the surfaces of the soil aggregates or in the aqueous phase. The general form of Fick's law of diffusion applies for such systems and for a non-steady state condition can be expressed as (Bird et al. 1960):

$$\frac{\partial C}{\partial t} = D_{eff} \nabla^2 C \quad (5.1)$$

C = concentration of component A

D_{eff} = effective diffusivity

t = time

Equation 5.1 describes the concentration of solute in NAPL as a function of time and position. The analytical solution for equation 5.1, for the case of zero initial concentration and constant surface concentration, is provided by Carslaw and Jeager (1959). The solutions have been modified to meet the boundary conditions of our system (the details on developing the governing equations for the model has been explained in Appendix C, sections C.1. and C.2.). The volume average

concentrations for average concentration in the pores (\bar{C}_p) and in the film (\bar{C}_f)

diffusion are expressed by the following equations:

$$\bar{C}_p = C_s \left(1 - \frac{6}{\pi^2}\right) \sum_{n=1}^{\infty} \frac{1}{n^2} e^{-D_{eff} \pi^2 n^2 t / R^2} + C_0 \quad (5.2)$$

$$\bar{C}_f = \frac{8C_0}{\pi^2} \sum_{n=0}^{\infty} \frac{1}{(2n+1)^2} e^{-D_{NAPL} (2n+1)^2 \pi^2 t / 4l^2} \quad (5.3)$$

C_0 = initial concentration, mg of component A/kg of soil

D_{NAPL} = Diffusivity of component A in NAPL, cm²/s

D_{eff} = effective diffusivity in NAPL filled pores, cm²/s

R = the radius of soil aggregate, cm

l = film thickness, cm

Equations 5.2 and 5.3 are based on the following boundary conditions:

$$C_p(R, t) = 0 \quad (5.4)$$

$$C_f(l, t) = 0 \quad (5.5)$$

and the following initial condition:

$$C_p(r, 0) = C_0 \quad (5.6)$$

$$C_f(l, 0) = C_0 \quad (5.7)$$

The model assumes a uniform initial concentration of contaminants within the aggregates and a zero concentration at the surface of the aggregates at any time $t > 0$, because the biological activity reduces the aqueous phase concentration to negligible levels. This boundary condition provides the maximum driving force for diffusion in

soil aggregates. The required model inputs are aggregate size, initial concentration and thickness of the film of NAPL.

The effective diffusivity D_{eff} is defined by the following equation:

$$D_{eff} = \frac{D_{NAPL} \varepsilon_t}{\tau \varepsilon_{NAPL}} \quad (5.8)$$

$$\varepsilon_t = \varepsilon_{NAPL} + \varepsilon_{aq} \quad (5.9)$$

The concentration of the contaminants in the soil at any time ($t \geq 0$) can be expressed by a two compartment model consisting of NAPL film and NAPL pores, giving the residual concentration of contaminants in the soil at any time in the process of bioremediation.

$$\bar{C} = a \frac{A(t)}{A_{max}} \bar{C}_f + (1 - a \frac{A(t)}{A_{max}}) \bar{C}_p \quad (5.10)$$

A_{max} is the maximum external surface area of soil microaggregates available for mass transfer. $A(t)$ is the available external surface area for mass transfer at any time t and a is an adjustable parameter to correct for the available surface area. The coefficient $a \frac{A(t)}{A_{max}}$ corresponds to the fraction of NAPL that exists as a film surrounding the aggregates at any time t . For a sonicated soil $A(t)/A_{max}$ is equal to one. For non-sonicated soil in the bioreactor this ratio is a function of time as the aggregates break down continuously and the surface area for mass transfer increases over time. $A(t)$ and A_{max} were determined from experimental data. Values of D_{NAPL}

over time. $A(t)$ and A_{max} were determined from experimental data. Values of D_{NAPL} and α , as adjustable parameters, were determined by non-linear regression and by minimizing the sum of squared residuals between experimental and calculated values of \bar{C} in equation 5.10.

5.3 Results and discussion

5.3.1 Feasibility of the Model

The total porosity in a clean soil consists of air-filled porosity and water-filled porosity, however in the contaminated soil and the model we are considering a third type of porosity defined as NAPL-filled porosity. As mentioned in chapter 4, the microstructure analysis of distribution of NAPL in soil aggregates revealed two distinct physical structures: a NAPL film surrounding the aggregates and pores filled with NAPL. Diffusion of contaminants through the pore structure will take place through NAPL for the pores filled with this material, however, at some point during their journey the contaminants might pass through water-filled pores. In this model, we do not consider the diffusion through water-filled pores and we justify it by the following reasoning:

Different empirical models such as Stokes-Einstein equation, Wilke-Chang correlation and Tyn-Calus correlation (Reid et al., 1987) predict that diffusivity is inversely correlated to viscosity ($D \propto \mu^{-1}$). Some researchers have proposed that the relation may not hold for diffusion of solutes in viscous solvents. Davies found that diffusion coefficient of CO_2 in various solvents ranging in viscosity 1-27 cP (10^{-3}

kg/m.s) is in the form of $D \propto \mu^{-0.45}$. Hiss and Cussler (1973) studied diffusion of naphthalene through hydrocarbon oils, ranging in viscosity between 0.5 – 5000 cP. They suggested the following correlation for high viscosity liquids:

$$D \propto \mu^{-0.69} \quad (5.11)$$

Equation 5.11, as well as other empirical correlations, suggests that increasing the viscosity of the solvent will reduce the diffusion coefficient. For example diffusion coefficient of naphthalene in benzene ($\mu = 0.63$ cP) will drop from 1.19×10^{-5} cm²/s to 8.74×10^{-8} cm²/s in oil with viscosity of 1000 cP. It is reasonable to conclude that diffusion through the aqueous phase will at least be 100 times faster than oil with viscosity of 1000 cP. The viscosity of creosote can be in a wide range depending on the sources and composition as tabulated in Table 5.1. The presence of polychlorinated biphenyl compounds in the mixture can increase the viscosity significantly (Cohen and Mercer, 1993).

Table 5.1. Kinematic viscosity of NAPL from different sources

Source	Kinetic Viscosity, cP
Creosote (85% PAHs, 10% phenolic compounds, 5% N-, S- and O- heterocycles (Cohen and Mercer, 1993)	10 - 70
polychlorinated biphenyl compounds (Cohen and Mercer, 1993)	1900 - sticky resin
Coal tars (Lee et al., 1992, Ripp et al., 1993)	34 – 6600 @ 40°C
Hydrocarbon oils (Hiss and Cussler, 1973)	0.5 – 5000 @ 25°C

This simple analysis shows that diffusion coefficients of PAHs in water ($\mu = 1$ cP at 25° C) will be significantly higher than diffusion in typical NAPL. Thus, resistance to mass transfer in aqueous phase is negligible compared to resistance in NAPL if the diffusion lengths are comparable and as the molecules diffuse out of NAPL they will diffuse out of the aqueous phase at much accelerated rate. Therefore we can justify the assumption that diffusion through NAPL is the rate controlling step, rather than diffusion in aqueous phase as suggested by other researchers (Ghoshal et al. 1996; Mukherji et al, 1997). This analysis is consistent with the observation of Weber and Miller (1988) that in a well mixed system, resistance to external mass transfer was not significant compared to intraparticle diffusion, however they suggested that film diffusion may have a role in studies of packed columns. Ortiz et al. (1999) studied dissolution of PAHs from non-aqueous phase liquids with a wide range of viscosity. They concluded that dissolution of PAHs from highly viscous NAPLs such as petrolatum, paraffin and transmission oil was limited by transport in NAPL, and further, they observed a decrease in release of PAHs from NAPL with time.

5.3.2 Aggregate size Distribution and Corresponding Surface Area

The values of A_{max} and $A(t)$ were calculated from data for aggregate size. During bioremediation, slurry samples were taken from the bioreactor at different time intervals and particle size analysis was performed. Figure 5.1 illustrates the variation of different fractions of aggregates in bioremediation process. The most

dramatic change was observed in the aggregates $D_p < 38$ (μm), $1.981 > D_p > 991$ (μm) and $991 > D_p > 495$ (μm). The mass fraction for the four other size ranges remained almost constant. The mass fraction of the aggregates smaller than $38 \mu\text{m}$ showed an exponential increase, while the aggregates $1.981 > D_p > 991$ (μm) and $991 > D_p > 495$ (μm) had an exponential decrease in their mass fractions.

$$m_{D_p < 38} = 60.95 - 45.63e^{(-0.488t)} \quad (5.12)$$

$$m_{1.981 > D_p > 991} = 3.62 + 18.80e^{(-0.16t)} \quad (5.13)$$

$$m_{991 > D_p > 495} = 8.60 + 12.13e^{(-0.317t)} \quad (5.14)$$

The mass average diameter of the aggregates was determined in chapter 3 as:

$$D_{mean} = 182.61 + 414.66e^{(-0.22t)} \quad (3.1)$$

Cooney et al. (1983) suggested that the arithmetic average aggregate size should not be used in diffusion equations when a range of particle sizes exist. In our analysis we concluded that a mass average diameter was not a proper length scale to be used in diffusion equation when a wide range of aggregates existed, thus the average aggregate size in each sieve fraction and corresponding mass fractions were used in calculations. Further, our analysis showed that for sonicated soil more than 95% of the external surface area available for mass transfer originated from the fraction of aggregates in the size range less than $38 \mu\text{m}$.

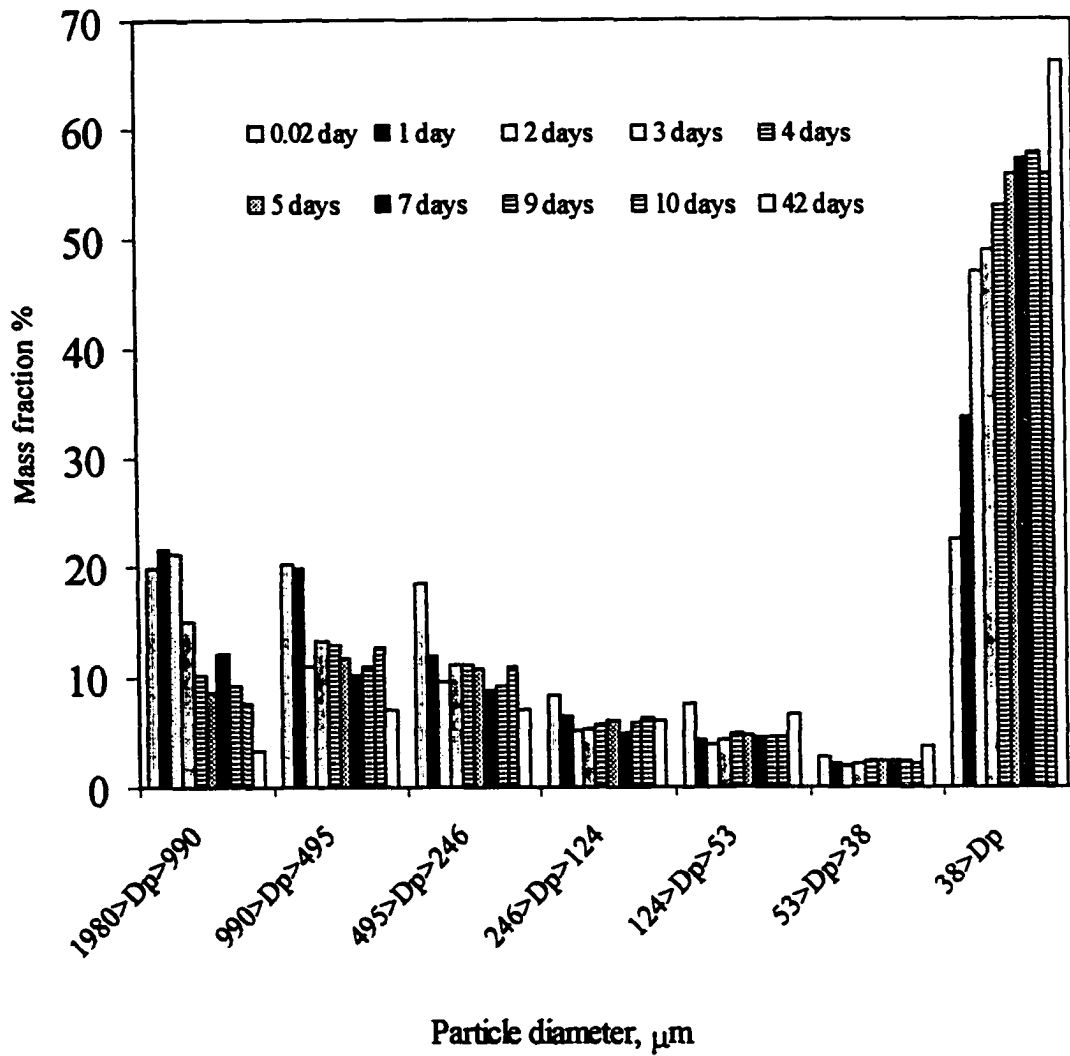


Figure 5.1. Aggregate size distribution in the process of bioremediation of Edmonton creosote-contaminated soil in slurry phase bioreactor

5.3.3 Determination of Model Parameters

Diffusivity of PAHs in NAPL (D_{NAPL}) and α , the correction factor for the available aggregate surface area for mass transfer, were the two adjustable parameters in this model. The value of $A(t)/A_{max}$ was calculated from the aggregate size distribution data and based on the surface area of the aggregates in different size fractions. The adjustable parameters were determined by non-linear regression (Nedler-Mead simplex method) and by minimizing the sum of squared residuals between experimental and calculated values of \bar{C} in equation 5.10. The average values of D_{NAPL} and $\alpha \frac{A(t)}{A_{max}}$ obtained from two experiments with sonicated soil were averaged and listed in Table 5.2 along with D_{NAPL} obtained from experiments with non-sonicated soil and the corresponding aqueous diffusivities for six PAHs. $\alpha \frac{A(t)}{A_{max}}$ represents the fraction of NAPL which is present as a film around the soil aggregates. This value ranged from 0.83 to 0.98 with an average of 0.9 for sonicated soil. For non-sonicated soil, $\alpha \frac{A(t)}{A_{max}}$ is a function of time. As the aggregates break down, an increasing fraction of NAPL appears as a film. The final values of $\alpha \frac{A(t)}{A_{max}}$ for non-sonicated soil are presented in Table 5.2. The data of Table 5.2 show that the calculated values for all PAHs are in close agreement, except for anthracene. Figure 5.2 shows the variation of $\alpha \frac{A(t)}{A_{max}}$ as a function of time for the average value of

$\alpha=1.1$ obtained from the data on non-sonicated soils, excluding the data on anthracene.

Table 5.2. Model Parameters Estimated from Experimental Data on Edmonton Creosote-Contaminated Soil¹

PAH	D in water ² ($\text{cm}^2/\text{s} \times 10^6$)	D_{NAPL} ($\text{cm}^2/\text{s} \times 10^{14}$)		$\alpha \frac{A(t)}{A_{\max}}$, film fraction of NAPL	
		Sonicated	Non-sonicated	Sonicated	Non-sonicated Final Value
Acenaphthene	5.9	4.5	1.9	0.95	0.92
Phenanthrene	5.8	4.4	1.8	0.98	0.88
Anthracene	5.9	2.0	4.8-13.1 ³	0.85	0.23-0.60 ³
Fluoranthene	5.8	4.8	0.84	0.95	0.99
Pyrene	5.6	4.4	1.1	0.86	0.89
Chrysene	5.1	2.3	0.52	0.83	0.86
Mean	5.7	3.8	1.6	0.91	0.91 ⁴
SD	0.29	1.6	1.2	0.06	0.07

1. The values of D_{NAPL} and $\alpha \frac{A(t)}{A_{\max}}$ are the average of the data obtained in parallel experiments with sonicated and non-sonicated soil.
2. Calculated from Wilke-Chang correlation.
3. The data on anthracene in non-sonicated soil were scattered.
4. The data on anthracene are not included in calculation of mean value in non-sonicated soil.

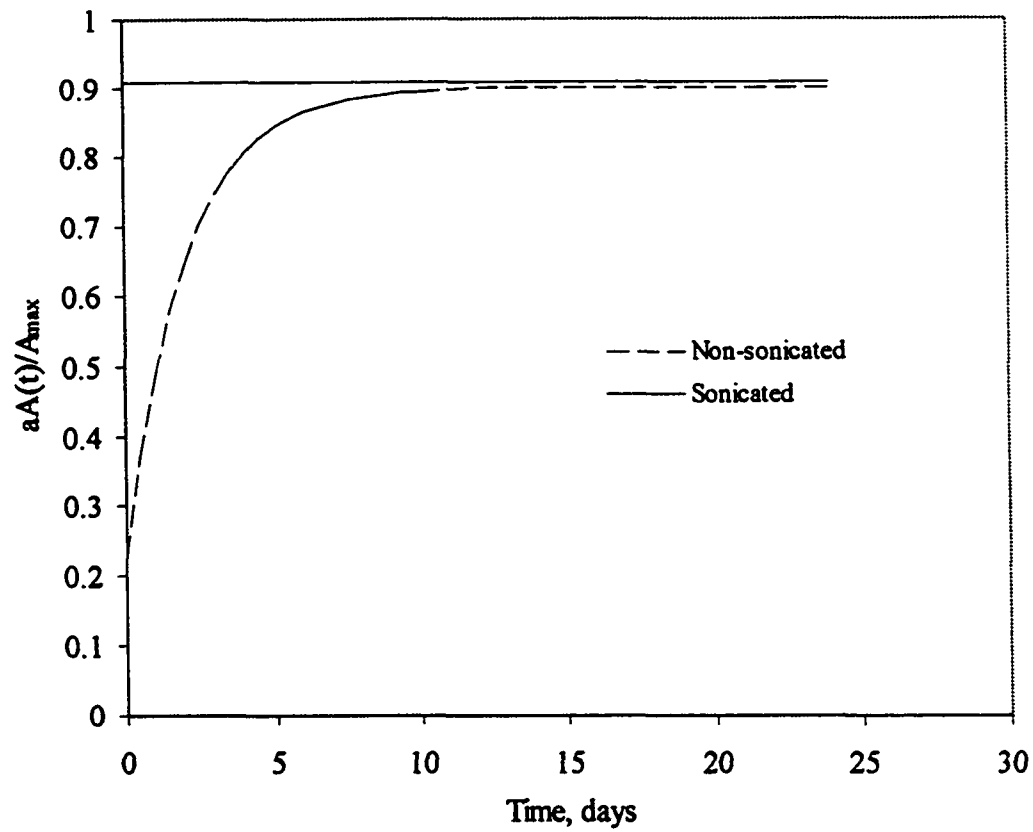


Figure 5.2. Variation of $aA(t)/A_{max}$ for non-sonicated soil during slurry phase bioremediation

Figures 5.3 and 5.4 show the experimental data for degradation of 6 PAHs and the corresponding model predictions. Good agreement between experimental data and model predictions is observed. As mentioned earlier the model applies only to phase two and three of the degradation curves i.e. from the point where the maximum rate of degradation started.

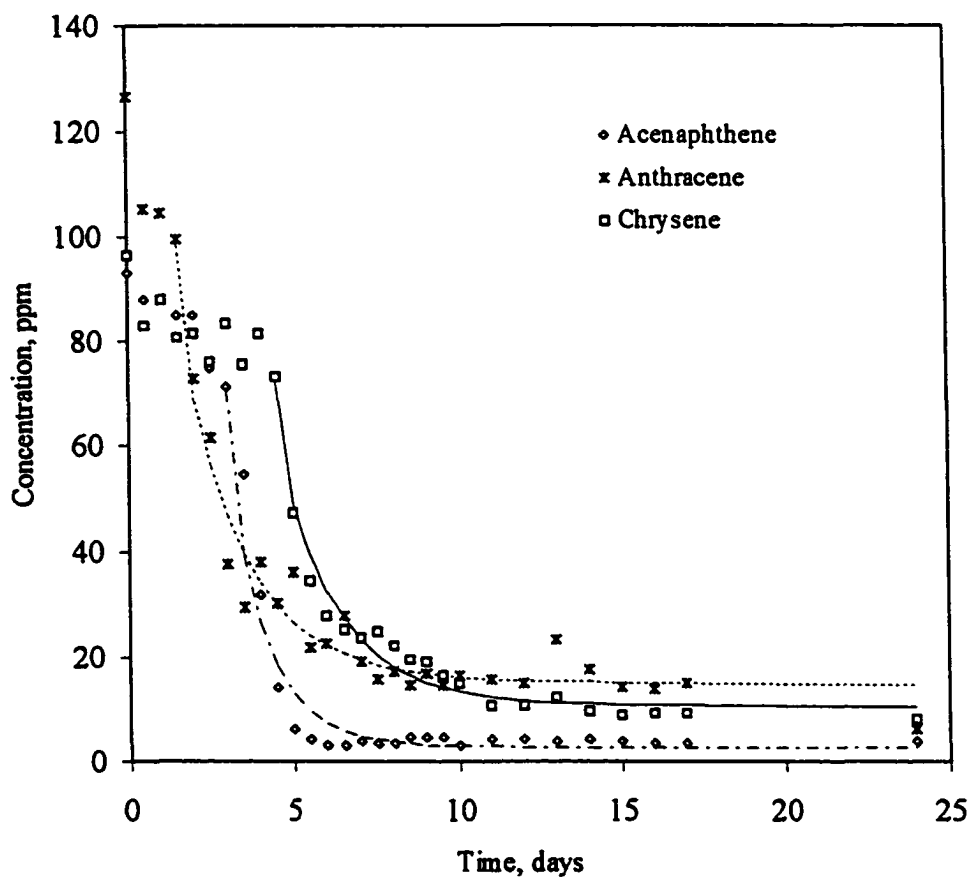


Figure 5.3. Time course of concentration of acenaphthene, anthracene and chrysene during bioremediation of Edmonton creosote-contaminated soil (sonicated) in slurry phase reactor. The solid lines were calculated from equation 5.10 using the data of Table 5.2 for diffusivity and fraction of NAPL in films

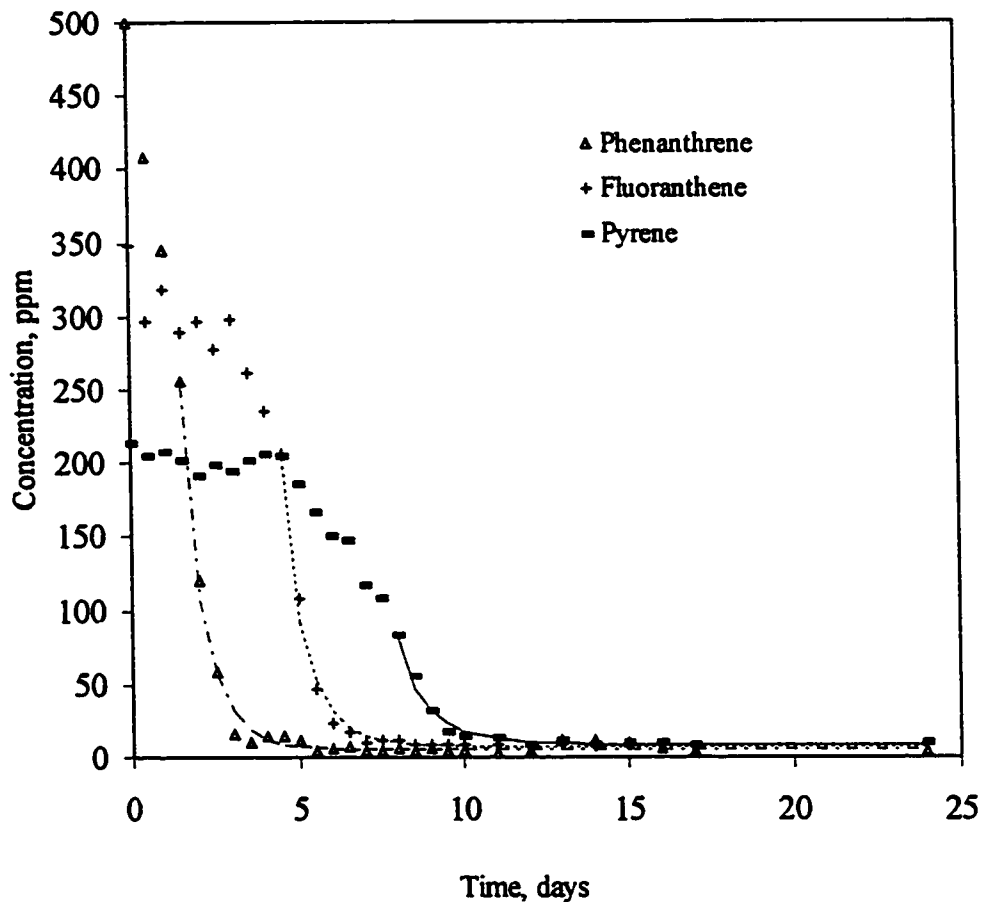


Figure 5.4. Time course of concentration of phenanthrene, fluoranthene and pyrene during bioremediation of Edmonton creosote-contaminated soil (sonicated) in slurry phase reactor. The solid lines were calculated from equation 5.10 using the data of Table 5.2 for diffusivity and fraction of NAPL in films

5.3.4 Estimated Diffusion Coefficients in NAPL

The first column in Table 5.2 shows the diffusion coefficients of six target PAHs in water. The aqueous diffusivities of PAHs were estimated from the Wilke-Chang correlation (Reid et al., 1987). These values are within 5% and there is no significant difference in aqueous diffusivity of the PAH homologous series. The calculated diffusivity of PAHs in NAPL was lower than their aqueous diffusivity by eight orders of magnitude. Excluding anthracene and chrysene, the diffusivity of the four PAHs (acenaphthene, phenanthrene, fluoranthene and pyrene) in NAPL fall within 4% of each other. This result is consistent with the variation of diffusivity of PAHs in water and with the dependence of diffusivity on molecular size. The diffusivity of anthracene and chrysene was significantly lower than their homologues (t test with 95% confidence). Similarly, the diffusion coefficients obtained from the non-sonicated experiments were significantly lower than the values obtained from sonicated experiments (t test with 95% confidence, excluding anthracene). Despite the variations between the diffusivity of different PAHs in sonicated and non-sonicated soils, both sets of data for D_{NAPL} are in the same order of magnitude for all components, which is in agreement with suggested correlations. However, Ortiz et al. (1999) reported two orders of magnitude difference in diffusivity of phenanthrene and pyrene in paraffin.

Physical structure and the shape of the molecule (Rogers et al., 1972) can have an impact on reducing the diffusivity of PAHs. Branched molecules, such as benzene with various functional groups, were suggested to have lower diffusivity in

polymers than unbranched molecules as they have potential for entanglement with polymer mesh (Brusseau et al., 1991).

5.3.5 The Effect of Solvent Molecular Weight and Viscosity

Creosote is a complex mixture that contains hundreds of organic compounds with different structures and physical properties. Haeseler et al. (1999), performing an analytical characterization on MGP contaminated soils, reported that the composition of organic matter in contaminated sites were qualitatively very similar to the composition of coal tar but with a lower proportion (28%) of total extractable organics and lower PAH content. The PAHs represented 10% of the total extractable fraction, 15% represented the resins and 3% were classified as other extractable organics. Such a combination, along with 72% non-extractable organic compounds, can have a very high viscosity. These data are consistent with our analysis where only 40% of the organic material was extractable by dichloromethane in creosote-contaminated soil. The measured viscosity of the extracts from creosote-contaminated soil used in our study was in the range of 1000 – 6000 cP (Table 5.3) for extractable free flowing organic matters. All viscosity measurements were performed on dichloromethane extractable materials using a Carri-Med CLS controlled stress rheometer. There is no method to measure the viscosity of non-extractable fraction, which is considered as semi-solid compounds or dense polymers. Obviously if we include the 60% non-extractable organic material, the viscosity of the resultant mixture may be in the range of 10000 – 530000 cP as was measured for the coal tar.

Such a high viscosity NAPL can reduce the diffusivity up to 3 – 4 orders of magnitude.

Table 5.3. Measured kinematic viscosity of creosote

Source	Kinetic Viscosity, cP
Non-bioremediated extract, creosote-contaminated soil	1000 @ 25°C
Free-flowing extract obtained from bioremediated creosote-contaminated soil	6000 @ 25°C
Coal tar	10000 @ 25°C
Coal tar (heated for 10 minutes at 60 °C)	530000 @ 25°C

5.3.6 Time Dependent Diffusivity

It is important to realize that the model assumed constant effective diffusivity. This is a simplistic assumption because transport of PAHs from NAPL can be substantially reduced by decreasing the effective diffusivity over time (Ortiz et al., 1999). The composition of NAPL changes continuously in the process of bioremediation as certain components are preferentially degraded and secondary metabolites are produced and deposited. The trend in NAPL composition leads to higher molecular weight compounds with higher viscosity that eventually decelerates the diffusive transport process. Rutherford et al. (1997) reported an increase of 36% in average molecular weight of dichloromethane extractable materials after bioremediation. The removal of PAHs during bioremediation, therefore, would tend to decrease D_{eff} with extent of bioremediation.

5.3.7 Formation of Semi-rigid Film on the Surface of NAPL

Some investigators have observed the development of a semi-rigid interfacial film at the interface of coal tar and water (Luthy et al, 1993, Nelson et al., 1996). Similar observations have been reported in crude oil-water systems (Dabros et al, 1999). Crude oil contains many surface-active components that accumulate at the oil-water interface to form adsorbed layers. In particular, adsorption of high molecular weight polar molecules, such as asphaltenes and resins, at the oil-water interface results in the formation of the films (Luthy, 1993). This film has been referred to as an interfacial skin or semi-rigid film. It behaves as a paper bag, as it crumples upon withdrawing the liquid inside and forms a spherical shape when more liquid is injected. The presence of such a film can play an important role in limiting mass transfer rates by adding an additional resistance to mass transfer. Such a resistance may contribute to the very low apparent diffusivity in NAPL in aged contaminated soils as observed in our model. Such films would be broken when shear force is applied, particularly in sonicated soil. This breakage and disruption of surface films would give higher D_{NAPL} in sonicated soil than non-sonicated soil, consistent with the data of Table 5.2.

5.3.8 Comparison of Diffusion Coefficients in NAPL with Literature Values

Diffusion controlled mechanisms in adsorption/desorption of organic compounds from soils and sediments has been the subject of a large number of studies. Some researchers have suggested that diffusion within soil organic matter

(SOM) (Brusseau, 1989, 1991, Pignatello, 1993) is the controlling mechanism while others have considered that diffusion within microporous mineral compounds (Ball, 1991; Miller, 1992; Wu, 1986) was responsible for retarded diffusion in natural sediments. A comparison between the diffusion coefficients obtained in each case show orders of magnitude differences. Pignatello and Xing (1996) suggested that diffusion coefficients from soil organic matter are in the range of 10^{-17} cm²/s or less and that the soil particle size should not affect desorption from such polymer structures. They concluded that the diffusion length for soil organic matter is in the range of 30 – 1000 nm. Diffusion in dense non-aqueous phase liquids such as creosote and coal tar are analogous to diffusion in soil organic matter because they have very complex composition consisting of asphaltene molecules and many other large undefined structures. Such structures have even larger partition coefficients than SOM (Rutherford et al., 1997), and may well retain the non-polar molecules such as PAHs leading to low diffusivities.

A few researchers have attempted to evaluate the diffusion coefficients in NAPL. Reported diffusivity values range over many orders of magnitude, from 10^{-6} to 10^{-21} . Diffusivity in this case is sensitive to the viscosity of NAPL as well as its composition. Table 5.3 summarizes the diffusion coefficients reported in different studies and covers diffusion in SOM, pore diffusion and diffusion in different NAPLs.

The diffusion coefficients obtained in this study were in the range of 1×10^{-14} to 4×10^{-14} cm²/s which is lower than the range obtained for diffusivity of PAHs in

various oil fractions. The diffusivities obtained in our study are at least two orders of magnitude lower than the data obtained by Ortiz et al. (1999), which may be attributed to higher viscosity of aged NAPL in contaminated soil.

Table 5.4. Diffusion coefficients of organic compounds in different media

Sample	Diffusion Coefficient, cm^2/s
Polychlorinated biphenyls in river sediments (Carroll, 1994)	$2.6 \times 10^{-18} - 7.3 \times 10^{-21}$
Naphthalene, phenanthrene and pyrene in petrolatum	$1.4 \times 10^{-8} - 4.5 \times 10^{-11}$
Naphthalene, phenanthrene and pyrene in transmission oil	$3.3 \times 10^{-9} - 6.2 \times 10^{-12}$
Naphthalene, phenanthrene and pyrene in paraffin Ortiz (1999)	$1.8 \times 10^{-9} - 7.1 \times 10^{-12}$
Lindane in water (Mott et al., 1991)	6.3×10^{-6}
Lindane in sand (Mott et al., 1991)	1.8×10^{-6}
Phenol in soil slurry (Fu et al., 1996)	$0.6 \times 10^{-5} - 4.5 \times 10^{-5}$
Lindane in subsurface sand (Miller, 1992)	1.47×10^{-11}
2,3,7,8-tetrachlorodibenzo-p-dioxin (Overcash, 1991)	
in ethyl oleate	$1.6 \times 10^{-6} - 2.2 \times 10^{-6}$
in ethyl oleate and soil	$1.8 \times 10^{-7} - 5.6 \times 10^{-7}$
in dimethyl sulfoxide	5.0×10^{-6}
in dimethyl sulfoxide and soil	$1.0 \times 10^{-6} - 1.5 \times 10^{-6}$
n-hexane in liquid hydrocarbons ($\mu = 0.5 - 5000$ cP)	$2.6 \times 10^{-5} - 5.5 \times 10^{-8}$
naphthalene in liquid hydrocarbons ($\mu = 0.5 - 5000$ cP) (Hiss & Cussler, 1973)	$2.37 \times 10^{-5} - 3.9 \times 10^{-8}$

5.3.9 Analogy to Diffusion in Polymers

The low diffusivity of PAHs in NAPL has encouraged researchers to look for explanations and find analogies for such systems. As a result, diffusion of contaminants in soil organic matter and humic materials has been compared to diffusion in polymers (Brusseau and Rao, 1991, Carroll, 1994; Oritz, 1999). Soil organic matter consists of complex humic substances with molecular weight ranging from 300 to 200000 (Carroll et al., 1994) which places them in the same class as synthetic polymers. There is very little information on diffusion in humic polymers (Pignatello, 1989; Ball, 1991) however, diffusion of low molecular weight substances in synthetic polymers has extensively been studied (Crank, 1968; Gusev et al. 1994). The rate of diffusion through organic materials and organic polymers is a function of the nature of the polymer (glassy or rubbery), the forces holding the polymer chain together and the size and shape of the diffusing molecule. Carroll et al. (1994) have used a two compartment model to describe the labile fraction and the resistant fraction of polychlorinated biphenyls in desorption from sediments. They simulated the soil organic matter in sediments as humic polymers containing both glassy and rubbery polymer fractions and applied a permeant/polymer diffusion model (Salame, 1986) to obtain diffusion coefficients of 7.3×10^{-21} cm²/s and 2.6×10^{-18} cm²/s for diffusivity of polychlorinated biphenyls in Hudson River sediments. These values for diffusion coefficients are much smaller than any published data on diffusion through NAPL or soil organic matter.

The data obtained in this study fall in between the diffusivity observed in various oil fractions and in polymers, which is reasonable given the physical and chemical properties of the aged NAPL. The 40% extractable fraction of NAPL has oil-like properties while the 60% non-extractable fraction demonstrates polymer properties. Such a combination may lead to intermediate transport properties as was observed here.

5.3.10 Fraction of NAPL as a Film

The last two columns in Table 5.2 show another parameter which was estimated by the model, corresponding to the fraction of NAPL that coated the aggregates as a film, predominantly the aggregates smaller than 38 μm . The parameter estimated from sonicated soil shows an average of 90% of NAPL as a film. Vigorous sonication reduced the mass average aggregate size to 78 μm . After sonication, the aggregates in the size range smaller than 38 μm comprised 75 weight% of the total aggregates. The model for distribution of NAPL, described in chapter 4, predicted that the NAPL initially present in the macropores would appear as a film around smaller aggregates when the aggregates are disrupted. The 90% film fraction of NAPL for sonicated soil is consistent with the NAPL distribution model. Further, the kinetic analysis of bioremediation data as listed in Table 5.4 implies that the fraction of the PAHs with slow desorption behavior ranges from 3% to 17% for different PAHs. These independent data are consistent with the information on film fraction of NAPL obtained by model simulation. Experimental data and model

simulation both agree that 90% of the contaminants are removed during the rapid phase of degradation, however, degradation of the last 10% occurs over a much longer time scale.

Table 5.5. The mass fraction of slow desorbing PAHs

Compound	Mass fraction in slow desorption %
Acenaphthene	3.45
Phenanthrene	3.25
Anthracene	17.1
Fluoranthene	5.95
Pyrene	7.55
Chrysene	13.15
Average	8.4

5.4 Summary and Conclusion

A two compartment model was developed to accommodate both film diffusion and pore diffusion of PAHs in NAPL and through the porous structure of soil aggregates. This model considered the changes in aggregate size distribution during the process of bioremediation and includes two adjustable parameters: diffusivity of PAHs in NAPL and a correction factor for the fraction of NAPL present as a film on the surface of microaggregates. Analytical solutions to the PDE's that describe the diffusion of PAHs through the NAPL in such systems were fitted to the experimental data and the two adjustable parameters were estimated.

The diffusion coefficients obtained for various PAHs in NAPL in the creosote-contaminated soil were on the order of $0.5 \times 10^{-14} - 5 \times 10^{-14} \text{ cm}^2/\text{s}$. These values are in the low range of the values for diffusion coefficients of organic species in oils, and are in the high range of the values suggested for polymers that have physical properties intermediate between liquids and solids. Model predictions were found to agree very well with experimental data.

5.5 Literature cited

Ball, W.P.; Roberts, P.V., "Long term sorption of halogenated organic chemicals by aquifer materials. 1. Equilibrium" *Environ. Sci. Technol.* 1991, 25, 1223.

Ball, W.P.; Roberts, P.V., "Long term sorption of halogenated organic chemicals by aquifer materials. 2. Intraparticle diffusion" *Environ. Sci. Technol.* 1991, 25, 1237.

Bird, R.B.; Stewart, W.E.; Lightfoot, E.N., "*Transport Phenomena*" John Wiley & Sons. USA. 1960.

Brusseau, M.L.; Rao, P.S.C., "Influence of sorbate structure on nonequilibrium sorption of organic compounds" *Environ. Sci. Technol.* 1991, 25, 1501.

Carroll, K.M.; Harkness, M.R.; Bracco, A.A.; Balcarcel, R.R., "Application of a permeant/polymer diffusional model to the desorption of polychlorinated biphenyl from Hudson River Sediments" *Environ. Sci. Technol.* 1994, 28, 253.

Carslaw, H.S.; Jaeger, J.C., "*Conduction of Heat in Solids*" Oxford University Press, Ely House, London W. 1959.

Cohen, R.M.; Mercer, J.W., "*DNAPL Site Evaluation*" CRC Press Inc., N.W. 1993.

Cooney, D.O.; Adesany, B.A., "Effect of particle size distribution on adsorption kinetics in stirred batch systems" *Chem. Eng. Sci.* 1983, 38(9), 1535-1541.

Cornelissen, G.; Rigterink, H.; Ferdinany, M.M.; Van Noort, P.C.M., "Rapidly desorbing fractions of PAHs in contaminated sediments as a predictor of the extent of bioremediation" *Environ. Sci. Technol.* 1998, 32, 966.

Crank, J.; Park, C.S., "*Diffusion in Polymers*" Academic Press, New York. 1968.

Dabros, T.; Yeung, A.; Masliyah, J.; Czanecki, J.; 1999. "Emulsification through area contraction" *J. Colloid and Interface Sci.* 210, 224.

Efroymsen, R.A.; Alexander, M., "Role of partitioning in biodegradation of phenanthrene dissolved in nonaqueous-phase liquids" *Environ. Sci. Technol.* 1994, 28, 1172.

Farrell, J.; Reinhard, M., "Desorption of halogenated organics from model solids, sediments, and soil under unsaturated conditions. 2. Kinetics." *Environ. Sci. Technol.* 1994, 28, 63.

Fu, C.; Pfanstiel, S.; Gao, C.; Yan, X.; Govind, R.; Tabak, H.H., "Studies on contaminant biodegradation in slurry, wafer, and compacted soil tube reactors" *Environ. Sci. Technol.* 1996, 32, 966-970.

Geerdink, M.J.; Van Loosdrecht, M.C.M.; Luyben, K.C.A.M., "Model for microbial degradation of nonpolar organic contaminants in a soil slurry reactor" *Environ. Sci. Technol.* 1996, 30, 779.

Ghoshal, S.; Ramaswami, A.; Luthy, R.G., "Biodegradation of naphthalene from coal tar and heptamethylnonane in mixed batch systems" *Environ. Sci. Technol.* 1996, 30, 1282.

Gusev, A.A.; Muller-Plathe, F.; Gunsteren, W.F.; Suter, U.W., "*Advances in Polymer Science*", Eds. Monnerie, E.L.; Suter, U.W., Springer-Verlag, New York. 1994.

Haeseler, F.; Blanchet, D.; Druelle, V.; Werner, P.; Vandecasteele, J.P., "Analytical characterization of contaminated soils from former manufactured gas plants" *Environ. Sci. Technol.* 1999, 33, 825.

Hiss, T.G.; Cussler, E.L., "Diffusion in high viscosity liquids" *AICHE J.* 1973, 19, 698.

Karickhoff, S.W., "Sorption kinetics of hydrophobic pollutants in natural sediments" *Contaminants and Sediments*. Vol 2. R.A. Baker, ed. Ann Arbor Science Publishers, Ann Arbor, Mich. 1980, 193.

Luthy, R.G.; Ramaswami, A.; Ghoshal, S.; Merkel, W. "Interfacial films in coal tar non-aqueous phase liquid-water systems" *Environ. Sci. Technol.* 1993, 27, 2914.

Mihelcic, J.R.; Luthy, R.G., "Sorption and microbial degradation of naphthalene in soil-water suspensions under denitrification conditions" *Environ. Sci. Technol.* 1991, 25, 169.

Miller, CT; Predit, J.A., "Use of a reactive surface diffusion model to describe apparent sorption-desorption hysteresis and abiotic degradation of lindane in a subsurface material" *Environ. Sci. Technol.* 1992, 26, 1417.

Mott, H.V.; Weber, W.J.Jr. "Factors influencing organic contaminant diffusivities in soil-bentonite cutoff barriers" *Environ. Sci. Technol.* 1991, 25, 1708.

Mukherji, S.; Peters, C.A.; Weber, W.J., Jr., "Mass transfer of polynuclear aromatic hydrocarbons from complex DNAPL mixtures" *Environ. Sci. Technol.* 1997, 31, 416.

Nelson, E.; Goshal, S.; Edwards, J.; Marsh, G.X.; Luthy, R.G., "Chemical characterization of coal tar-water interfacial films" *Environ. Sci. Technol.* 1997, 30, 1014.

Ortiz, E.; Kraatz, M.; Luthy, R.G., "Organic phase resistance to dissolution of polycyclic aromatic hydrocarbon compounds" *Environ. Sci. Technol.* 1999, 33, 235-242.

Overcash, M.R.; McPeters, A.L.; Dougherty, E.J.; Carbonell, R.G., "Diffusion of 2,3,7,8-tetrachlorodibenzo-p-dioxin in soil containing organic solvents" *Environ. Sci. Technol.* 1991, 25, 1479.

Pignatello, J.J., "Sorption dynamics of organic compounds in soils and sediments" in *Reactions and Movements of Organic Chemicals in Soils*, B.L. Sawhney and K. Brawn (Eds.), *Soil Sci. Soc. Am., Inc. & Am. Soc. Of Agronomy, Inc.*, Madison, WI, 1989.

Pignatello, J.J.; Ferrandino, F.J.; Huang, L.Q., "Elusion of aged and freshly added herbicides from a soil" *Environ. Sci. Technol.* 1993, 17, 1563.

Pignatello, J.J.; Xing, B., "Mechanism of slow sorption of organic chemicals to natural particles" *Environ. Sci. Technol.* 1996, 30, 1.

Ried, R.C.; Prausnitz, J.M.; Poling, B.E., "*Properties of Gases and Liquids*" McGraw-Hill, New York. 1987.

Ripp, J. "*Chemical and physical characteristics of tar samples from selected manufactured gas plant (MGP) sites*" Prepared for Electric Power Research Institute, Palo Alto, CA., 1993.

Rogers, C.E.; Fels, M.; Li, N.N., "*Recent development in separation Science*" Li, N.N., Ed.; CRC Press: Cleveland, OH, Vol. II, 1972.

Rutherford, P.M.; Gray, M.R.; Dudas, M.J., "Desorption of ¹⁴C naphthalene from bioremediated and nonbioremediated soils contaminated with creosote compounds" *Environ. Sci. Technol.* 1997, 31,2515.

Salame, M., "Prediction of gas barrier properties of high polymers" *Poly. Eng. & Sci.* 1986, 26, 1543.

Weber, W.J.Jr.; Miller, C.T., "Modeling the sorption of hydrophobic contaminants by aquifer materials. I. Rates and equilibria" *Water Res.* 1988, 22, 457.

Wu, S.; Gschwend, P.M., "Sorption kinetics of hydrophobic organic compounds to natural sediments and soils" *Environ. Sci. Technol.* 1986, 20, 717.

6. Inhibitory Effects with Multiple Carbon Sources

6.1 Introduction

Some bacteria have the enzymatic capability to degrade a wide range of structurally diverse PAHs. In the past decade, considerable research has made progress towards understanding the metabolism involved in degradation of PAHs by soil indigenous communities. These investigations have shown that degradation of different PAHs does not happen to the same extent. Low molecular weight PAHs are used as the energy source, while some of high molecular weight PAHs may only be co-metabolized. In a mixed culture, the co-metabolic products can serve as energy source for different species of microbial culture.

Many investigators have reported sequential degradation of hydrocarbons in a mixture. Comparing the composition of aliphatic hydrocarbons in oil, cycloparaffins are the most resistant to biodegradation followed by isoparaffins, aromatics and finally n-alkanes (Perry and Scheld, 1968). Oberbremer et al. (1989) observed two phases of degradation for a mixture of hydrocarbons containing tetradecane, pentadecane, hexadecane, pristane (2,6,10,14-tetramethylpentadecane), trimethylcyclohexane, phenyldecane and naphthalene. They reported that in the first phase naphthalene was degraded and degradation of the rest of the hydrocarbons started in the second phase after the interfacial tension was lowered by the production of surfactants.

Rittman (1994) suggested that the initial step in biodegradation of organic pollutants require co-substrate, meaning that concentration of materials other than the target contaminant controls the rate of degradation.

Two independent phenomena could result in sequential degradation in a mixed carbon source leading to the kinetic behavior observed in this study. Competitive inhibition of the substrates for the same enzyme in the pathway and catabolic repression due to induction of a new enzyme when the substrate changes are the possible mechanisms suggested to explain the lag phase observed in degradation of phenanthrene, pyrene and chrysene.

1. In degradation of analogue PAHs, the competition for the initial enzyme in the pathway (e.g. di-oxygenase) may result in competitive inhibition of substrates with larger molecular weight. This phenomenon can lead to faster degradation of specific compounds and hinders the degradation of other analogues (Stringfellow et al., 1995). The inhibited substrate may be used as growth substrate or co-metabolite.

2. Catabolite repression

Consideration should be given to the acclimation period needed for the cells to adjust to a different carbon source. Control and regulation of enzyme activity inside the cells requires an adaptive period in which the enzyme is produced and activated by specific molecules such as vitamins and cofactors. This activation period is manifested as a lag phase when the microorganisms are transferred to a

different carbon source. Different enzymes are generally required for each carbon source. When the medium contains multiple carbon sources, multiple lag phases may be observed. This phenomenon referred to as diauxic growth is caused by a shift in metabolic patterns. After one carbon source is depleted the microorganisms produce enzymes that enable them to use a different carbon source. The possible explanation for the serial utilization phenomenon is catabolite repression. The use of one carbon source may lead to repression of enzymes that are essential for transformation of other carbon sources. The repressor can be the carbon source or any of the metabolites in the pathway.

Most of the research in this area have been conducted with pure cultures. It is not clear whether such diauxic phenomenon applies to mixed microbial cultures such as soil microorganisms.

6.2 Qualitative Discussion

A critical analysis of biodegradation data in this study revealed that the intrinsic microbial activities limited degradation of contaminants in the first phase of bioremediation. The kinetic analysis of biodegradation of 6 PAHs showed an initial lag phase during which no significant degradation occurred. The duration of this phase depended on the PAH compound. The microorganisms showed a preference for compounds with simple chemical structure, and higher solubility therefore, the more complex chemicals with low solubility had longer lag phases. The presence of

an alternative carbon source apparently inhibited degradation of four and higher-ring compounds. Similar observations were reported by other researchers. Preferential degradation of 1,2,4-trichlorobenzene over chlorobenzenes, α -hexachlorocyclohexane over hexachlorocyclohexanes (Feidieker et al., 1995) and n-alkanes over branched alkanes (De Jonge et al., 1997) are some examples.

Before any attempt at modeling the inhibitory effect of multi-substrate carbon source, reproducible experimental data are essential. In all experiments, either with sonicated soil or non-sonicated soil, the inhibitory effect was observed and degradation of target PAHs occurred in the same sequence and order as illustrated in Figure 6.1. Among the 6 PAHs, phenanthrene was the most readily degradable. Degradation of phenanthrene started at zero time and reached its maximum rate in about one day. Fluoranthene and chrysene had lag phases of 4 and 4.5 days. The rate of degradation during the lag phase was very low and in many cases negligible. Statistical analysis (t test with 95% confidence) was performed on the data obtained in six experiments. For fluoranthene and chrysene 33% of the experiments showed non-zero slopes during the lag period i.e. definite degradation. Pyrene had two distinct phases before the maximum rate of degradation started. An initial lag phase of 5 days was followed by a phase of degradation at a slow rate. In one out of six experiments, no degradation of pyrene occurred during the lag phase.

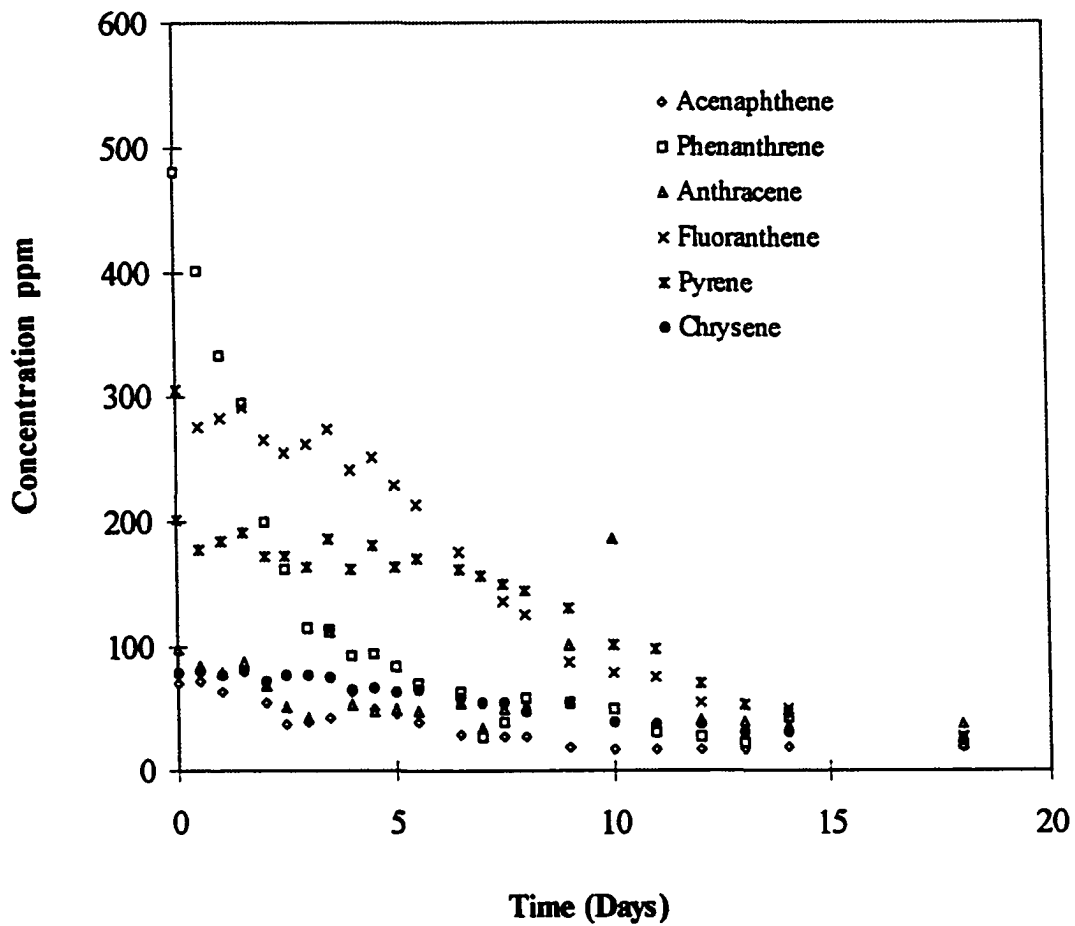


Figure 6.1. Time course concentration of 6 PAHs in the process of bioremediation of creosote-contaminated soil in slurry phase reactor.

Table 6.1 Statistical analysis of the slope of the lag phase in bioremediation of creosote-contaminated soil

PAH	Number of experiments	Number of experiments with zero slope (95% confidence)
Fluoranthene	6	2
Pyrene	6	1
Chrysene	6	3

6.3 Experiments with C-horizon soil

Experiments were conducted with pristine soil spiked with each individual PAH to investigate the occurrence and duration of the lag phase when the PAHs were used as the sole carbon source and in combination with other PAHs. These experiments were conducted with fluoranthene, pyrene and chrysene. Further, experiments were conducted with combination of the three PAHs and also combination of 6 PAHs: aacenaphthene, phenanthrene, anthracene, fluoranthene, pyrene and chrysene. The protocol for the methods used to spike the soil and bioremediation experiments were described in chapter 3. The only difference here is that the spiked C-horizon soils were inoculated with 10% slurry of creosote-contaminated soil which contained active culture to degrade all 6 PAHs.

6.3.1 Results

The results of the experiments with C-horizon soil are presented in Figures 6.2, 6.3 and 6.4. Figure 6.2 presents the data on degradation of fluoranthene in three different conditions: 1. As the sole carbon source; 2. in combination with pyrene and chrysene; 3. in combination with 5 PAHs. Fluoranthene did not show any lag phase in cases 1 and 2, however the rate of degradation was low for the first two days. When fluoranthene was degraded in combination with 5 other PAHs a lag phase of 4.5 days was observed. Similarly chrysene had no lag phase when it was the only carbon source (Figure 6.3), however, in combination with fluoranthene and pyrene a lag phase of 2.5 days was observed, which increased to 5 days when it was degraded in combination with 5 PAHs.

Pyrene (Figure 6.4) had completely different behavior. A lag phase of 4.5 to 5.5 days was observed in all experiments, independent of the environment. 80% of the experiments showed zero slope during the lag phase. The results of these experiments are summarized in Table 6.2.

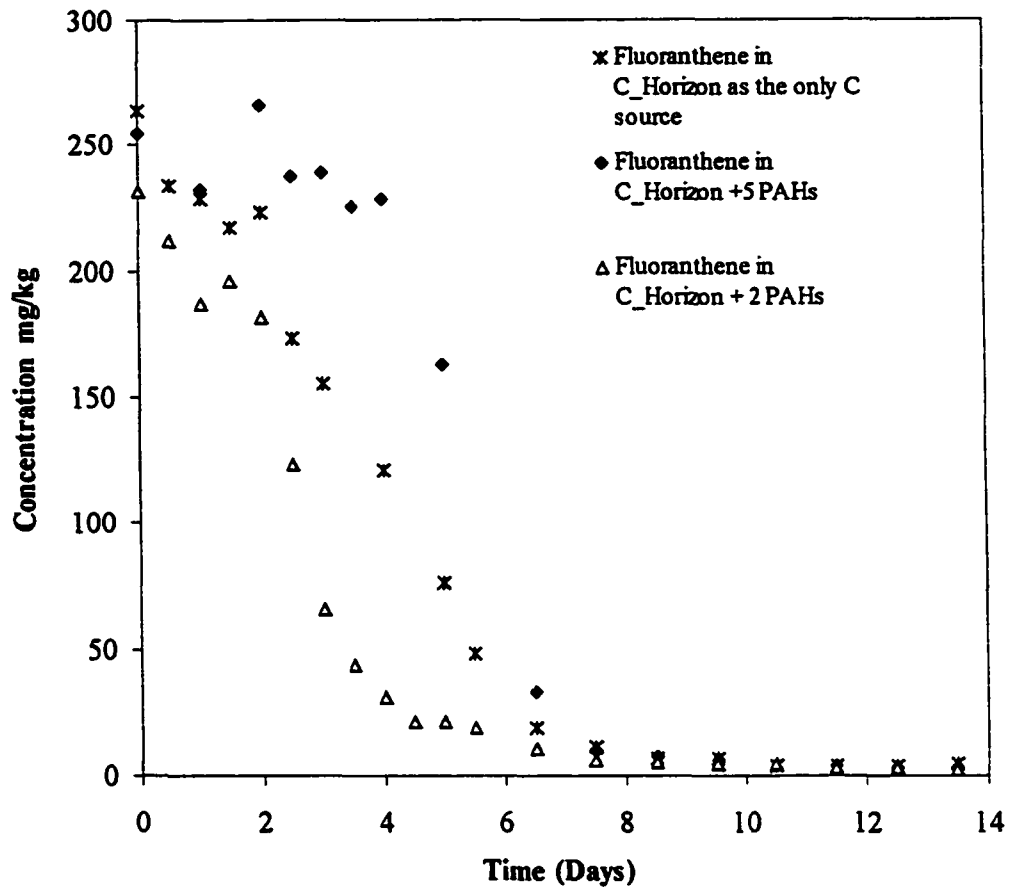


Figure 6.2. Time course of degradation of fluoranthene in spiked C-horizon soil

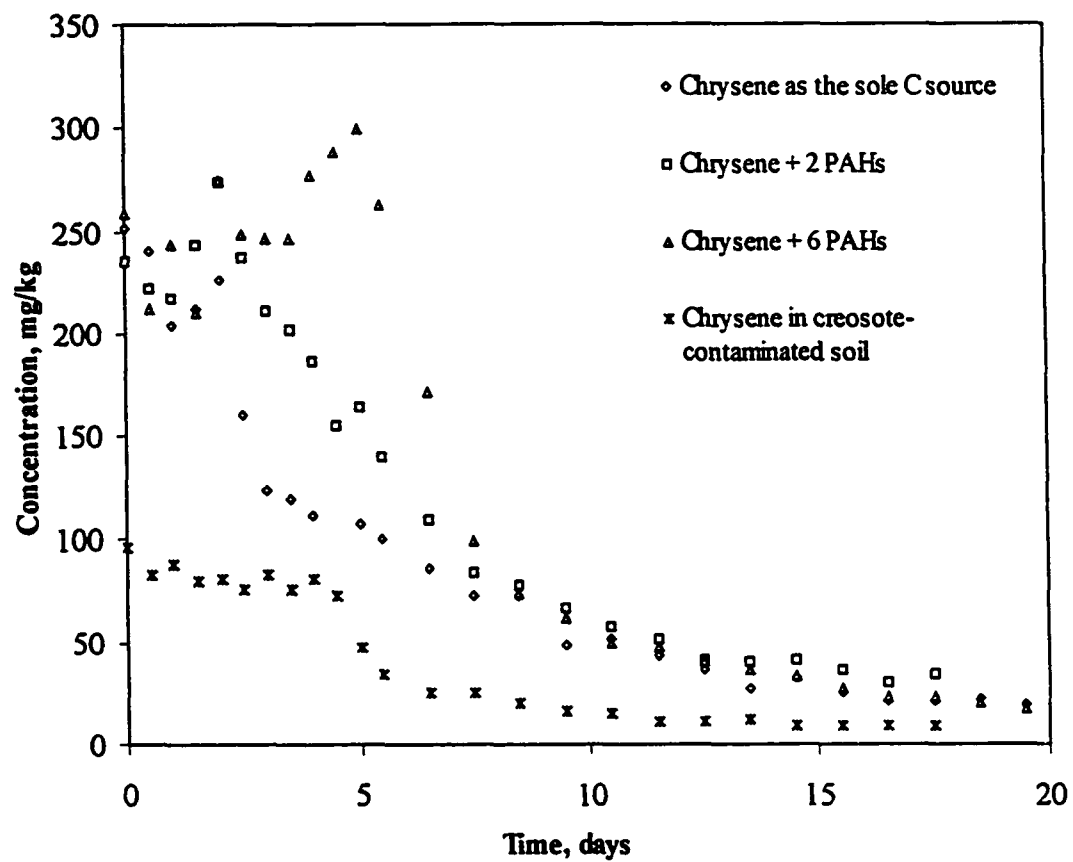


Figure 6.3. Time course of degradation of Chrysene in spiked C-horizon soil

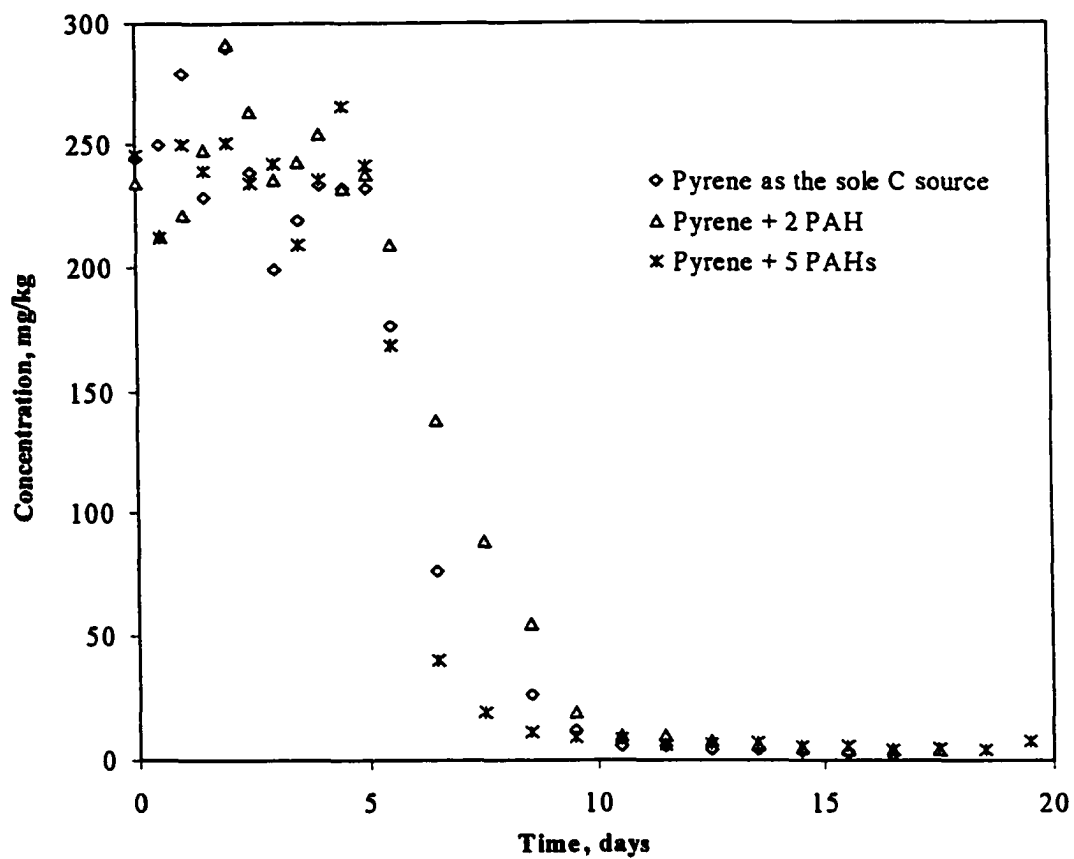


Figure 6.4. Time course of degradation of pyrene in spiked C-horizon soil

Table 6.2. Data on the first phase of degradation of PAHs in C-horizon soil

PAH	lag phase, days	Number of experiments, zero slope (t test, 95% confidence)
Sole carbon source		
fluoranthene 300 & 600 ppm	0	
pyrene 300 ppm	5	1
pyrene 600 ppm	4	1
chrysene 300 ppm	0	
Combination of 3 PAHs		
fluoranthene	0	
pyrene	5.5	1
chrysene	2.5	1
Combination of 6 PAHs¹		
Fluoranthene	4.5	1 out of 2
Pyrene	5	1 out of 2
Chrysene	5.25	2

¹ Data are the average of two parallel experiments.

6.4 Modeling

The observations on both creosote-contaminated soil and spiked C-horizon soil implied that competitive inhibition of the substrates could partly explain the kinetic behavior in the first phase of degradation. However, it doesn't rule out catabolic repression or a combination of different mechanisms that may have been involved in the process of bioremediation. Specifically the data on pyrene suggest

that an induction period for a specific enzyme is the most likely the explanation for degradation kinetics of this compound.

6.4.1 Development of a Substrate Inhibition Model

Modeling of competitive inhibition in cometabolism can be accomplished using a modified Michaelis-Menten enzyme kinetics expression (Ely et al., 1995; Strand et al., 1990; Chang et al., 1996).



$$\frac{dS}{dt} = \frac{v_{max}S}{K_S + S + \frac{K_S}{K_I}S_I} \quad (6.4)$$

where S = substrate concentration in aqueous phase

S_I = inhibitor concentration in aqueous phase

v_{max} = maximum rate of degradation

K_S & K_I = enzyme half saturation constants for the substrate and the inhibitor

As mentioned in Chapter 5 in developing the diffusion-degradation model, it was assumed that active degradation happens only in the aqueous phase. The overall rate of biotransformation of PAHs released from NAPL can be altered by the intrinsic microbial degradation rates. The dynamic change in the aqueous phase concentration of the inhibitor can be described by the following equation:

$$\frac{dS_I}{dt} = Flux_I - k_{bio}S_I \quad (6.5)$$

where

$Flux_I$ = flux of inhibitor from NAPL

k_{bio} = apparent first order rate constant for biodegradation

When the microorganisms are actively degrading the PAHs:

$$\frac{dS_I}{dt} = 0 \quad (6.6)$$

and

$$S_I = \frac{Flux_I}{k_{bio}} \quad (6.7)$$

The first term in the right hand side of equation (6.5) represents the rate of input of PAHs to the aqueous phase while the second term represents the rate of removal of PAHs from aqueous phase due to biodegradation. The intrinsic biodegradation rate constant is expressed as pseudo-first order coefficient and can be derived from Michaelis-Menten kinetics in the condition of low substrate concentration:

$$\frac{dS_I}{dt} = \frac{v_{\max,I} S_I}{K_I + S_I} \quad (6.8)$$

At low concentrations of substrate, $S_I \ll K_I$ resulting in the following equation:

$$\frac{dS_I}{dt} = \frac{v_{\max,I}}{K_I} S_I = k_{bio} S_I \quad (6.9)$$

$$k_{bio} = \frac{v_{\max,I}}{K_I} \quad (6.10)$$

Substituting equation (6.7) in (6.4) and considering the partition coefficient that relates the concentration of PAHs in aqueous phase to the concentration in soil (6.11) we can derive the rate equation for the inhibitory effect of the substrates:

$$K_p = \frac{C}{S} \quad (6.11)$$

K_p is the equilibrium partition coefficient between soil and aqueous phase and C is the concentration in soil phase.

$$\frac{dC}{dt} = \frac{v_{\max} C}{K_1 + C + \left(\frac{K_1}{K_2}\right) Flux_I} \quad (6.12)$$

where

$$K_1 = K_S K_p \quad (6.13)$$

$$K_2 = K_I k_{bio} \quad (6.14)$$

Equation (6.12) was used as a model to test the inhibitory effect of phenanthrene on degradation of fluoranthene and chrysene in bioremediation of creosote-contaminated soil.

6.4.2 Results and Discussions

6.4.2.1 Evaluation of Model Parameters

To calculate model parameters K_1 and K_2 from equation 6.12, it was required that the value of v_{max} was estimated. This value was calculated based on the data obtained from degradation of phenanthrene in sonicated soil. It was assumed that the maximum rate of degradation for PAH analogues were limited by degradation rate of phenanthrene in a diffusion controlled system i.e. $v_{max}^{Fluoranthene} \leq v_{max}^{Phenanthrene}$.

With this assumption Michaelis-Menten kinetics was applied to phenanthrene data and the two model parameters v_{max} and K_S were calculated.

$$\frac{dS}{dt} = \frac{V_{max} S}{K_S + S} \quad (6.15)$$

Applying equation 6.11 to equation 6.15 we can convert the aqueous phase concentrations to soil phase concentrations:

$$\frac{dC}{dt} = \frac{V_{max} C}{K_S K_P + C} = \frac{V_{max} C}{K_1 + C} \quad (6.16)$$

Equation 6.16 was used to calculate v_{max} and K_1 for phenanthrene. Knowing v_{max} , K_1 and K_2 were calculated for fluoranthene, pyrene and chrysene based on equation 6.12. It was assumed that phenanthrene was the inhibitor for degradation of the fluoranthene and chrysene. Similarly phenanthrene and fluoranthene acted as inhibitors for degradation of pyrene. The calculated values of model parameters are listed in Table 6.3.

Table 6.3 Model parameters for degradation of PAHs based on competitive inhibition kinetics

PAH	v_{max} , mg/kg soil. d	K_1 , mg/kg soil	K_2 , (mg/kg soil). d ⁻¹
Phenanthrene	217	67.1	
Fluoranthene		781	17.6
Pyrene		448	77.3
Chrysene		3984	46.4

6.4.2.2 Validity of the Competitive Inhibition Model

As a first step, a competitive inhibition model based on Michaelis-Menten kinetics was developed and fitted to the data for degradation of fluoranthene, pyrene and chrysene. Degradation of fluoranthene showed a lag phase of 4 days. During this time period the concentration of phenanthrene dropped to 3% of its initial value. As illustrated in Figure 6.2, this lag phase was not observed when fluoranthene was

spiked into the soil and used as the sole carbon source. Similarly, chrysene did not show a lag phase when it was used as the only carbon source (Figure 6.3), while a lag phase of 4.5 days was observed in degradation of chrysene in creosote-contaminated soil and when more readily degradable PAHs such as phenanthrene was present. These data suggest that competitive inhibition in the multi-substrate environment of creosote-contaminated soil might explain the kinetic behavior of degradation of PAH compounds. Bouchez et al. (1995) also observed the inhibition of PAH substrate with or without cometabolization of the second PAH. In the experiment with creosote-contaminated soil, degradation of pyrene did not start before the total concentration of phenanthrene and fluoranthene depleted to 25% of its initial value.

Figures 6.5 to 6.7 represent the data from the inhibition model based on Michaelis-Menten enzyme kinetics. The plots in Figure 6.5 contain the data on: 1. the experimental data on degradation of phenanthrene (as inhibitor); 2. the experimental data on degradation of fluoranthene; 3. data from a model based on inhibition kinetics (equation 6.12); 4. data from a modified Michaelis-Menten kinetics (equation 6.16); 5. the diffusion controlled model. Strong deviation from the experimental data was observed when the inhibition model was extended to longer periods of times. The main reason was that the model parameters were estimated from the data points in the lag phase. Figure 6.5 also shows a plot of modified Michaelis-Menten kinetics where the inhibition was completely removed after the lag phase. The parameters for this part of the plot were taken from the data obtained on

degradation of phenanthrene ($K_f=67.1$ mg/kg soil). Figures 6.6 and 6.7 show similar plots for chrysene and pyrene.

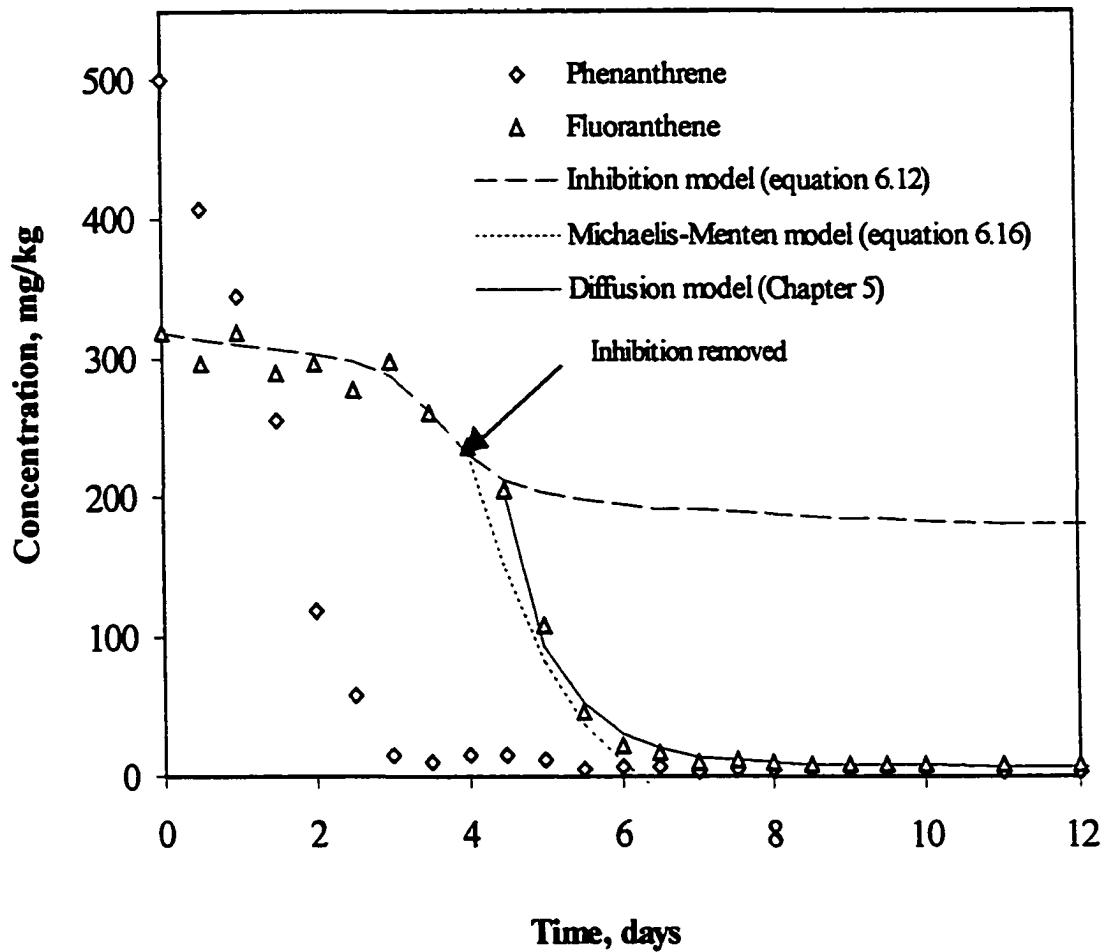


Figure 6.5. The time course of concentration of fluoranthene during bioremediation of creosote-contaminated soil in slurry phase reactor. The solid line represents the diffusion model and the dashed lines compare the inhibition model with Michaelis-Menten model.

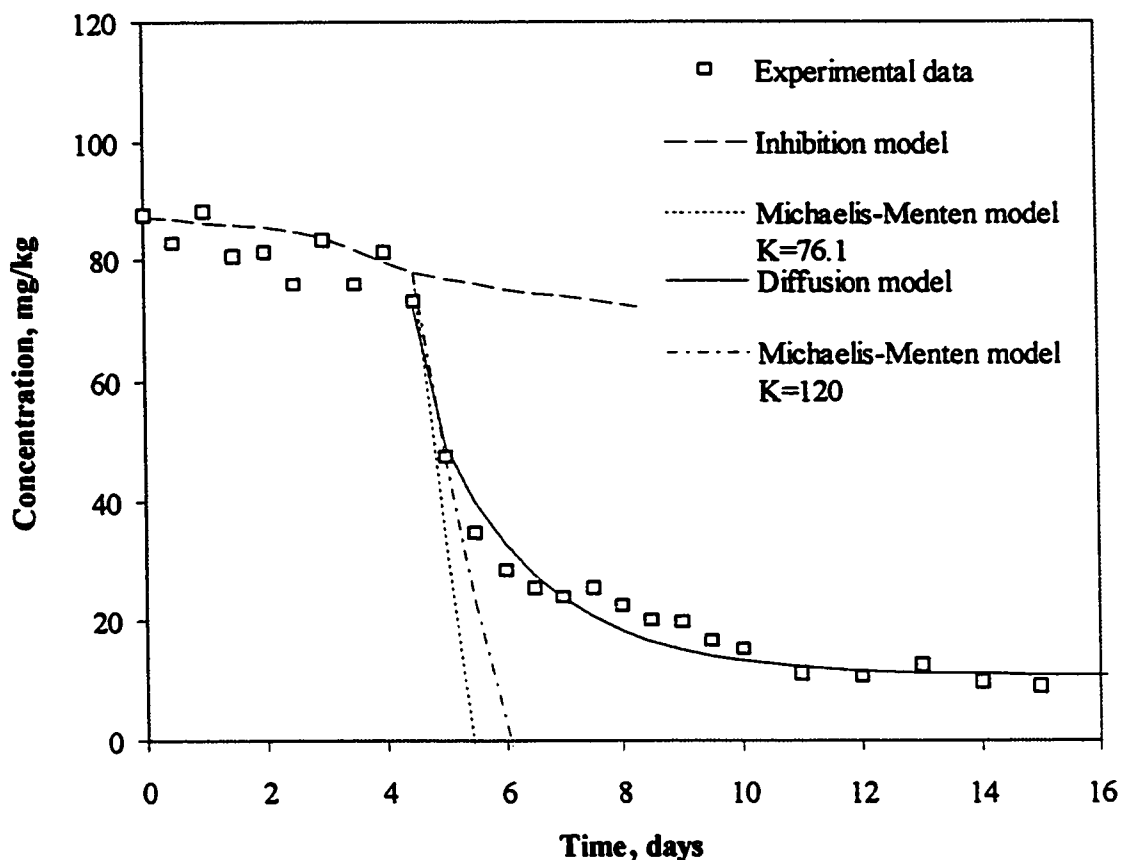


Figure 6.6. The time course of concentration of chrysene during bioremediation of creosote-contaminated soil in slurry phase reactor. The solid line represents the diffusion model and the dashed lines compare the inhibition model with Michaelis-Menten model (different values of K_1 are plotted).

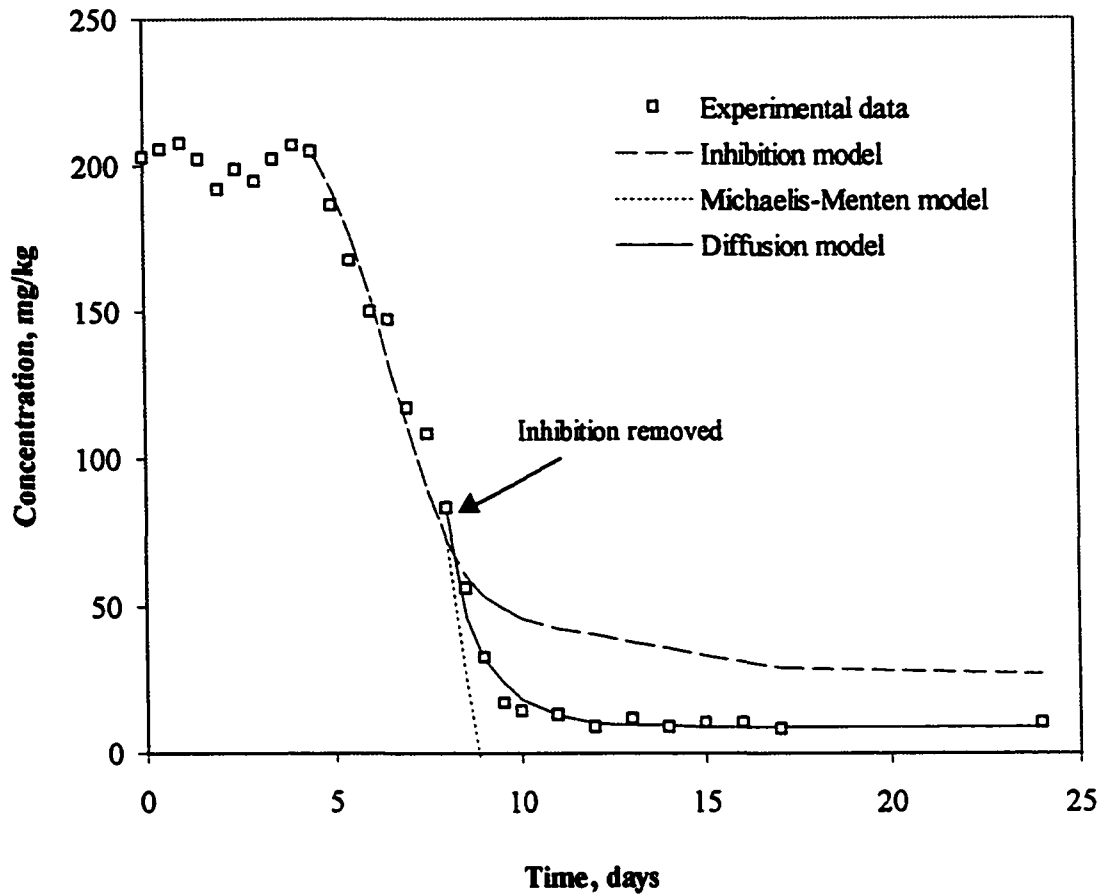


Figure 6.7. The time course of concentration of pyrene during bioremediation of creosote-contaminated soil in slurry phase reactor. The solid line represents the diffusion model and the dashed lines compare the inhibition model with Michaelis-Menten model.

Comparing all the plots in Figures 6.5 and 6.6 implies that a simple inhibition model is inadequate to explain the kinetics of biodegradation of fluoranthene and chrysene in the first phase. Models with more adjustable parameters could possibly fit the data, however they might not have any mechanistic significance. It is important to note here that the Michaelis-Menten enzyme kinetics were developed based on constant enzyme concentration, however, in our system the concentration of enzymes is variable and depends not only on the growth kinetics of microbial population but the intrinsic metabolic activities related to the production of enzymes.

The K_i value obtained from phenanthrene data has been used to demonstrate the kinetic behavior in degradation of fluoranthene, pyrene and chrysene in the conditions when the inhibition was removed. These values may not be a true representative. Especially in case of chrysene, it is expected that the K_i value be much larger than 67.1 that was used in calculations. A plot with K_i values of 120 mg/kg is plotted in Figure 6.6 to demonstrate the effect of this variable.

In the case of pyrene, the lag phase was observed even when pyrene was used as the sole carbon source. Mechanisms other than competitive inhibition are, therefore, responsible for the kinetics observed in the first phase of degradation for this compound. Rittmann (1995) suggested that the initial step in biodegradation of the contaminants required cosubstrates. The presence of cosubstrate is essential to increase the intracellular electron donor units such as nicotinamide adenine dinucleotide phosphate (NADH). Saez and Rittmann (1993) showed that the initial monooxygenation of 4-chlorophenol was rapid only when the cosubstrate phenol was

being oxidized to create a high concentration of NADH. Stringfellow et al. (1995) reported that the presence of phenanthrene and salicylate induced the metabolism of four ring PAHs such as fluoranthene and pyrene, neither of which was a growth substrate for the strain they used. It is expected that the presence of a mixed culture in soil with multi-substrate environment can cause complex behavior as observed by Bouchez et al. (1995). They studied the interactions in the degradation of a mixture of two PAHs by individual strains of *Pseudomonas* and *Rhodococcus*. They reported that fluorene as a cosubstrate increased the utilization of phenanthrene, but the pattern most usually observed was a lower degradation of the substrate PAH when a second PAH was added. The inhibition occurred whether or not the second PAH was cometabolized. In the case of naphthalene, strong inhibition (toxicity behavior) prevented degradation of substrate PAH. They concluded that a diverse interaction was happening during degradation of PAHs, where each strain presented a limited capacity for PAH degradation and that degradation of PAH mixtures implied a wide variety of strains and complex metabolic interactions.

6.5. Conclusion

A simple inhibition model based on Michaelis-Menten enzyme kinetics could not explain the kinetic behavior of PAH degradation in the first phase, suggesting that more complex mechanisms such as catabolic repression might have a determinative role in the kinetics of bioremediation. In the soil environment with a wide variety of

strains and complex hydrocarbon and PAH mixtures, complex metabolic interactions are expected. These effects are not explicitly included in our model.

6.6. Literature Cited:

Bouchez, M.; Blanchet, D.; Besnainou, B.; Vandecasteele, JP., "Diversity of metabolic capacities among strains degrading polycyclic aromatic hydrocarbons" in *Microbial Processes in Bioremediation*. Ed: Hincsee, R.E. & Brockman, F.J., Columbus: Battelle Press. 1995, 153.

Chang, H.L.; Alvarez-Cohen, L., "Transformation capacities of chlorinated organics by mixed cultures enriched on methane, propane, toluene or phenol" *Biotech. Bioeng.* 1995, 45, 440.

De Jonge, H; Freijer, J.I.; Verstraten, J.M.; Westerveld, J., "Relation between bioavailability and fuel oil hydrocarbon composition in contaminated soils." *Environ. Sci. Technol.* 1997, 31:771-775.

Ely, R.L.; Hyman, M.R.; Arp, D.J.; Geunther, R.B.; Williamson, K.J., "A cometabolic kinetic model incorporating enzyme inhibition, and recovery: II. Model development, analysis and testing" *Biotech. Bioeng.* 1995, 46, 218.

Feidieker, D.; Kampfer, P.; Dott, W., "Field scale investigations on the biodegradation of chlorinated aromatic compounds and HCH in the subsurface environment" *J. Contam. Hydrol.* 1995, 19, 145.

Oberbremer, A.; Muller-Hurtig, R., "Aerobic stepwise hydrocarbon degradation and formation of biosurfactants by an original soil population in a stirred reactor" *Appl. Microbiol. Biotech.* 1989, 31, 582.

Perry, J.J.; Scheld, H.W., "Oxidation of hydrocarbons by microorganisms isolated from soil" *Can. J. Microbiol.* 1968, 14, 403.

Rittmann, B.E., "Dissolution and cosubstrate effects in the transfer of biodegradation kinetics to the field" in *Microbial Processes for Bioremediation*. Ed: Hincsee, R.E. & Brockman, F.J., Battelle Press., Columbus, 1995, 1.

Rittmann, B.E.; Seagren, E.; Wrenn, B.; Valocchi, A.J.; Ray, C.; Raskin, L., *In situ Bioremediation*, 2nd ed., Noyes Publisher, Inc., Park Ridge, NY, 1994.

Saez, P.B.; Rittmann, B.E., "Biodegradation kinetics of a mixture containing a primary substrate (phenol) and an inhibitory cometabolite (4-chlorophenol)" *Biodegradation*. 1993, 4, 3.

Strand, S.E.; Bjelland, M.D.; Stensel, H.D., "Kinetics of chlorinated hydrocarbons degradation by suspended cultures of methane-oxidizing bacteria" *Research journal WPCF*. 1990, 62, 124.

Stringfellow, W.T.; Chen, S.H.; Aitken, M.D., "Induction of PAH degradation in a phenanthrene degrading *Pseudomonad*" in *Microbial Process for Bioremediation*. Ed: Hinchee, R.E. & Brockman, F.J., Columbus: Battelle Press., 1995, 83.

Walker, J.D.; Colwell, R.R., "Microbial petroleum degradation: use of mixed hydrocarbon substrates" *Appl. Microbiol.* 1974, 27, 1053.

7. Conclusions and Recommendations

7.1. Conclusions

7.1.1 Kinetics of Bioremediation

Bioremediation experiments were conducted on two types of soils: A) C-horizon soil spiked with anthracene; B) Creosote-contaminated soil. The soils were sonicated and the effect of aggregate size on the kinetics of bioremediation was investigated. The results suggested that:

1. Degradation rate of anthracene in sonicated soil was twice the rate in the non-sonicated soil in a slurry phase reactor, consistent with diffusion limitation in soil aggregates.
2. Biodegradation kinetics of six PAHs in a creosote-contaminated soil showed three distinct phases.
 - An initial lag phase during which no degradation occurred. The duration of this phase depended on the PAH molecule. The microorganisms showed a preference to compounds with simple chemical structure, therefore, the more complex chemicals had longer lag phases.
 - In the rapid phase of degradation considerable amounts of PAHs were degraded.
 - A slow rate of degradation was observed and attributed to a resistant fraction of contaminants in the soil.
3. The effect of sonication was more profound in the rapid phase of degradation. The apparent rate constants for degradation of six target PAHs in creosote-

contaminated soil were increased up to 5 fold by sonication, however, the extent of bioremediation was not affected.

4. The mass average diameter of the aggregates was reduced to 78 μm by vigorous sonication. In slurry phase reactor, the mass average diameter of the aggregates was reduced from the initial value of 580 μm to asymptotic value of 180 μm in three weeks. The following model was obtained for distribution of mass average diameter of the aggregates in the bioreactor in the process of bioremediation:

$$D_{mean} = 182.61 + 414.66 \text{EXP}(-0.22t) \quad (3.1)$$

5. The extent of bioremediation for non-sonicated soil was comparable to sonicated soil due to the fact that the aggregate size during bioreactor operation was reduced to a comparable value to sonication.
6. The apparent rate constants for six PAHs was linearly correlated to $1/R^2$, consistent with diffusion controlled transport.

7.1.2 Characterization of Contaminated Soils

The microstructure of contaminated soils and the distribution of NAPL in soil aggregates were investigated using two microscopy methods: confocal scanning laser microscopy and cryo-scanning electron microscopy. The images from the two techniques gave consistent information on distribution of NAPL in soil aggregates. It

was concluded that the NAPL fills the pores, likely in the size range down to at least 0.05 μm .

A model was proposed for distribution of NAPL in soil aggregates. This model suggested that the distribution of NAPL changes from NAPL-filled pores for large aggregates, to a surface film for small aggregates. It was concluded that the size of the aggregates determines the nature of diffusion process to liberate the contaminants from NAPL.

7.1.3 Modeling

1. A two-compartment non-steady state diffusion model based on the combination of film diffusion and pore diffusion could explain the dynamics behavior of the system in the second and third phase of bioremediation. This model considers the changes in the aggregate size distribution in the bioreactor. It also considers the physical model developed for distribution of NAPL in soil aggregates and the fact that pore diffusion changes to film diffusion as the aggregates break down in the bioreactor.

$$\bar{C} = a \frac{A(t)}{A_{\max}} \bar{C}_f + (1 - a \frac{A(t)}{A_{\max}}) \bar{C}_p \quad (5.10)$$

2. Analytical solutions to the PDF's were fit to the experimental data and the two model parameters: diffusion coefficient and a correction factor for the fraction of NAPL as a film were estimated.

3. The diffusion coefficients obtained for various PAHs in NAPL were in the order of $0.5 \times 10^{-14} - 5 \times 10^{-14} \text{ cm}^2/\text{s}$.
4. Degradation of fluoranthene and chrysene consistently showed a lag phase in the presence of lower molecular weight PAHs. Fluoranthene had a lag phase of 4.5 days in the presence of 5 PAHs (acenaphthene, phenanthrene, anthracene, pyrene and chrysene), while no lag phase was observed when fluoranthene was used as the sole carbon source or in combination with pyrene and chrysene. Similarly, chrysene had no lag phase as the only carbon source, however in combination with fluoranthene and pyrene a lag phase of 2.5 days was observed which increased to 4.5 days in the presence of 5 PAHs. Similar behavior was observed in the degradation of chrysene.
5. A competitive inhibition model was developed using a modified Michaelis-Menten enzyme kinetics. Phenanthrene was assumed to have an inhibitory effect on degradation of fluoranthene and chrysene. This model could partly explain the kinetic behavior of degradation of fluoranthene and chrysene in the first phase but did not rule out the more complex mechanisms such as catabolite repression.

$$\frac{dC}{dt} = \frac{v_{\max}C}{K_1 + C + \left(\frac{K_1}{K_2}\right)Flux_I} \quad (6.12)$$

6. Pyrene exhibited a lag phase of 5 days whether it was used as the sole carbon source or in combination with other PAHs. It was concluded that the long induction period for specific enzyme was responsible for the consistent lag phase in degradation of pyrene.

7.2. Recommendations

1. The studies on the microstructure of contaminated soils suggested that the distribution of water and oil within the pore structure is partially affected by pore size and it was concluded that NAPL filled the available pores up to 0.05 μm . Further studies are required to investigate the pore size distribution in soil aggregates and the pore size ranges available to accommodate the oil. Mercury intrusion technique can be used to study the pore size distribution in soil aggregates. Nitrogen absorption can be used as complementary technique to cover the smaller size range, which could not be captured by mercury porosimetry.
2. More studies are needed to investigate the effect of composition and viscosity of the NAPL on diffusion coefficients of different compounds. Further, the composition and the characteristics of the interfacial film and its contribution to increased resistance to the mass transfer needs to be investigated.
3. More studies on biological aspect of bioremediation are required. These studies need to focus on:
 - The transport processes through cell membrane
 - The interactions of multiple carbon sources
 - Recognition of specific enzymes for degradation of PAHs and quantifying the level of enzymes at different stages of degradation.
4. The results reported here for sonicated soil demonstrated the limits of bioremediation. Further reduction of aggregate size is impractical and the

microstructures responsible for holding the contaminants will not be affected. There are cases where this limit of bioremediation is insufficient or this level of clean up may not even be reached because of limited microbial activity. In these situations and considering the fact that the main structure of NAPL persists in the soil after bioremediation mobilization of NAPL by surface wetting agents would be a reasonable approach.

Appendices

Appendix A

This appendix contains the raw data of the bioremediation experiments on C-horizon soil and Edmonton-creosote-contaminated soil. These data were used to calculate the degradation rate constants for different PAHs in sonicated soils and non-sonicated soils.

A.1. Raw data on bioremediation of C-horizon soil and Edmonton creosote-contaminated soil

The raw data on degradation of PAHs in C-horizon soil and creosote-contaminated soil have been presented as graphs, where the time course concentrations of PAHs were plotted against time. These data are presented for two sets of data for C-horizon soil and ten set of experiments for Edmonton Creosote-contaminated soil

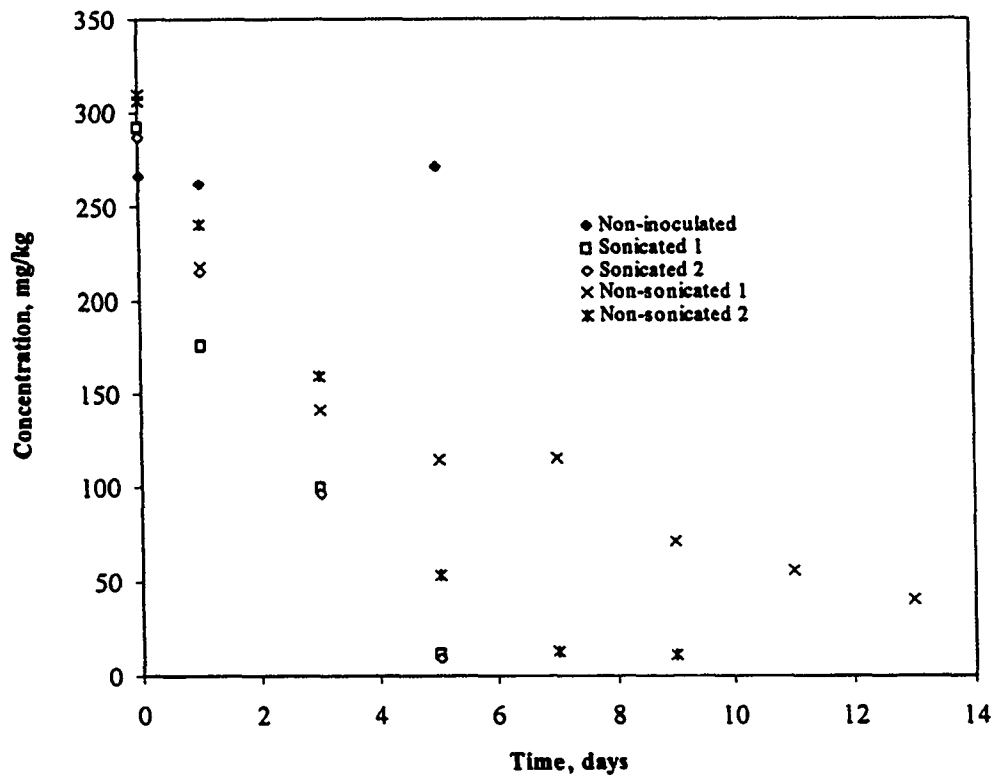


Figure A.1. Effect of sonication on degradation of Anthracene in C-horizon soil (experiment 1)

C-horizon soil was loaded with anthracene with a concentration of 400 ppm and left for 17 days prior to experiment. 200 g of soil was sonicated in 100 ml water for 21 minutes.

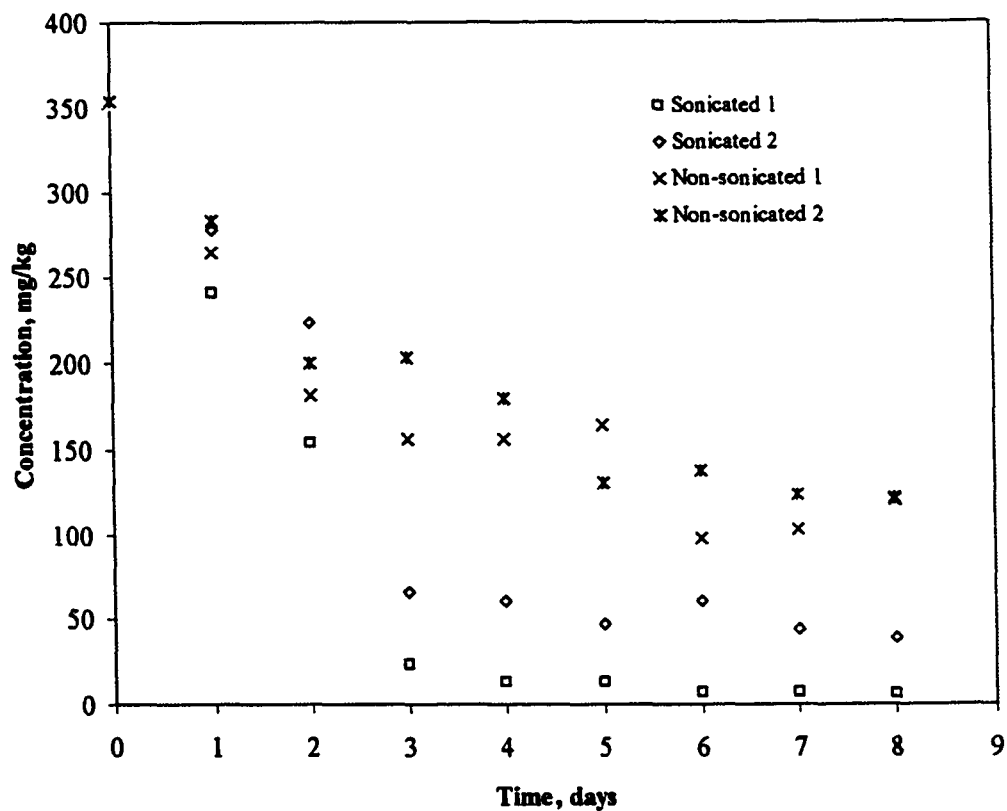


Figure A.2. Effect of sonication on degradation of Anthracene in C-horizon soil (experiment 2)

C-horizon soil was loaded with anthracene with a concentration of 400 ppm and left for 17 days prior to experiment. 200 g of soil was sonicated in 100 ml water for 21 minutes.

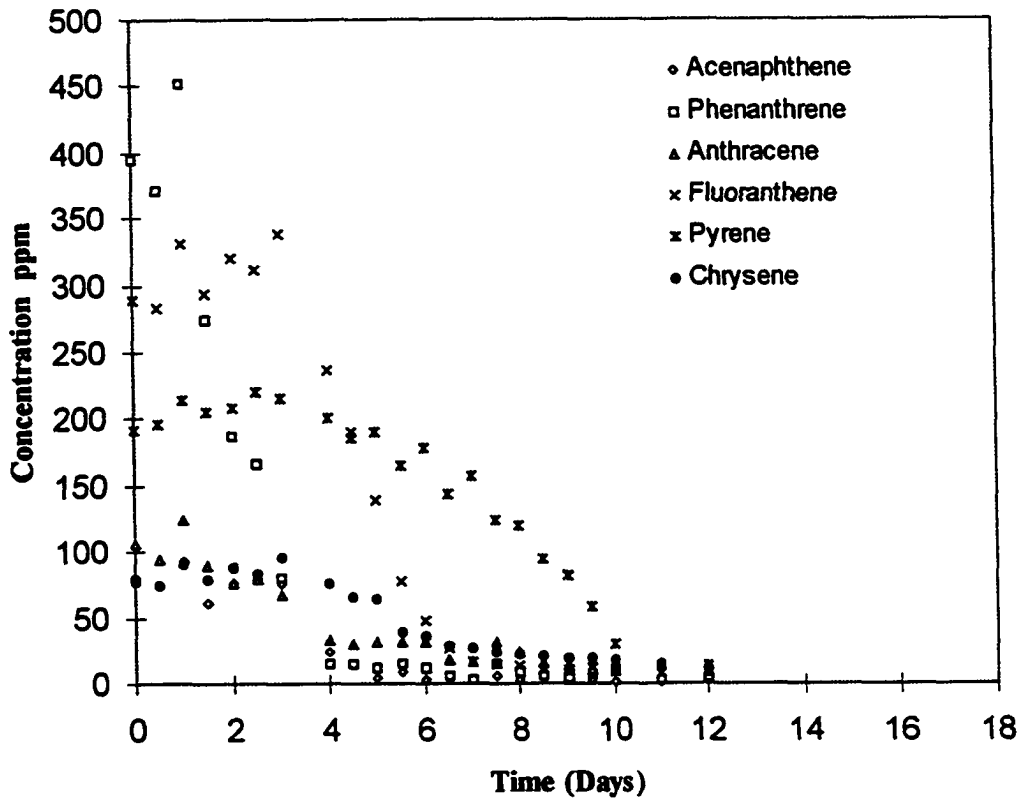


Figure A.3. Degradation of six target PAHs in a sonicated creosote-contaminated soil (experiment B)

50 g of soil was sonicated in 200 ml water for 30 minutes.

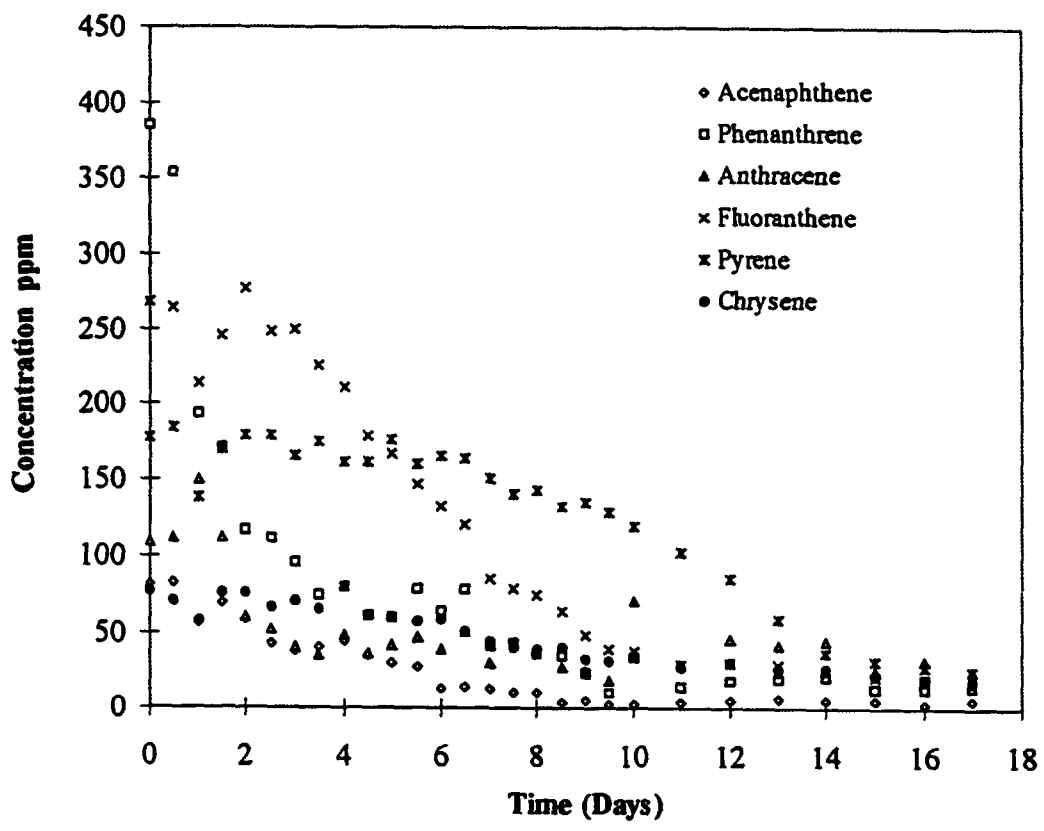


Figure A.4. Degradation of six target PAHs in a Non-sonicated creosote-contaminated soil (experiment C)

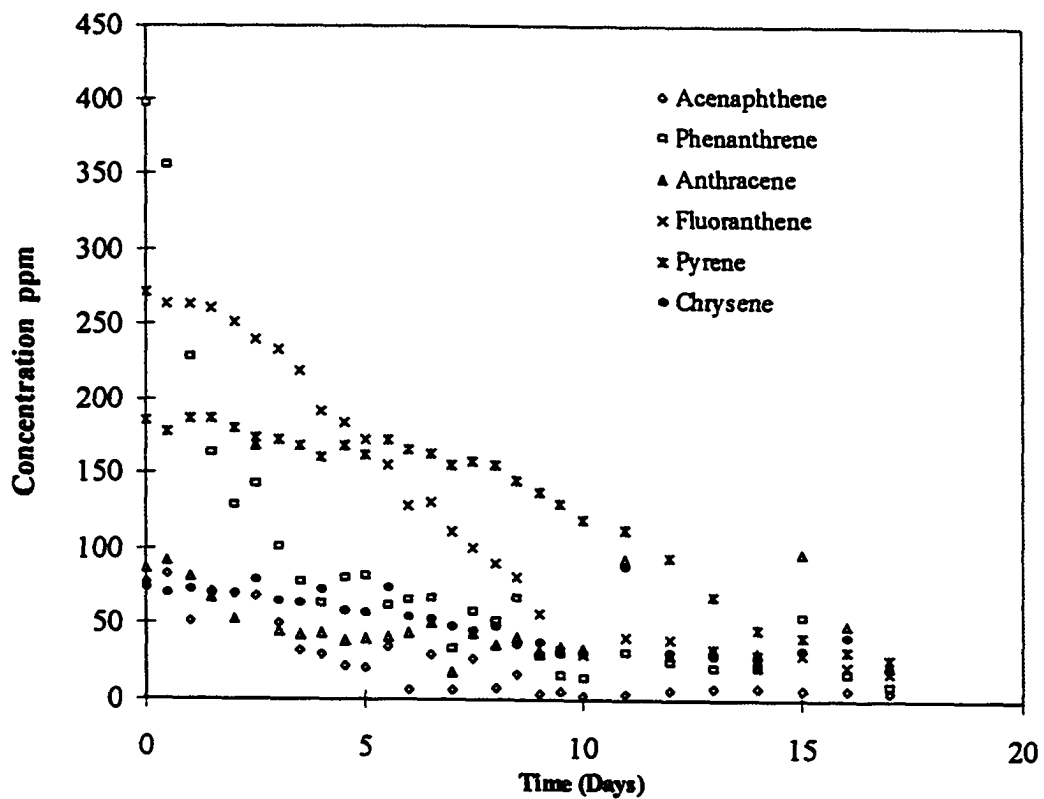


Figure A.5. Degradation of six target PAHs in a Non-sonicated creosote-contaminated soil (experiment D)

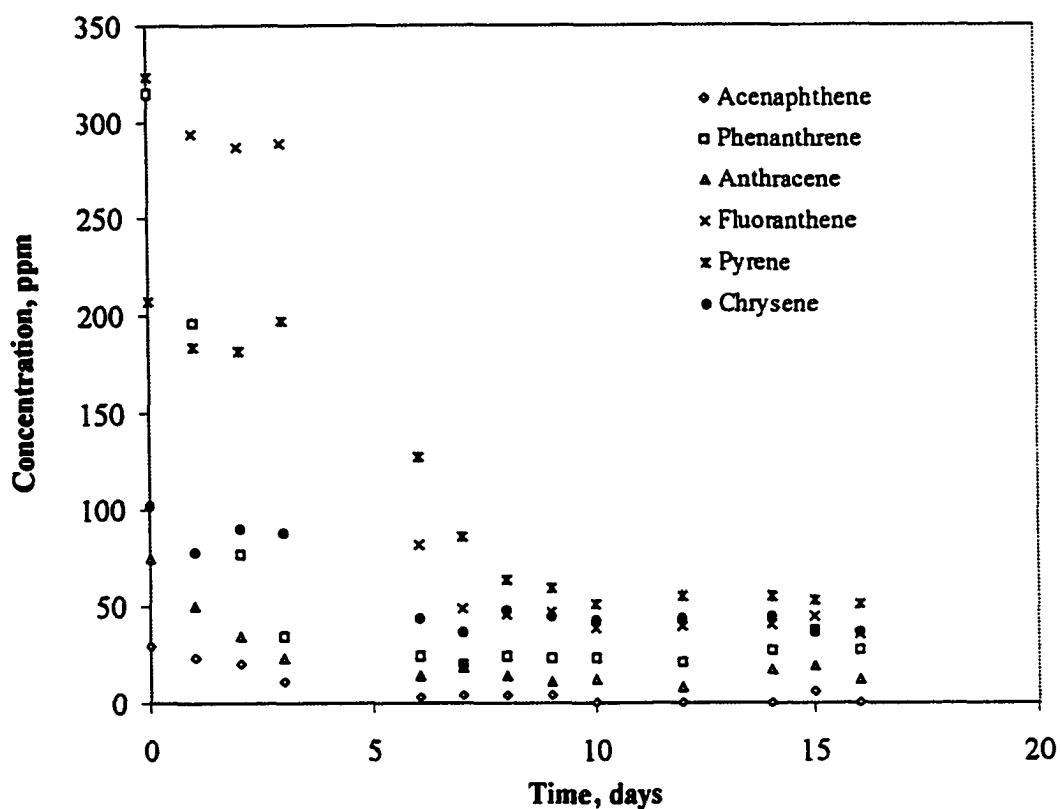


Figure A.6. Degradation of six target PAHs in a sonicated creosote-contaminated soil (experiment E)

50 g of soil was sonicated in 200 ml water for 21 minutes.

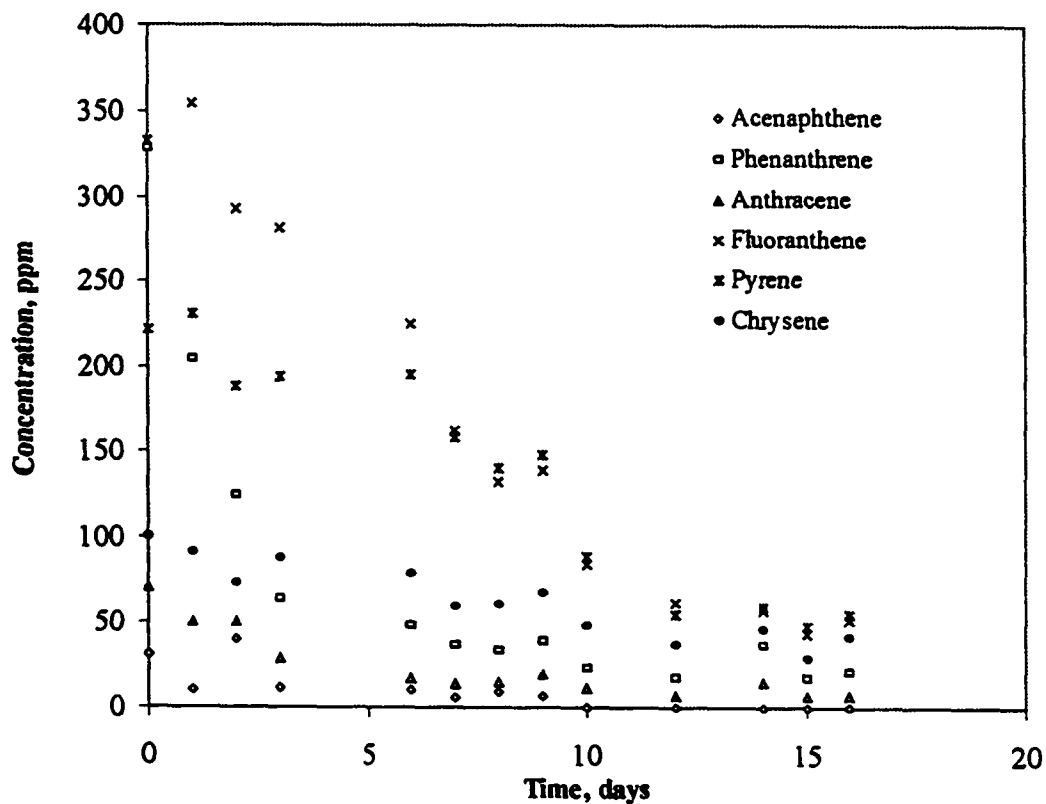


Figure A.7. Degradation of six target PAHs in a Non-sonicated creosote-contaminated soil (experiment F)

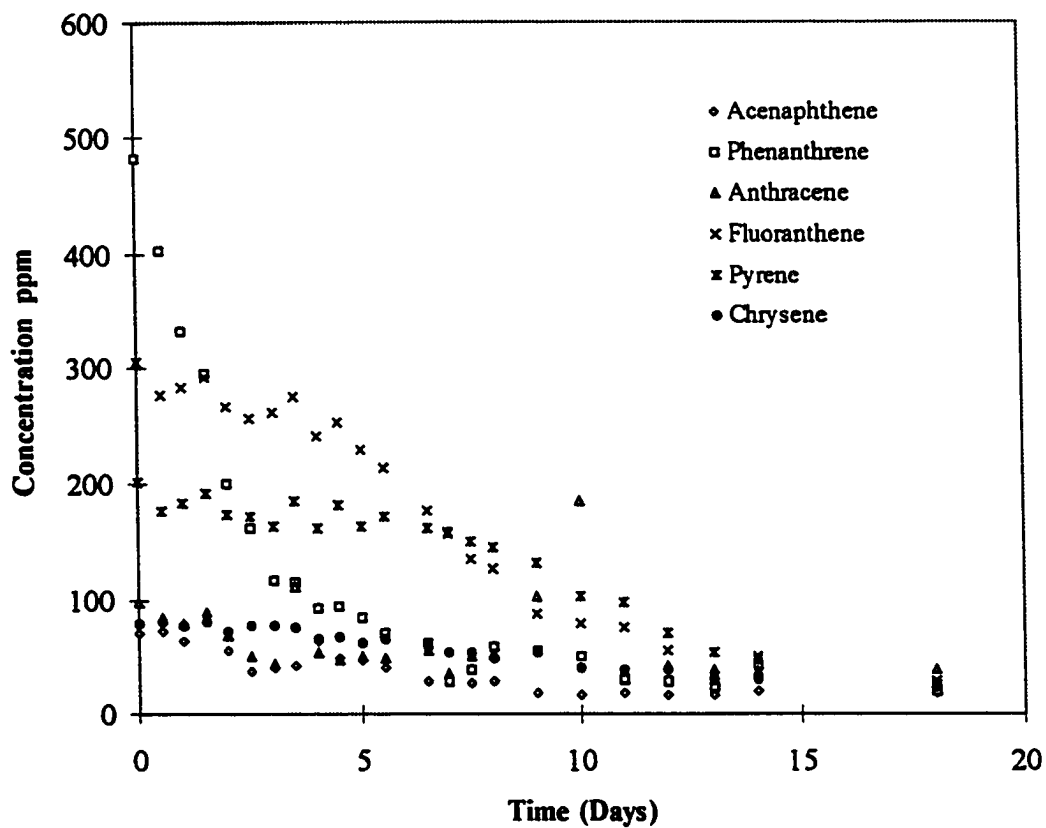


Figure A.8. Degradation of six target PAHs in a Non-sonicated creosote-contaminated soil (experiment G)

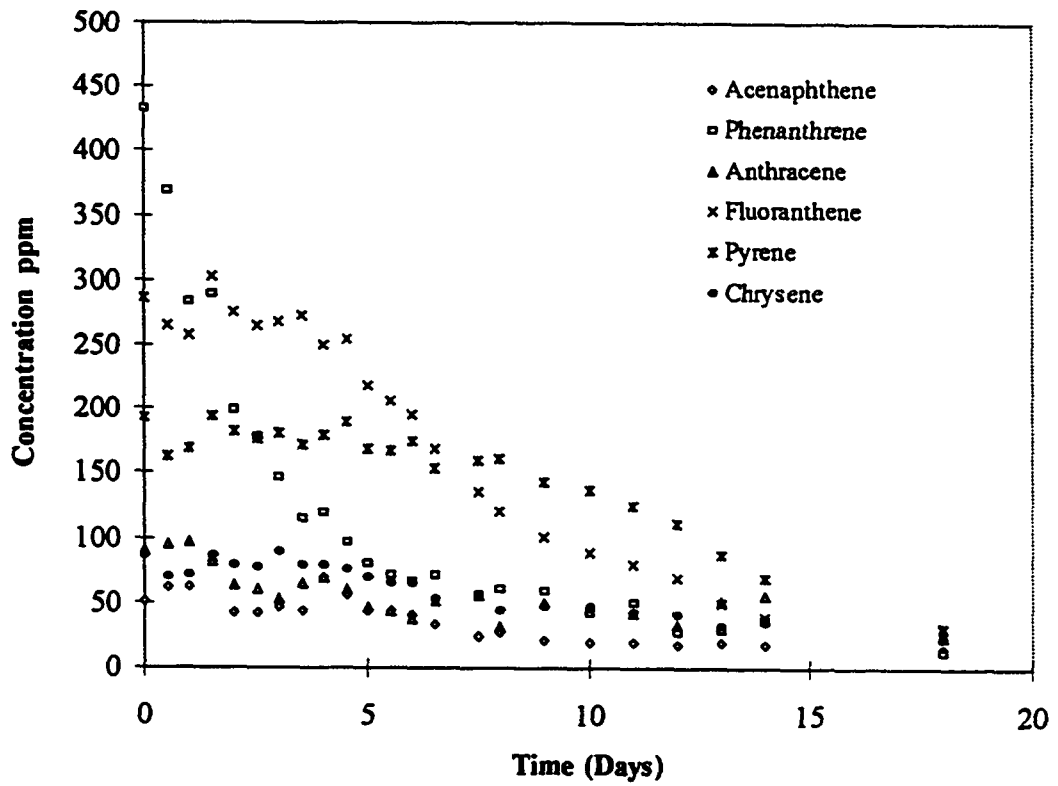


Figure A.9. Degradation of six target PAHs in a Non-sonicated creosote-contaminated soil (experiment H)

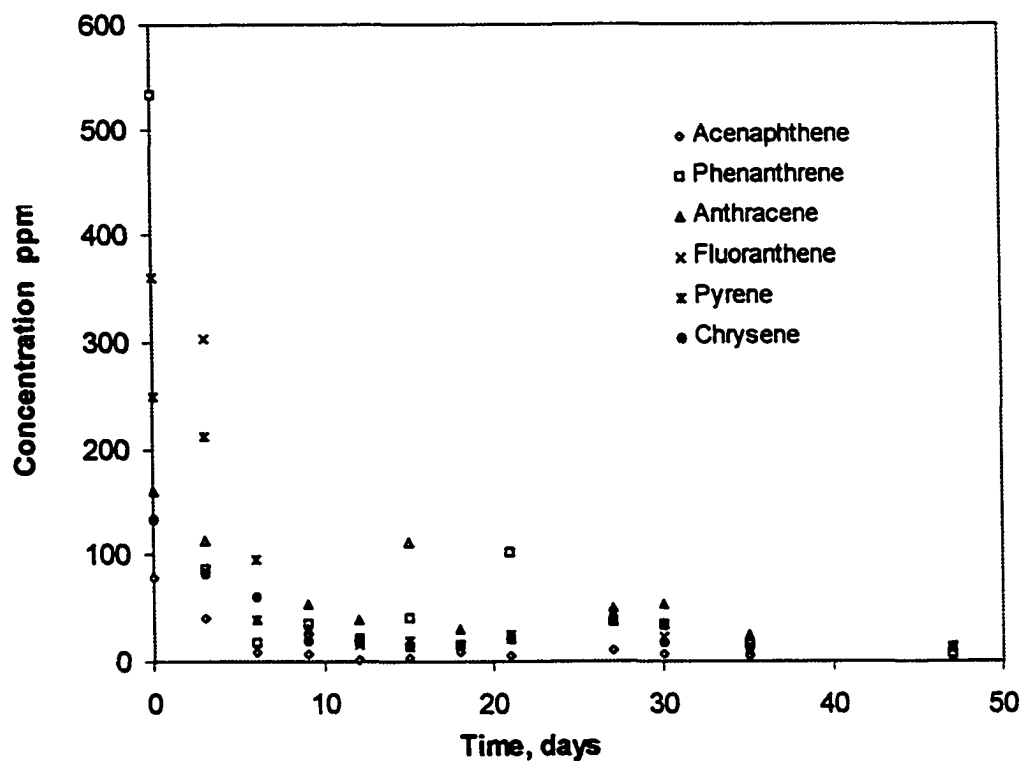


Figure A.10. Degradation of six target PAHs in a Sonicated creosote-contaminated soil (experiment I)

50 g of soil was sonicated in 200 ml water for 21 minutes.

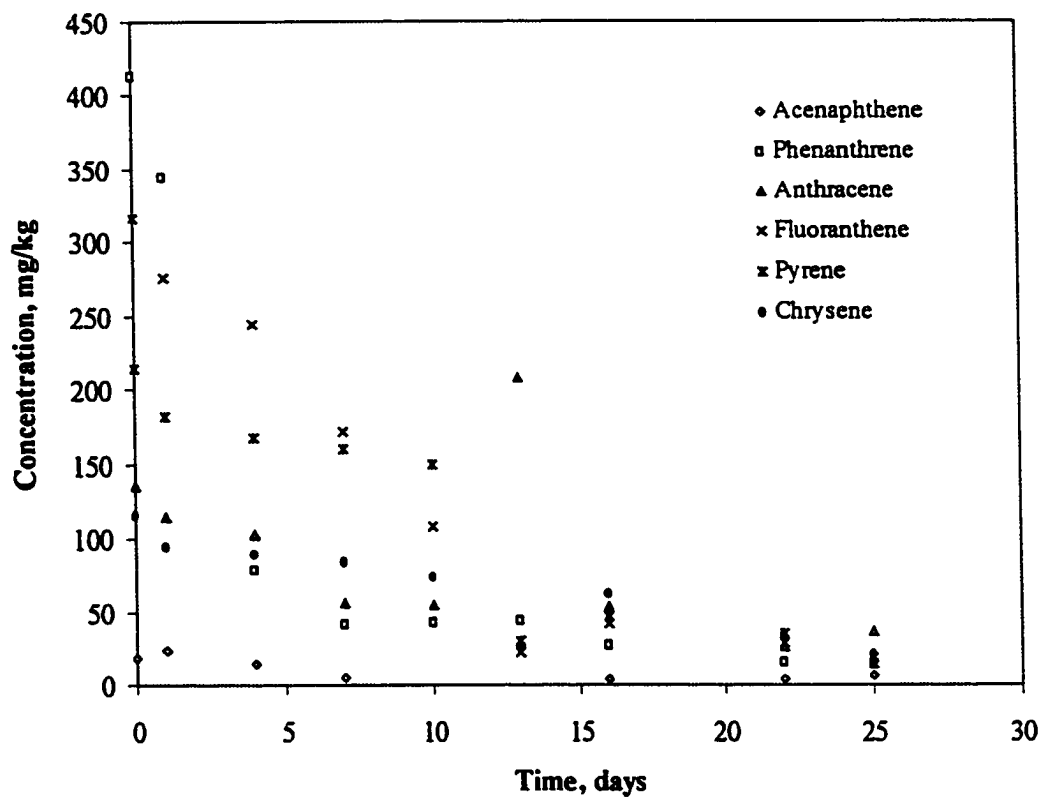


Figure A.11. Degradation of six target PAHs in a Non-sonicated creosote-contaminated soil (experiment J)

A.2. Sample Calculation of the Rate Constants

Based on the data presented in section A.1., the apparent rate constants for the rapid phase of degradation were estimated for all six PAHs in each experiment. The following is a sample calculation for degradation of fluoranthene in sonicated creosote-contaminated soil of experiment B.

A.2.1. Estimation of the Apparent First Order Rate Constants

The apparent rate constant for the rapid phase of degradation was calculated assuming first order kinetics for degradation of PAHs.

$$\frac{dC}{dt} = -kC \quad C(0) = C_0 \quad (\text{A.1})$$

$$\text{Ln}\left(\frac{C_0}{C}\right) = kt \quad (\text{A.2})$$

$\text{Ln}(C_0/C)$ was plotted against time and the slope was estimated by linear regression.

The statistical analysis on calculation of the slope is presented for the sample calculations.

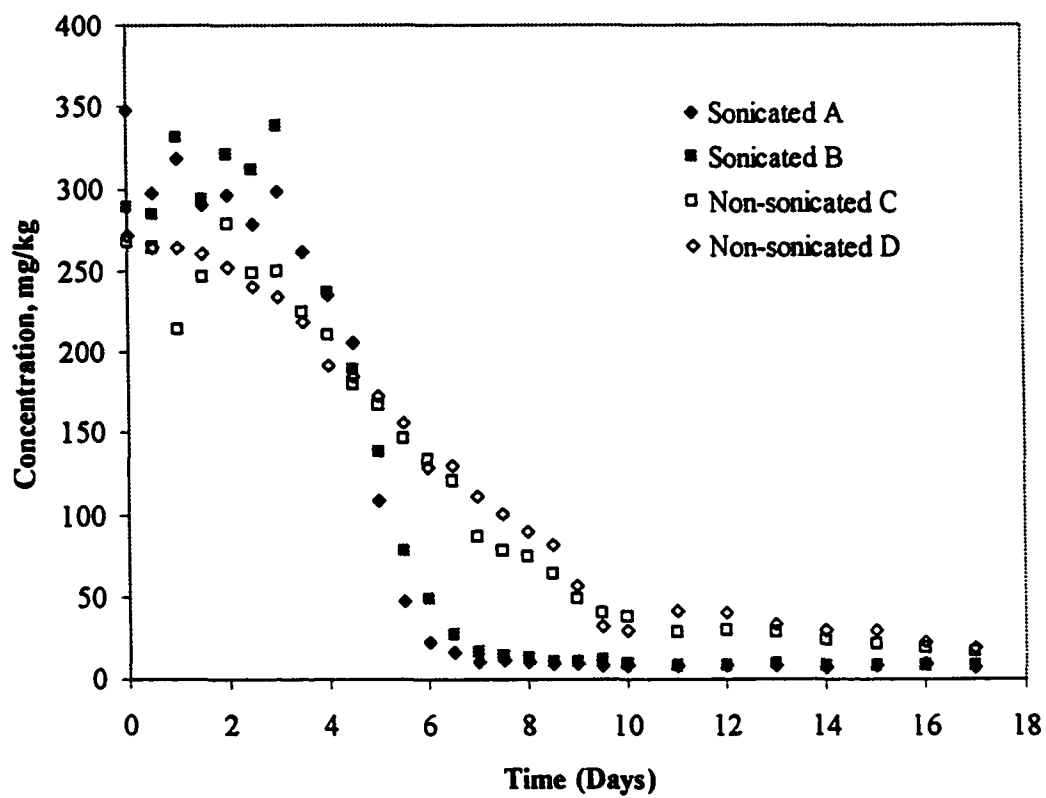


Figure A.12. Degradation of Fluoranthene in creosote-contaminated soil.

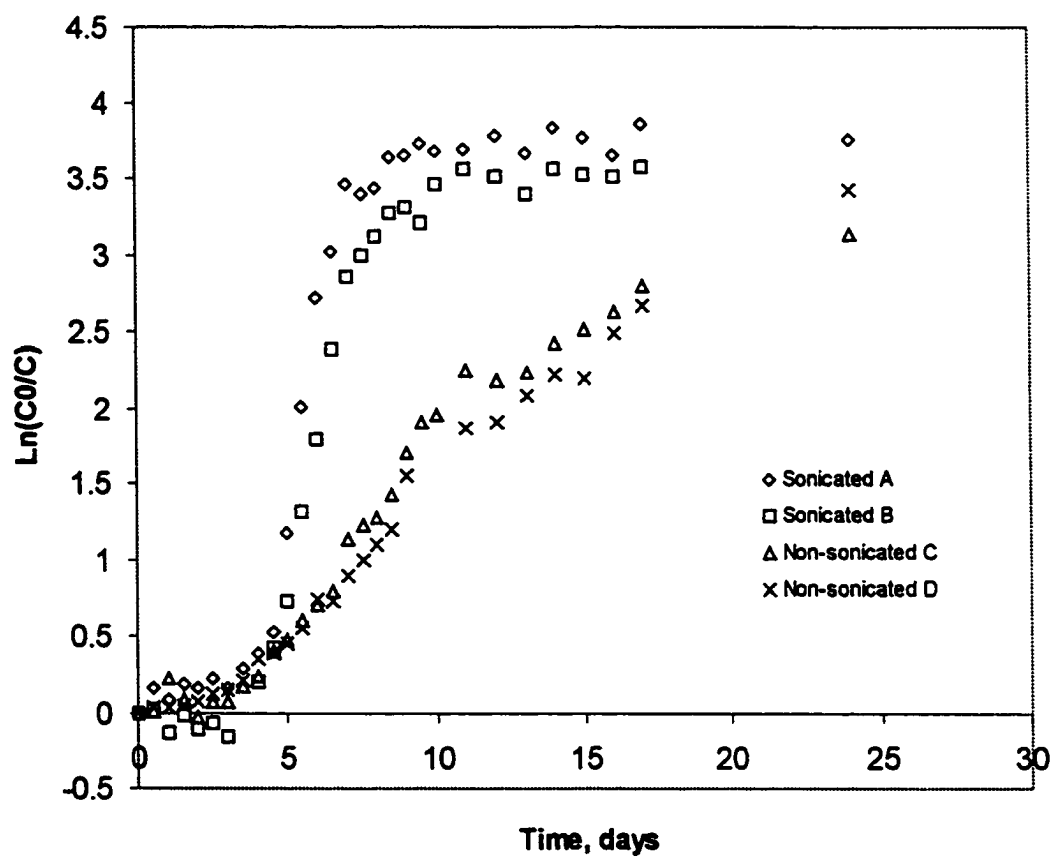


Figure A.13. The apparent first order rate constant of degradation of fluoranthene in creosote-contaminated soil.

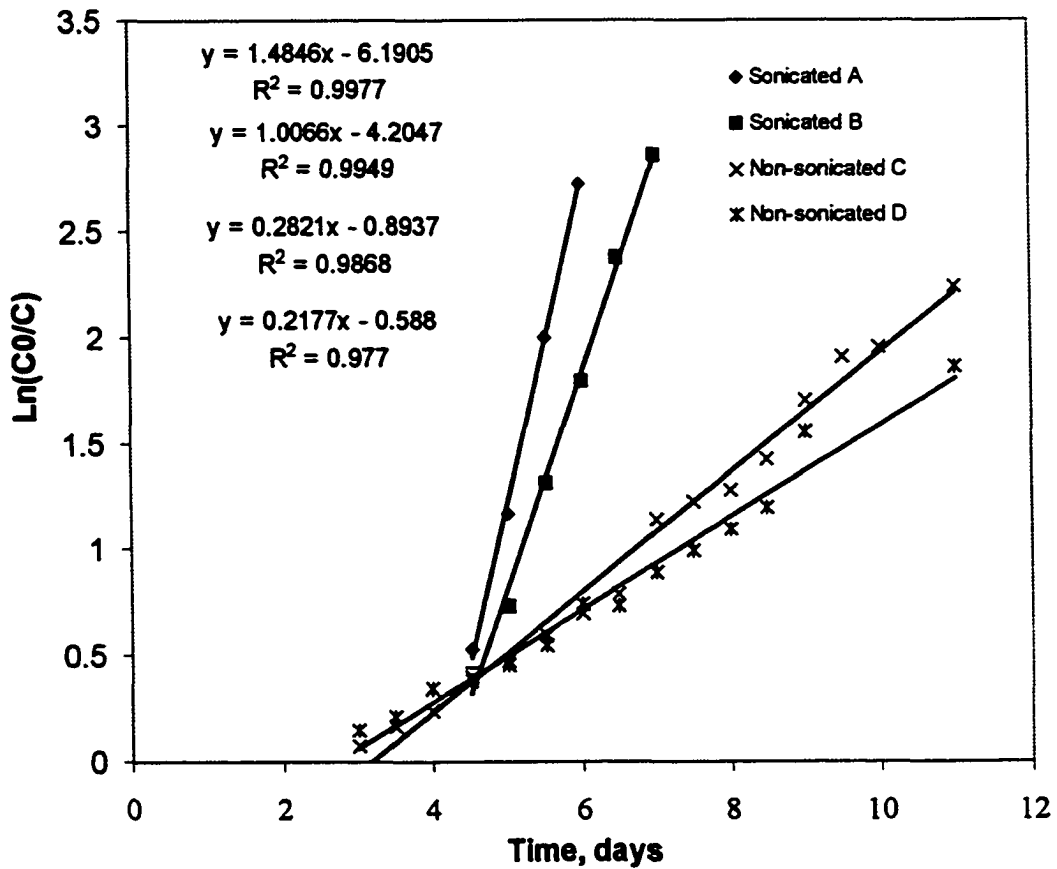


Figure A.14. The apparent first order rate constant of degradation of fluoranthene in creosote-contaminated soil in the rapid phase of degradation.

A.2.2. Statistical analysis

Samples of the statistical analysis for calculation of the slopes are presented for fluoranthene in four experiments.

Sonicated A		Non-sonicated C		Non-sonicated D	
Time	Ln(C0/C)	Time	Ln(C0/C)	Time	Ln(C0/C)
4.5	0.524693162	3	0.069487973	3	0.146189841
5	1.166146912	3.5	0.171017922	3.5	0.209673122
5.5	2.003619778	4	0.237594296	4	0.344010519
6	2.719856211	4.5	0.396919589	4.5	0.384010735
		5	0.470201495	5	0.449470232
		5.5	0.596880893	5.5	0.55083769
		6	0.696504977	6	0.744912826
Sonicated B		6.5	0.791281413	6.5	0.728319486
Time	Ln(C0/C)	7	1.135061131	7	0.889234023
4.5	0.42066889	7.5	1.224383963	7.5	0.988908622
5	0.733287302	8	1.276245729	8	1.096870602
5.5	1.310694866	8.5	1.428972785	8.5	1.195361145
6	1.793468189	9	1.707189488	9	1.551292342
6.5	2.383826611	9.5	1.907443667	11	1.863455369
7	2.856791962	10	1.95253105		
		11	2.24235527		

Experiment A:

SUMMARY OUTPUT

<i>Regression Statistics</i>	
Multiple R	0.998834957
R Square	0.997671271
Adjusted R Squa	0.996506906
Standard Error	0.056703909
Observations	4

ANOVA

	<i>df</i>	<i>SS</i>	<i>MS</i>	<i>F</i>	<i>Significance F</i>
Regression	1	2.755018253	2.755018253	856.837541	0.001165043
Residual	2	0.006430667	0.003215333		
Total	3	2.76144892			

	<i>Coefficients</i>	<i>Standard Error</i>	<i>t Stat</i>	<i>P-value</i>	<i>Lower 95%</i>	<i>Upper 95%</i>	<i>Lower 95.0%</i>	<i>Upper 95.0%</i>
Intercept	-6.190531099	0.267772164	-23.11865058	0.001865771	-7.342662535	-5.03839966	-7.34266253	-5.03839966
X Variable 1	1.484592403	0.050717518	29.27178746	0.001165043	1.266372384	1.702812421	1.266372384	1.702812421

RESIDUAL OUTPUT

<i>Observation</i>	<i>Predicted Y</i>	<i>Residuals</i>	<i>Standard Residuals</i>
1	0.490134714	0.034558448	0.609454422
2	1.232430915	-0.066284003	-1.168949447
3	1.974727116	0.028892662	0.509535628
4	2.717023318	0.002832893	0.049959397

PROBABILITY OUTPUT

<i>Percentile</i>	<i>Y</i>
12.5	0.524693162
37.5	1.166146912
62.5	2.003619778
87.5	2.719856211

Experiment B:

SUMMARY OUTPUT

<i>Regression Statistics</i>	
Multiple R	0.99745497
R Square	0.994916416
Adjusted R Squa	0.993645521
Standard Error	0.07524809
Observations	6

ANOVA

	<i>df</i>	<i>SS</i>	<i>MS</i>	<i>F</i>	<i>Significance F</i>
Regression	1	4.432692256	4.432692256	782.8465094	9.70753E-06
Residual	4	0.0226491	0.005662275		
Total	5	4.455341356			

	<i>Coefficients</i>	<i>Standard Error</i>	<i>t Stat</i>	<i>P-value</i>	<i>Lower 95%</i>	<i>Upper 95%</i>	<i>Lower 95.0%</i>	<i>Upper 95.0%</i>
Intercept	-4.204664917	0.209127554	-20.10574327	3.61195E-05	-4.785297294	-3.62403254	-4.78529729	-3.62403254
X Variable 1	1.006571806	0.035975468	27.97939437	9.70753E-06	0.906687688	1.106455925	0.906687688	1.106455925

RESIDUAL OUTPUT

<i>Observation</i>	<i>Predicted Y</i>	<i>Residuals</i>	<i>Standard Residuals</i>
1	0.324908212	0.095760678	1.272599445
2	0.828194115	-0.094906813	-1.261252116
3	1.331480018	-0.020785153	-0.276221666
4	1.834765922	-0.041297733	-0.548821008
5	2.338051825	0.045774787	0.608318253
6	2.841337728	0.015454234	0.205377092

PROBABILITY OUTPUT

<i>Percentile</i>	<i>Y</i>
8.333333333	0.42066889
25	0.733287302
41.66666667	1.310694866
58.33333333	1.793468189
75	2.383826611
91.66666667	2.856791962

Experiment C:

SUMMARY OUTPUT

<i>Regression Statistics</i>	
Multiple R	0.993360233
R Square	0.986764552
Adjusted R Squa	0.985819162
Standard Error	0.082356369
Observations	16

ANOVA					
	<i>df</i>	<i>SS</i>	<i>MS</i>	<i>F</i>	<i>Significance F</i>
Regression	1	7.079413802	7.079413802	1043.765443	1.49909E-14
Residual	14	0.094956002	0.006782572		
Total	15	7.174369804			

	<i>Coefficients</i>	<i>Standard Error</i>	<i>t Stat</i>	<i>P-value</i>	<i>Lower 95%</i>	<i>Upper 95%</i>	<i>Lower 95.0%</i>	<i>Upper 95.0%</i>
Intercept	-0.893716088	0.062681804	-14.25798292	9.93926E-10	-1.028155306	-0.75927687	-1.02815531	-0.75927687
X Variable 1	0.282060176	0.008730524	32.30735896	1.49909E-14	0.263335047	0.300785304	0.263335047	0.300785304

RESIDUAL OUTPUT

<i>Observation</i>	<i>Predicted Y</i>	<i>Residuals</i>	<i>Standard Residuals</i>
1	-0.047535561	0.117023534	1.420940912
2	0.093494526	0.077523396	0.941316338
3	0.234524614	0.003069682	0.037273161
4	0.375554702	0.021364887	0.259419971
5	0.51658479	-0.046383295	-0.563202279
6	0.657614878	-0.060733984	-0.737453395
7	0.798644965	-0.102139989	-1.240219665
8	0.939675053	-0.148393641	-1.801847774
9	1.080705141	0.05435599	0.660009545
10	1.221735229	0.002648735	0.032161867
11	1.362765317	-0.086519588	-1.050551266
12	1.503795404	-0.074822619	-0.90852256
13	1.644825492	0.062363996	0.757245577
14	1.78585558	0.121588087	1.476365312
15	1.926885668	0.025645382	0.311395251
16	2.208945843	0.033409426	0.405669006

PROBABILITY OUTPUT

<i>Percentile</i>	<i>Y</i>
3.125	0.069487973
9.375	0.171017922
15.625	0.237594296
21.875	0.396919589
28.125	0.470201495
34.375	0.596880893
40.625	0.696504977
46.875	0.791281413
53.125	1.135061131
59.375	1.224383963
65.625	1.276245729
71.875	1.428972785
78.125	1.707189488
84.375	1.907443667
90.625	1.95253105
96.875	2.24235527

Experiment D:

SUMMARY OUTPUT

<i>Regression Statistics</i>	
Multiple R	0.988415847
R Square	0.976965886
Adjusted R Squa	0.975046377
Standard Error	0.079989214
Observations	14

ANOVA					
	<i>df</i>	<i>SS</i>	<i>MS</i>	<i>F</i>	<i>Significance F</i>
Regression	1	3.256506891	3.256506891	508.9664323	3.40308E-11
Residual	12	0.076779293	0.006398274		
Total	13	3.333286184			

	<i>Coefficients</i>	<i>Standard Error</i>	<i>t Stat</i>	<i>P-value</i>	<i>Lower 95%</i>	<i>Upper 95%</i>	<i>Lower 95.0%</i>	<i>Upper 95.0%</i>
Intercept	-0.588034868	0.064962048	-9.051975526	1.03891E-06	-0.729575009	-0.44649473	-0.72957501	-0.44649473
X Variable 1	0.217697019	0.009649569	22.5602844	3.40308E-11	0.196672415	0.238721623	0.196672415	0.238721623

RESIDUAL OUTPUT

<i>Observation</i>	<i>Predicted Y</i>	<i>Residuals</i>	<i>Standard Residuals</i>
1	0.065056189	0.081133652	1.014307399
2	0.173904699	0.035768423	0.447165573
3	0.282753209	0.061257311	0.765819634
4	0.391601718	-0.007590983	-0.094900087
5	0.500450228	-0.050979996	-0.637335878
6	0.609298737	-0.058461047	-0.730861624
7	0.718147247	0.026765579	0.334614851
8	0.826995757	-0.098676271	-1.233619703
9	0.935844266	-0.046610243	-0.582706597
10	1.044692776	-0.055784154	-0.697395944
11	1.153541286	-0.056670683	-0.708479059
12	1.262389795	-0.067028651	-0.837971109
13	1.371238305	0.180054037	2.250978945
14	1.806632343	0.056823026	0.710383599

PROBABILITY OUTPUT

<i>Percentile</i>	<i>Y</i>
3.571428571	0.146189841
10.71428571	0.209673122
17.85714286	0.344010519
25	0.384010735
32.14285714	0.449470232
39.28571429	0.55083769
46.42857143	0.728319486
53.57142857	0.744912826
60.71428571	0.889234023
67.85714286	0.988908622
75	1.096870602
82.14285714	1.195361145
89.28571429	1.551292342
96.42857143	1.863455369

A.2.3. Apparent Rate Constants for 6 PAHs

Acenaphthene	Slope, k	SE	R ²
Non-sonicated C	<u>0.29838178</u>	<u>0.02513296</u>	0.92154169
Non-sonicated D	<u>0.38947563</u>	<u>0.05063371</u>	0.85542282
Non-sonicated F	<u>0.20964927</u>	<u>0.04789445</u>	0.90548614
Non-sonicated G	<u>0.20506758</u>	<u>0.01518725</u>	0.95796567
Non-sonicated H	<u>0.19311188</u>	<u>0.0166394</u>	0.95059718
Non-sonicated J	<u>0.18276879</u>	<u>0.05173109</u>	0.86190207

Sonicated A	<u>1.21263235</u>	<u>0.09975234</u>	0.97364586
Sonicated B	<u>1.01169353</u>	<u>0.16153732</u>	0.90745888
Sonicated E	<u>0.4916273</u>	<u>0.0227635</u>	0.99786068
Sonicated I	<u>0.31893244</u>	<u>0.03313532</u>	0.96863353

Phenanthrene	Slope, k	SE	R ²
Non-sonicated C	<u>0.40240414</u>	<u>0.05550531</u>	0.89754107
Non-sonicated D	<u>0.44816565</u>	<u>0.04222711</u>	0.94942704
Non-sonicated F	<u>0.54265064</u>	<u>0.03292053</u>	0.99269302
Non-sonicated G	<u>0.4713105</u>	<u>0.03097514</u>	0.9788601
Non-sonicated H	<u>0.4713105</u>	<u>0.03097514</u>	0.9788601
Non-sonicated J	<u>0.34741397</u>	<u>0.04380551</u>	0.96918243

Sonicated A	<u>1.67596777</u>	<u>0.13305157</u>	0.98144353
Sonicated B	<u>1.16065472</u>	<u>0.18472146</u>	0.92937766
Sonicated E	<u>0.75393</u>	<u>0.06480321</u>	0.98543901
Sonicated I	<u>0.57079113</u>	<u>0.02069474</u>	0.99868721

Anthracene	Slope, k	SE	R²
Non-sonicated C	<u>0.35794473</u>	<u>0.02957984</u>	0.98652595
Non-sonicated D	<u>0.28413774</u>	<u>0.04749546</u>	0.95043717
Non-sonicated F	<u>0.2432611</u>	<u>0.0304772</u>	0.95502802
Non-sonicated G	<u>0.35407763</u>	<u>0.08129815</u>	0.86344157
Non-sonicated H	<u>0.30104958</u>	<u>0.03380405</u>	0.96355329
Non-sonicated J	<u>0.11504502</u>	<u>0.02685194</u>	0.90175017
Sonicated A	<u>0.53660251</u>	<u>0.05741588</u>	0.95621028
Sonicated B	<u>0.536988</u>	<u>0.06637071</u>	0.97035282
Sonicated E	<u>0.38695789</u>	<u>0.0033264</u>	0.99985223
Sonicated I	<u>0.23113092</u>	<u>0.06804974</u>	0.92023107

Fluoranthene	Slope, k	SE	R²
Non-sonicated C	<u>0.28206018</u>	<u>0.00873052</u>	0.98676455
Non-sonicated D	<u>0.21769702</u>	<u>0.00964957</u>	0.97696589
Non-sonicated F	<u>0.20957712</u>	<u>0.02504639</u>	0.94595765
Non-sonicated G	<u>0.22453385</u>	<u>0.0131137</u>	0.97994422
Non-sonicated H	<u>0.20584311</u>	<u>0.00736369</u>	0.99238013
Non-sonicated J	<u>0.18629616</u>	<u>0.05839902</u>	0.77232123
Sonicated A	<u>1.4845924</u>	<u>0.05071752</u>	0.99767127
Sonicated B	<u>1.00657181</u>	<u>0.03597547</u>	0.99491642
Sonicated E	<u>0.43895655</u>	<u>0.01884572</u>	0.99816015
Sonicated I	<u>0.39619221</u>	<u>0.1670458</u>	0.84906198

Pyrene	Slope, k	SE	R²
Non-sonicated C	<u>0.32217069</u>	<u>0.03032994</u>	0.97410023
Non-sonicated D	<u>0.2706455</u>	<u>0.02545788</u>	0.97414249
Non-sonicated F	<u>0.20644488</u>	<u>0.03198261</u>	0.91240721
Non-sonicated G	<u>0.19726444</u>	<u>0.01438333</u>	0.9741061
Non-sonicated H	<u>0.20201139</u>	<u>0.00641767</u>	0.99698136
Non-sonicated J	<u>0.17606487</u>	<u>0.08957454</u>	0.65890438

Sonicated A	<u>1.06528822</u>	<u>0.08634034</u>	0.98703255
Sonicated B	<u>0.90305925</u>	<u>0.06515701</u>	0.98969563
Sonicated E	<u>0.35200306</u>	<u>0.02535096</u>	0.99484
Sonicated I	<u>0.32691561</u>	<u>0.03414801</u>	0.98920689

Chrysene	Slope, k	SE	R²
Non-sonicated C	<u>0.1697469</u>	<u>0.01788714</u>	0.93753767
Non-sonicated D	<u>0.16047762</u>	<u>0.01997911</u>	0.90212169
Non-sonicated F	<u>0.11513608</u>	<u>0.01631026</u>	0.94321534
Non-sonicated G	<u>0.0814541</u>	<u>0.00419538</u>	0.96418969
Non-sonicated H	<u>0.08492811</u>	<u>0.00487958</u>	0.95281931
Non-sonicated J	<u>0.03415298</u>	<u>0.00568391</u>	0.90026074

Sonicated A	<u>0.57228688</u>	<u>0.05488606</u>	0.9731468
Sonicated B	<u>0.45429952</u>	<u>0.07703242</u>	0.92059423
Sonicated E	<u>0.21855251</u>	<u>0.01433667</u>	0.9957153
Sonicated I	<u>0.19581306</u>	<u>0.0449177</u>	0.9047807

Appendix B

This appendix contains more images form Scanning electron microscopy and confocal scanning laser microscopy.



Figure B.1. Cryogenic scanning electron microscopy of Devon hydrocarbon-contaminated soil. X1000. The image illustrates the microorganisms associated with clay aggregates.

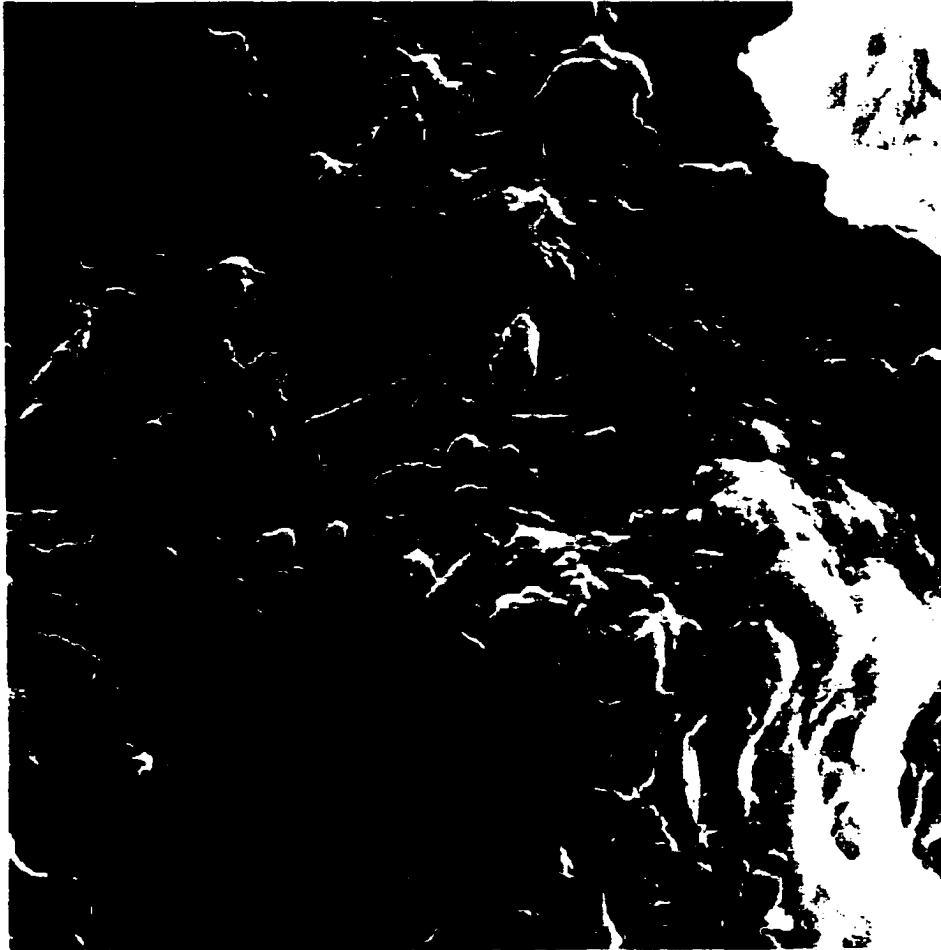


Figure B.2. Cryogenic scanning electron microscopy of Devon hydrocarbon-contaminated soil. X3700. The image illustrates the microorganisms associated with clay aggregates.

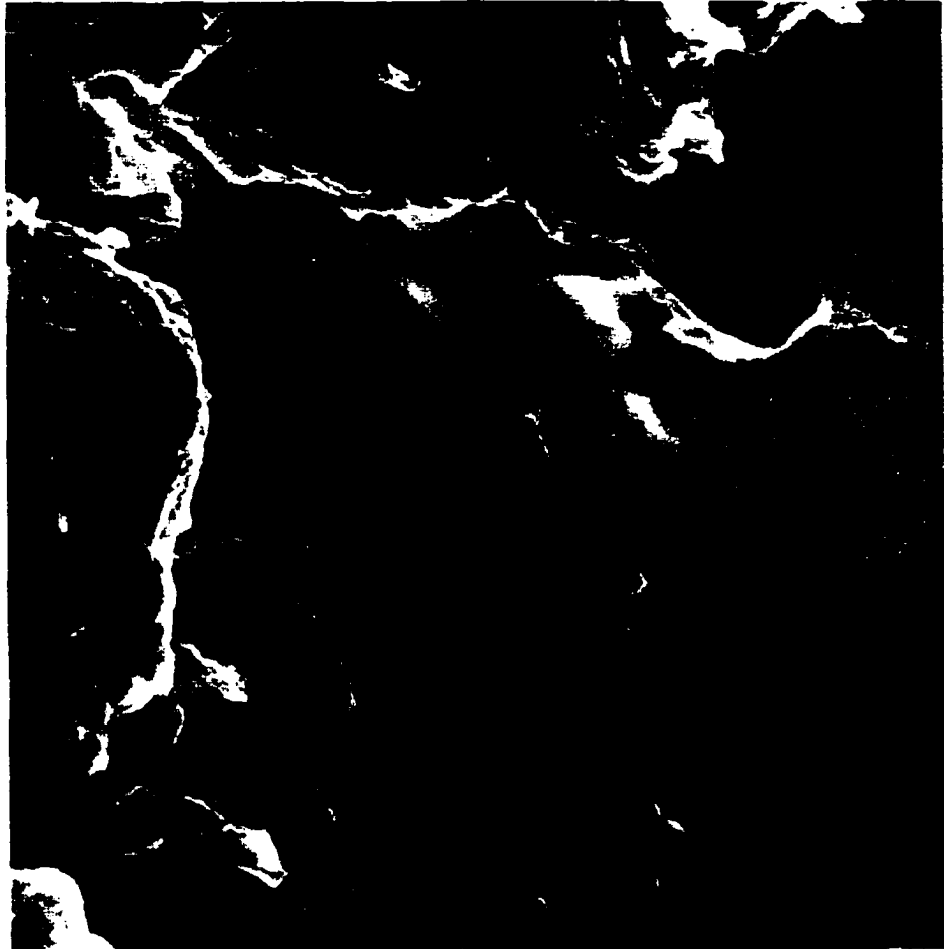


Figure B.3. Cryogenic scanning electron microscopy of Devon hydrocarbon-contaminated soil. X4000.

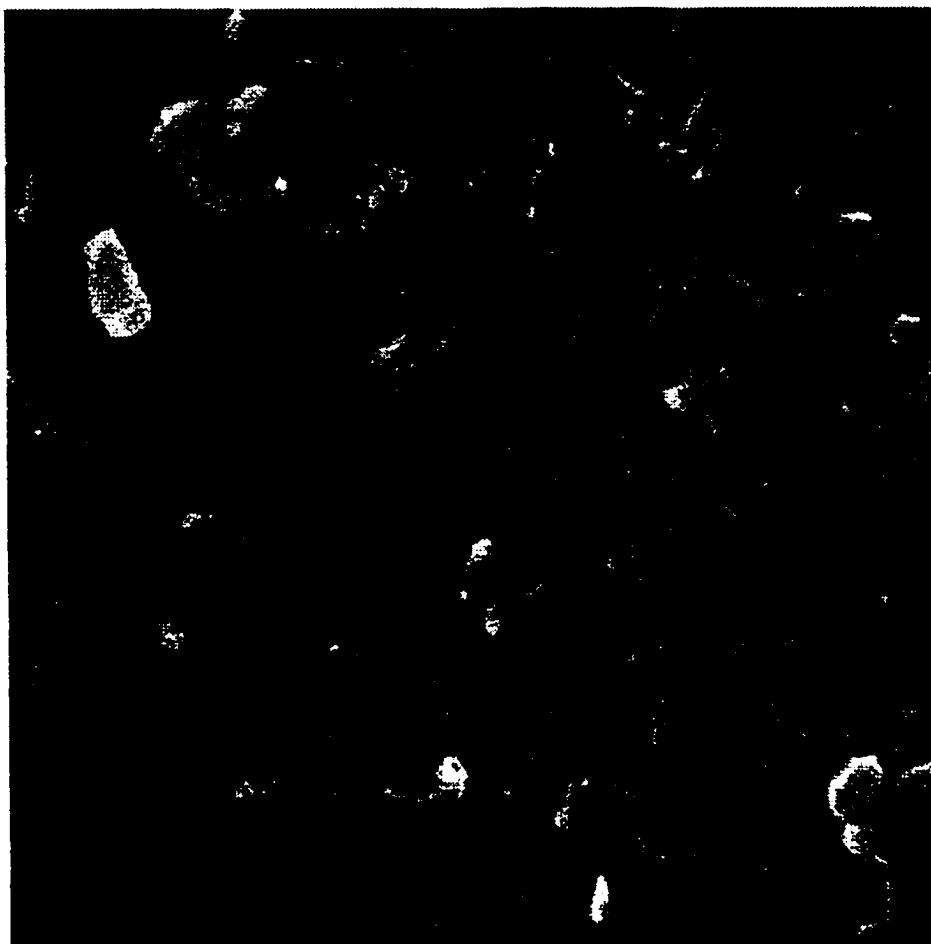


Figure B.4. Cryogenic scanning electron microscopy of Edmonton creosote-contaminated soil. X12000.



Figure B.5. Electron microscopy of Edmonton creosote-contaminated soil, X13000.



Figure B.6. Electron microscopy of Edmonton creosote-contaminated soil, X4300.

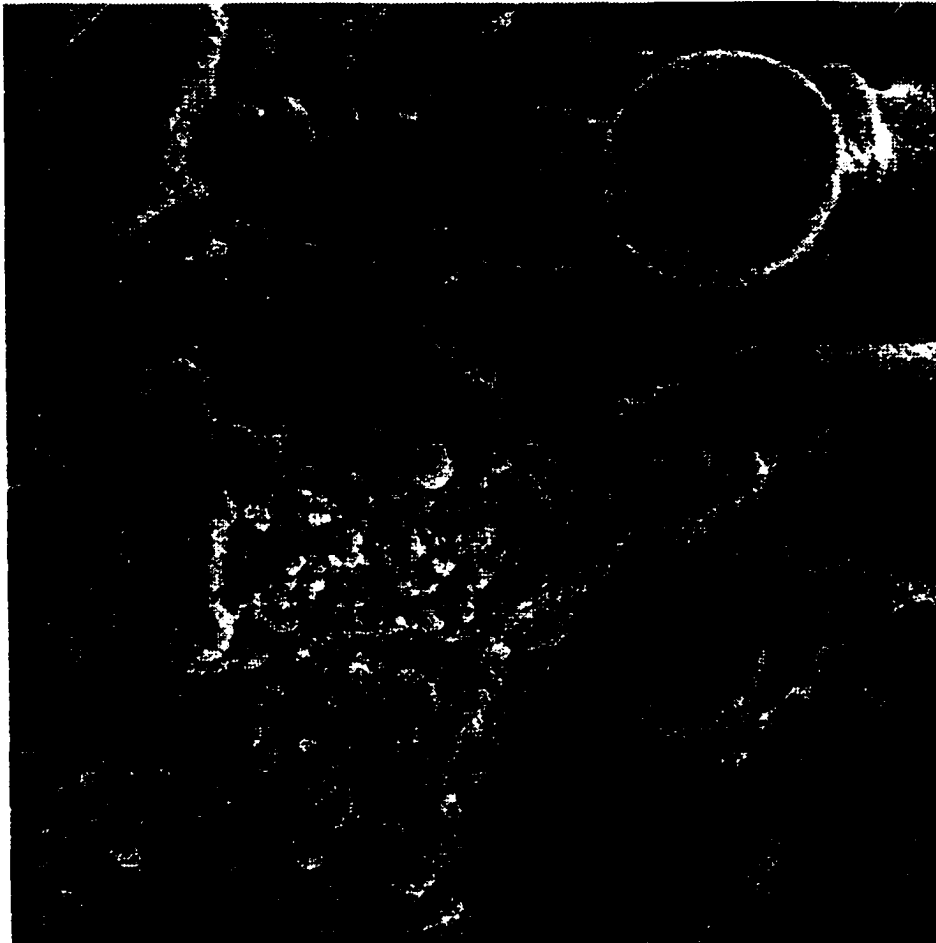


Figure B.7. Cryogenic scanning electron microscopy of Edmonton creosote-contaminated soil. X10000. The sample was freeze fractured.

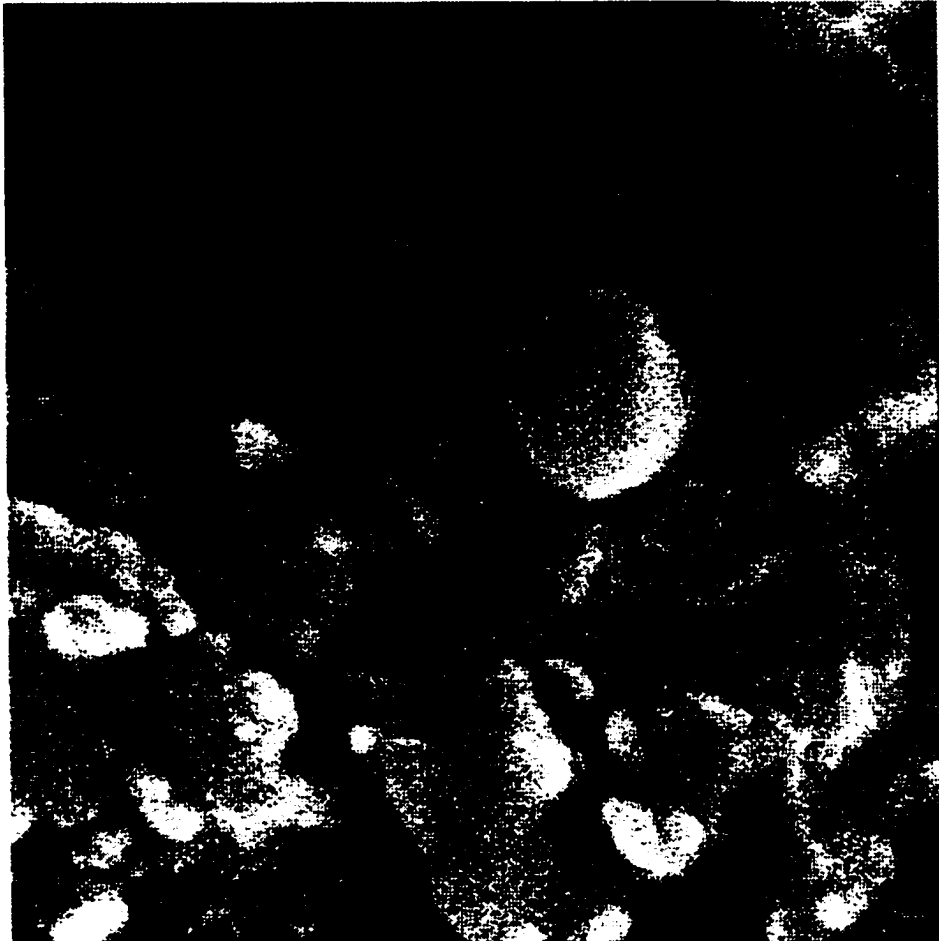


Figure B.8. Cryogenic scanning electron microscopy of Edmonton creosote-contaminated soil. X45000. The sample was freeze fractured.



Figure B.9. Cryogenic scanning electron microscopy of Edmonton creosote-contaminated soil. X10000. The sample was freeze fractured.

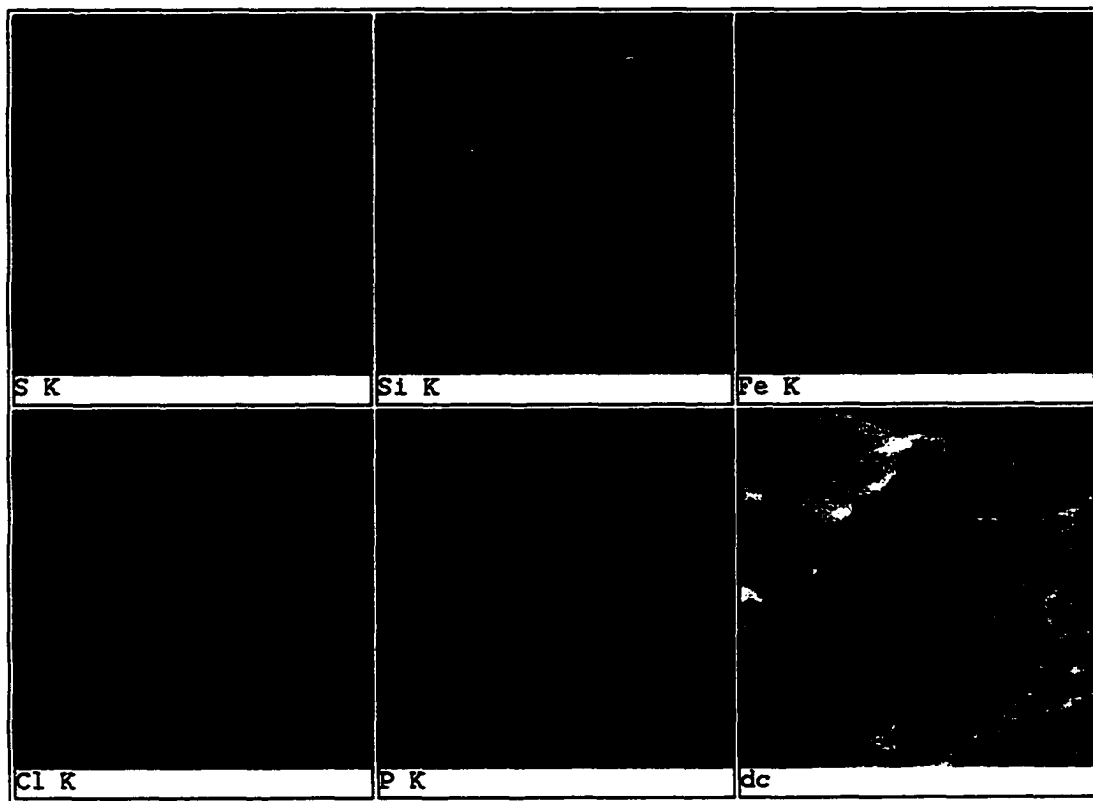
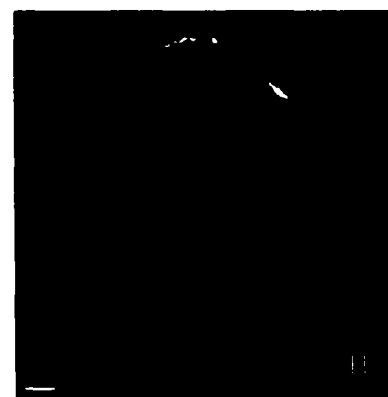
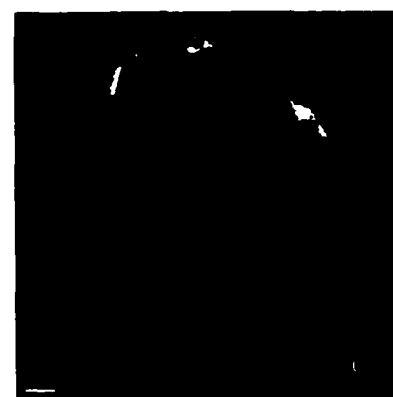
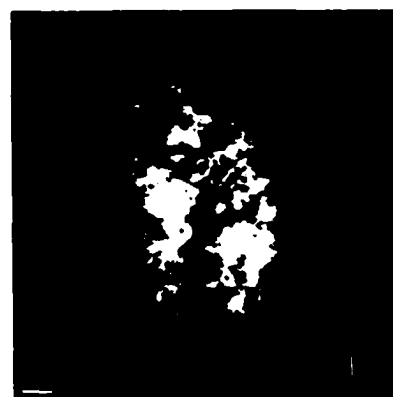
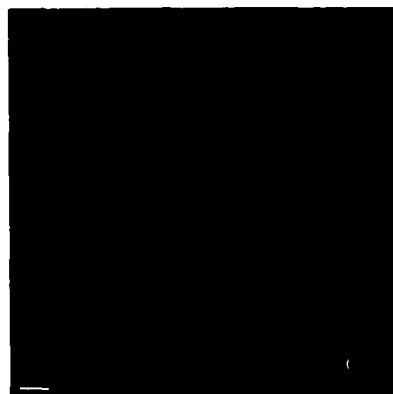
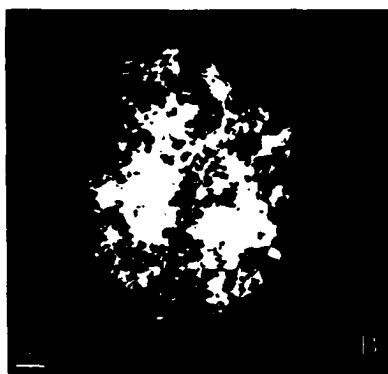
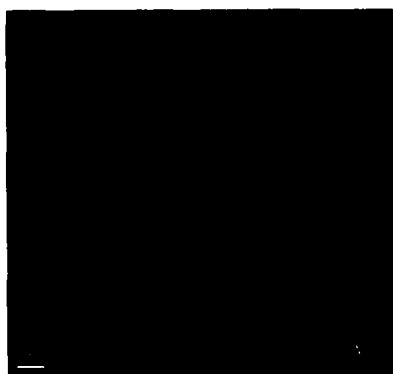


Figure B.10. A map of Devon hydrocarbon-contaminated soil, which shows the distribution of chemical elements obtained by elemental analysis of EDX. The distribution of Cl, Fe and P followed the same pattern as Si the major component of clay. S was used as precursor for the presence of organic materials in soil. The map of S shows its relative abundance and similar distribution as Si, Cl and Fe.

Figure B.11. An aggregate of Prince Albert creosote contaminate soil; A) 3D construction of 530 DF30 filter FITC signal, the 3D image was constructed by collecting 70 series of images at 1.2 μm focus intervals; B) 3D construction using pseudo-colour; C) the image from the first plane of focus; D, E, F, G, H) the images from 10th, 15th, 25th, 45th and 65th planes of focus respectively.



Appendix C

C.1. Mass Balance and Governing Equations for Pore Diffusion

A non-steady state diffusion equation was developed to explain the transport of contaminants within the porous structure of soil aggregates. The soil aggregates were considered as spheres.

$$JA \Big|_r - JA \Big|_{r+dr} = V \varepsilon_{NAPL} \rho_{NAPL} \frac{dC_{A/NAPL}}{dt} \quad \text{mg/day} \quad (C.1)$$

$$J = -D_{\text{eff}} \rho_{NAPL} \frac{dC_{A/NAPL}}{dr} \quad \text{mg/cm}^2 \cdot \text{s} \quad (C.2)$$

$$D_{\text{eff}} = D_{NAPL} \varepsilon_t / \tau \quad \text{cm}^2 / \text{s} \quad (C.3)$$

Equations (A.1) to (A.3) can be reduced to the following partial differential equation:

$$\frac{d^2 C_{A/NAPL}}{dr^2} + \frac{2}{r} \frac{dC_{A/NAPL}}{dr} = \frac{1}{D'_{\text{eff}}} \frac{dC_{A/NAPL}}{dt} \quad (C.4)$$

$$D'_{\text{eff}} = \frac{D_{\text{eff}}}{\varepsilon_{NAPL}} \quad (C.5)$$

$C_{A/NAPL}$ = concentration of component A in NAPL, mg/kg

J = flux of component A, mg/cm².d

A = area, cm²

V = volume of the aggregate, cm³

ϵ_{NAPL}	= NAPL filled porosity
ϵ_t	= total porosity, ($\epsilon_{NAPL} + \epsilon_{water}$)
ρ_{NAPL}	= density of NAPL, g/ cm ³
D_{eff}	= effective diffusivity of component A in NAPL and through pores, cm ² /s

To following equation can be used to convert the concentration in equation (C.4) from NAPL base to soil base, which is the unit used in experiments.

$$C = \frac{\epsilon_{NAPL} \rho_{NAPL}}{\rho_{soil}} C_{A/NAPL} \quad (C.6)$$

Substituting in equation (C.4) for $C_{A/NAPL}$ we get a similar equation that the concentration is expressed as soil base concentration.

$$\frac{d^2C}{dr^2} + \frac{2}{r} \frac{dC}{dr} = \frac{1}{D'_{eff}} \frac{dC}{dt} \quad (C.7)$$

$$D'_{eff} = \frac{D\epsilon_t}{\tau\epsilon_{NAPL}} \quad (C.8)$$

The analytical solution for equation C.1, for the case of zero initial concentration and constant surface concentration (C_s), is provided by Carslaw and Jeager (1959) in the following form:

$$C = C_s \left(1 + \frac{2R}{\pi r}\right) \sum_{n=1}^{\infty} \frac{(-1)^n}{n} \text{Sin}\left(\frac{n\pi r}{R}\right) e^{-D'_{eff} n^2 \pi^2 t / R^2} \quad (C.9)$$

The integrated form of equation (C.9) over the volume of sphere with radius R. will result in the following equation expressing the average concentration:

$$\bar{C} = C_s \left(1 - \frac{6}{\pi^2}\right) \sum_{n=1}^{\infty} \frac{1}{n^2} e^{-D_s \pi^2 n^2 t / R^2} \quad (\text{C.10})$$

The solution in equations (C.9) and (C.10) was obtained for zero initial concentration and constant surface concentration (C_s). However the boundary conditions in our system are:

$$C_p(R, t) = 0 \quad (\text{C.11})$$

$$C_p(r, 0) = C_0 \quad (\text{C.12})$$

where

C_p = concentration of component A in soil

C_0 = initial concentration of component A in soil

To meet the boundary conditions the variable C in equations (C.9) and (C.10) was transformed by the following equation:

$$C = C_p - C_0 \quad (\text{C.13})$$

So the boundary conditions are still valid:

$$C(r, 0) = C_p - C_0 = 0 \quad (\text{C.14})$$

$$C(R, t) = C_p - C_0 = -C_0 = C_s \quad (\text{C.15})$$

With this transformation the equations (C.9), (C.10) have been modified and are expressed by the following equations in polar coordinates:

$$C_p = C_s \left(1 + \frac{2R}{\pi r}\right) \sum_{n=1}^{\infty} \frac{(-1)^n}{n} \operatorname{Sin}\left(\frac{n\pi r}{R}\right) e^{-D_s n^2 \pi^2 t / R^2} + C_0 \quad (\text{C.16})$$

$$\bar{C}_p = C_s \left(1 - \frac{6}{\pi^2}\right) \sum_{n=1}^{\infty} \frac{1}{n^2} e^{-D_s \pi^2 n^2 t / R^2} + C_0 \quad (\text{C.17})$$

C.2. Mass Balance and Governing Equation for Film Diffusion

A non-steady state diffusion equation was developed to explain the transport of contaminants within the film of NAPL surrounding the soil aggregates.

$$JA \Big|_x - JA \Big|_{x+\Delta x} = A\Delta x \rho_{NAPL} \frac{dC_{A/NAPL}}{dt} \quad (C.18)$$

$$J = -D_{NAPL} \rho_{NAPL} \frac{dC_{A/NAPL}}{dx} \quad (C.19)$$

$$\frac{d^2 C_{A/NAPL}}{dx^2} = \frac{1}{D_{NAPL}} \frac{dC_{A/NAPL}}{dt} \quad (C.20)$$

The concentration in equation (C.18) is based on the NAPL mass. The following conversion will provide concentration based on soil mass.

$$C = mC_{A/NAPL} \quad (C.21)$$

where m is the NAPL mass fraction in soil. Substituting equation (C.19) in (C.18) provides a partial differential equation that the concentration of contaminants is expressed based on soil mass.

$$\frac{d^2 C}{dx^2} = \frac{1}{D_{NAPL}} \frac{dC}{dt} \quad (C.22)$$

$$C \rightarrow C_f$$

$$C_f = \frac{4C_0}{\pi} \sum_{n=0}^{\infty} \frac{(-1)^n}{(2n+1)} e^{-D_{soil}(2n+1)^2 x^2 / 4t^2} \cos \frac{(2n+1)\pi x}{2l} \quad (C.23)$$

$$\bar{C}_f = \frac{8C_0}{\pi^2} \sum_{n=0}^{\infty} \frac{1}{(2n+1)^2} e^{-D_{NAPL}(2n+1)^2 \pi^2 l / 4t^2} \quad (\text{C.24})$$

C_f = film concentration of component A, mg/kg soil

\bar{C}_f = average film concentration of component A, mg/kg soil

C.3. Calculation of average concentration in the Pores (C_{av})

Calculation of C_{av} based on analytical solution (Carlaw, 1959) and performing necessary change of variables.

$$\bar{C}_p = C_s \left(1 - \frac{6}{\pi^2}\right) \sum_{n=1}^{\infty} \frac{1}{n^2} e^{-D' \pi^2 n^2 t / R^2} + C_0 \quad (5.2)$$

$$\text{Boundary condition:} \quad (i) \quad C_p(R, t) = 0 \quad (5.4)$$

$$\text{Initial condition:} \quad (ii) \quad C_p(r, 0) = C_0 \quad (5.6)$$

This program introduces “function ca” as average concentration in the pores and calculates “ca” based on equations (5.2), (5.4) and (5.6).

function ca=cav(D,time)

global R Cs t C_m ca C0

suml=0; alpha=(D*pi^2*time)/R^2;

for n=1:40

argl=(1/n^2)*(exp(-alpha*n^2));

suml=suml+argl;

end

ca=C_s*(1-(6/pi^2)*suml)+C_0;

return

C.4. Calculation of average concentration in the film (C_{av})

Calculation of C_{av} based on analytical solution (Carlaw, 1959) and performing necessary change of variables.

$$\bar{C}_f = \frac{8C_0}{\pi^2} \sum_{n=0}^{\infty} \frac{1}{(2n+1)^2} e^{-D_{NAFL} (2n+1)^2 \pi^2 t / 4l^2} \quad (5.3)$$

Boundary condition: (i) $C_f(l, t) = 0$ (5.5)

Initial condition: (ii) $C_f(l, 0) = C_0$ (5.7)

This program introduces “function ca” as average concentration in the pores and calculates “ca” based on equations (5.3), (5.5) and (5.7).

```
function ca=cav_f(D,time)
global R Cs t C_m ca C0 l
```

```
    sum1=0; alpha=(D*pi^2*time)/(4*l^2);
    for n=0:40
        arg1=(1/(2*n+1)^2)*(exp(-alpha*(2*n+1)^2));
        sum1=sum1+arg1;
    end
    ca=(8*C0/pi^2)*sum1;
    return
```


C.5. Non-linear Regression for Diffusivity in NAPL

Non-linear regression was applied to get diffusion coefficient for various PAHs in NAPL using the analytical solution to partial diffusion equation. This model considers the combination of pore diffusion and film diffusion as transport mechanisms for contaminants in soil aggregates.

`%mainprog_fp2 used for sonicated sample.`

`global R Cs t C_m ca C0 mf Rad l`

`% Inputs:`

`C0= ;`

`Cs ;`

`l = ;`

`u= ;`

`% Reads the experimental data from file and calls them C_m (measured concentration).`

`data=csvread('phen.csv',42,12,[42 12 67 13]);`

`t=data(:,1)*86400;`

`C_m=data(:,2); % measured concentration ppm`

`% Initial guess for Df as cm2/s, and initial guess for the fraction of NAPL as a film`

`Df=input('initial guess for the diffusivity in film=');`

`a=input('initial guess for the fraction of NAPL in film=');`

`% Setting the initial values to zero.`

`nt=length(t);`

`for i=1:nt;`

`C_p1(i,1)=0;`

```

C_p(i,1)=0;
C_pf(i,1)=0;
C_p2(i,1)=0;
end

% Input the average size of the aggregates (cm) and the mass fractions

Rad=[20 45.5 88.5 185 370.5 743 1486]*(1e-4)/2;
mf=[74.55 5.68 3.74 4.46 3.74 3.39 4.41]/100;

% Calculates the average film concentration (C_pf) and average pore concentration (C_p)
and combines them by equation (5.10) to calculate the overall average concentration in an
aggregate (C_p2).

nR=length(Rad);
for i=1:nt,
C_pf(i,1)=cav_f(Df,t(i)); %Calculation of film diffusion
Dp=Df/10;
for j=1:nR, % calculation of pore diffusion
R=Rad(j);
m=mf(j);
C_p1(i,1)=cav(Dp,t(i));
C_p(i,1)=C_p(i,1)+m*C_p1(i,1);
end

% A(t)/Amax =1 for sonicated soil.

b(i,1)=a*A(t)/Amax
C_p2(i,1)=b(i)*C_pf(i,1)+(1-b(i))*C_p(i,1);
end

```

% Non-linear regression uses the function 'fmins' to get the best fit between experimental data (C_m) and the model prediction (C_p2). The values of Df and a are calculated.

```
options = 0;
options(2) = 1e-6; options(3) = 1e-6;
options(13) = 0;
X0=[Df a];
[X,opt]=fmins('regress_fp2',X0,options)
Df=X(1); a=X(2);
```

% plots the best fit as the result of regression.

```
plot(t/86400,C_p2, 'c');
s=num2str(Df);
q=num2str(a);
gtext(['Df='s]);
gtext(['a='q]);
```

% In case of Non-sonicated soil the values for mf (mass fraction of each class of aggregates) and A(t)/Amax (surface area associated with aggregates) were calculated from the following equations:

$$mf = [60.9546 - 45.6374 \cdot \exp(-0.488 \cdot ((t(i))/86400 + u)) \dots \\ 2.362 \dots \\ 4.712 \dots \\ 5.6802 + 3.3282 \cdot \exp(-1.7999 \cdot ((t(i))/86400 + u)) \dots \\ 9.7373 + 10.4272 \cdot \exp(-1.6462 \cdot ((t(i))/86400 + u)) \dots \\ 8.6080 + 12.1355 \cdot \exp(-0.3175 \cdot ((t(i))/86400 + u)) \dots \\ 3.6220 + 18.8067 \cdot \exp(- \\ 0.1610 \cdot ((t(i))/86400 + u))] / (0.95 \cdot 100)$$

$$A(t) / A_{max} = (60.95 - 45.63 \cdot \exp(-0.488 \cdot ((t(i))/86400 + u))) / 74.44;$$